Invited Speaker

35 Electron and x-ray spectroscopy for real-space electronic structure mapping in superconducting nickelates
Berit Goodge[1]
[1]Max Planck Institute for Chemical Physics of Solids, Dresden, Germany
549 Simulations of phonon and magnon EELS/EEGS including dynamical effects and multiple inelastic excitations
José Ángel Castellanos-Reyes[1], Paul Zeiger[1], Jan Rusz[1]
[1]Department of Physics and Astronomy, Uppsala University, Uppsala, Sweden

Oral Presentation

164 Structure Prediction using Data Derived Potentials and EELS
Thomas Ginnis[1], Professor Rebecca J Nicholls[1], Professor David Armstrong[1]
[1]Department of Materials, University of Oxford, Oxford, United Kingdom
393 Atomic Imaging of Lattice and Electron Ordering in Tensile-Strained LaCoO3 Films
Dr. Hongguang Wang[1], Dr. Bonan Zhu[2], Prof. David O. Scanlon[2], Prof. Peter A. van Aken[1]
[1]Max Planck Institute for Solid State Research, Heisenbergstr. 1, 70569, Stuttgart, Germany, [2]Department of Chemistry, University College London, London WC1H 0AJ, United Kingdom
415 Seeking peak precision in atomic EELS mapping with counting mode direct electron detection
Dr Duncan Alexander[1], Dr Chih-Ying Hsu[1,2], Dr Pau Torruella[1], Sebastian Cozma[1], Lucia Varbaro[2], Prof. Jean-Marc Triscone[2], Prof. Cécile Hébert[1]
[1]Electron Spectrometry and Microscopy Laboratory (LSME), Institute of Physics (IPHYS), École Polytechnique Fédérale de Lausanne (EPFL), Lausanne, Switzerland, [2]Department of Quantum Matter Physics (DQMP), University of Geneva, Geneva, Switzerland
463 Analytical electron tomography, fine structure EELS and nanoscale X-ray CT of nanoporous Copper materials
Tatiana Kormilina[1], Georg Haberfehlner[2], Samuel Graf[3], Eva-Maria Steyskal[3], Erdmann Spiecker[4], Gerald Kothleitner[1,2]
[1]Graz Centre for Electron Microscopy, Graz, Austria, [2]Institute of Electron Microscopy and Nanoanalysis, Graz University of Technology, Graz, Austria, [3]Institute of Materials Physics, Graz University of Technology, Graz, Austria, [4]Institute of Micro- and Nanostructure Research and Center for Nanoanalysis and Electron Microscopy, Friedrich-Alexander University, Erlangen, Germany
651 Multi Element ELNES Mapping of Compounds
Daen Jannis[1,2], Mr. Nicolas Gauquelin[1,2], Ms. Maria Meledina[3], Mr. Yuchen Zhao[4], Mr. Yunzhong Chen[4], Mr. Jo Verbeeck[1,2]
[1]EMAT, Universiteit Antwerpen, Antwerpen, Belgium, [2]NANOlab, Universiteit Antwerpen, Antwerpen, Belgium, [3]Thermo Fisher Scientific, Eindhoven, Netherlands, [4]Beijing National Laboratory of Condensed Matter Physics, Chinese Academy of Sciences, Beijing, China
1000 PolSpec – broadband cost-effective hyperspectral imaging
Huihui Liu[1], Sunil Kumar[1,2], Edwin A Garcia Castano[1], Paul French[1,2]
[1]Physics Department, Imperial College London, SW7 2AZ, , UK, [2]Francis Crick Institute, 1 Midland Road, NW1 1AT, , UK
119 Unveiling Metal-Insulator Transitions in (V1-xCrx)2O3 through in situ Monochromatized STEM/EELS
Dr. Abdelali Khelfa[1], Mr. Jean-Denis Blazit[1], Mr. Luiw H. G. Tizei[1], Mr. Etienne Janod[2], Mr. Julien Tranchant[2], Mr. Benoît Corraze[2], Mr. Laurent Cario[2], Mrs. Odile Stephan[1], Mrs. Laura Bocher[1]
[1]Laboratoire de Physique des Solides - Université Paris Saclay - CNRS, Orsay (91405), France, [2]Institut des Matériaux Jean Rouxel - Université de Nantes - CNRS, Nantes (44322), France

136 An accessible Secondary Electron Hyperspectral Imaging approach to draw meaningful insights from scanning electron microscopy
James Nohl[1,2], Jingqiong Zhang[1], Lyudmila Mihaylova[1], Serena Cussen[3], Cornelia Rodenburg[1]
[1]Department of Materials Science and Engineering, The University of Sheffield, Mappin Street, Sheffield, UK, [2]The Faraday Institution, Quad One, Becquerel Avenue, Harwell Campus, Didcot, UK, [3]School of Chemistry, University College Dublin, Belfield, Dublin 4, Ireland
272 Measuring hybridisation in Van der Waals heterostructures using momentum-resolved EELS
Hannah Nerl[1], Dr Ana Valencia[2], Mr Khairi Elyas[3], Juan Pablo Guerrero Felipe[1], Dr Katja Höflich[3], Prof Caterina Cocchi[1,2], Prof Christoph Koch[1]
[1]Department of Physics and IRIS Adlershof, Humboldt Universität zu Berlin, Berlin, Germany, [2]Institute of Physics and Center for Nanoscale Dynamics (CeNaD), Carl-von-Ossietzy Universität Oldenburg, Oldenburg, Germany, [3]Ferdinand-Braun-Institut gGmbH, Leibniz-Institut für Höchstfrequenztechnik, Berlin, Germany
303 Phonon dispersion surfaces from the electron microscope compared with calculations including dynamical diffraction
Dr. Benedikt Haas[1], Steven Quillin[2], Tracy Lovejoy[2], Niklas Dellby[2], Ondrej Krivanek[2,3], Adnan Hammud[4], Tim Schröder[1], Christoph Koch[1], Peter Rez[2]
[1]Department of Physics & Center for the Science of Materials Berlin, Humboldt-Universität zu Berlin, Berlin, Germany, [2]Bruker AXS (formerly Nion Co. R&D), Kirkland, USA, [3]Department of Physics, Arizona State University, Tempe, USA, [4]Department of Inorganic Chemistry, Fritz-Haber Institute of the Max-Planck Society, Berlin, Germany
397 Assessing the Precision of Local Temperature Measurement by Plasmon Energy in In-Situ Heating Electron Microscopy
Yi-Chieh Yang[1], Luca Serafini[2], Nicolas Gauquelin[2], Johan Verbeeck[2], Joerg Jinschek[1]
[1]Nanolab, Technical University of Denmark (DTU) , Kongens Lyngby, Denmark, [2]EMAT, University of Antwerp, Antwerp, Belgium
728 Unravelling the collagen mineralization using multiscale in situ X-ray-scattering/Raman spectroscopy and ex situ electron microscopy/nano-Xray-fluorescence
Prof. Dr Roland Kröger[1], Dr Julia Parker[2], Ms Emma Tong[1]
[1]University of York, York, United Kingdom, [2]Diamond Light Source, Harwell, United Kingdom
123 Quantitative chemical analysis by STEM-EDS and machine learning: Are AgAu alloyed at the nanoscale?
Dr Murilo Moreira[1,2], Dr. Emmanuel Cottancin[1], Dr. Michel Pellarin[1], Dr. Lucian Roiban[3], Dr. Karine Massenelli-Varlot[3], Dr. Daniel Ugarte[2], Dr. Varlei Rodrigues[2], Dr. Matthias Hillenkamp[1,2]
[1]Institute of Light and Matter, University Lyon, University Claude Bernard Lyon 1, CNRS, UMR5306, Villeurbanne F-69622, France, [2]Institute of Physics Gleb Wataghin, State University of Campinas, Campinas, 13083-970, Brazil, [3]INSA Lyon, Universite Claude Bernard Lyon 1, CNRS, MATEIS, UMR5510, Villeurbanne , France
291 5D-ToF-STIM Hyperspectral Imaging with a keV He+ Focused Ion Beam
Dr. Dustin Andersen[1], Michael Mousley[1], Saba Tabean[1], Radek Holeňák[2], Eleni Ntemou[2], Gerhard Hobler[3], Tom Wirtz[1], Daniel Primetzhofer[2], Santhana Eswara[1]
[1]Advanced Instrumentation for Nano-Analytics (AINA), MRT Department, Luxembourg Institute of Science and Technology (LIST), Belvaux, Luxembourg, [2]Department of Physics and Astronomy, Uppsala University, Uppsala, Sweden, [3]Institute of Solid-State Electronics, TU Wien, Vienna, Austria
373 Atomic Lensing Model for Atomic Scale Multi-Elemental Quantification in STEM
Dr Zezhong Zhang[1,2,3], Dr. Annick De Backer[1,2], Dr. Ivan Lobato[4], Prof. Sandra Van Aert[1,2], Prof. Peter Nellist[3]
[1]EMAT, University of Antwerp, Antwerp, Belgium, [2]NANOlab Center of Excellence, University of Antwerp, Antwerp, Belgium, [3]Department of Materials, University of Oxford, Oxford, United Kingdom, [4]Rosalind Franklin Institute, Harwell Research Campus , United Kingdom

417 Use of prior knowlege and physics-guided NMF for improved phase segmentation of EDX datasets.
Prof. Cécile Hébert[1], Dr. Adrien Teurtrie[1,2], Dr. Pau Torruella-Besa[1], M. Sebastian Cozma[1], Dr. Hui Chen[1], Dr. James Badro[3], Dr. Duncan T.L. Alexander[1]
[1]EPFL-IPHYS-LSME, Lausanne, Switzerland, [2]Unité Matériaux et Transformations, UMR-CNRS 820, Lille, France, [3]Institut de Physique du Globe, Paris, France
734 Direct visualization of chemical transport in solid-state chemical reactions by time-of-flight secondary ion mass spectrometry
Sang Pham[1], Sean Collins[1,2]
[1]Bragg Centre for Materials Research & School of Chemical and Process Engineering, University of Leeds, Leeds, United Kingdom, [2]School of Chemistry, University of Leeds, Leeds, United Kingdom
755 Electron beam propagation impact on high-resolution quantitative chemical analysis of GaN/AlGaN 1 nm-thick quantum wells
Florian Castioni[1,2], Sergi Cuesta[3], Patrick Quéméré[2], Eric Robin[3], Vincent Delaye[2], Eva Monroy[3], Pascale Bayle-Guillemaud[3], Nicolas Bernier[2]
[1]Université Paris-Saclay, CNRS, Laboratoire de Physique des Solides, Paris, France, [2]Université Grenoble Alpes, CEA, LETI, Grenoble , France, [3]Université Grenoble Alpes, CEA, IRIG, Grenoble, France
994 SEM-Cathodoluminescence Imaging and Spectroscopy - Applications in Archeology and Life Science
Dr. Ifat Kaplan-Ashiri[1]
[1]Electron Microscopy Unit, Department of Chemical Research Support, Weizmann Institute of Science, Rehovot, Israel
1005 Hyperspectral CT allows for non-destructive elemental imaging in museum specimen
Henrik Lauridsen[1], Daniel Klingberg Johansson[2], Christina Carøe Ejlskov Pedersen[3], Kasper Hansen[3], Michiel Krols[4], Kristian Murphy Gregersen[5], Julie Nogel Jæger[5], Catherine Jane Alexandra Williams[6], Ditte-Mari Sandgreen[7], Aage Kristian Olsen Alstrup[1,8], Mads Frost Bertelsen[9,10], Peter Rask Møller[2]
[1]Department of Clinical Medicine, Aarhus University, , Denmark, [2]Natural History Museum of Denmark, University of Copenhagen, , Denmark, [3]Department of Forensic Medicine, Aarhus University, , Denmark, [4]TESCAN XRE, , Belgium, [5]Institute of Conservation, Royal Danish Academy, , Denmark, [6]Department of Animal and Veterinary Sciences, Aarhus University, , Denmark, [7]Givskud Zoo-Zootopia, , Denmark, [8]Department of Nuclear Medicine & PET, Aarhus University Hospital, , Denmark, [9]Center for Zoo and Wild Animal Health, Copenhagen Zoo, , Denmark, [10]Department of Veterinary Clinical Sciences, University of Copenhagen, , Denmark

Poster Presentation

121 Multidimensional Characterisation and Multivariate Analysis of Cu3P Nanocages for Catalysis
Dr. Andrea Griesi[1], Mr. Rundong Mao[2], Mr. Sirous Khabbazabkenar[1], Mr. Yurii Ivanov[1], Mr. Guohua Jia[2], Mr. Giorgio Divitini[1]
[1]Ististuto Italiano di Tecnologia, Genova, Italy, [2]Curtin University , Perth, Australia
163 EELS at Extreme Energy Losses; complementary Information to X-ray Absorption Spectroscopy (XAS) in a TEM
Dr Sorin Lazar[1], Mrs. Maria Meledina[1], Mrs. Claudia S. Schnohr[2], Mr. Thomas Hoeche[3], Mr. Peter Tiemeijer[1], Mr. Paolo Longo[1], Mr. Bert Freitag[1]
[1]Thermo Fisher Scientific, Eindhoven, Netherlands, [2]Felix Bloch Institute for Solid State Physics, Leipzig, Germany, [3]Fraunhofer-Institut für Mikrostruktur von Werkstoffen und Systemen IMWS, Halle (Saale), Germany
249 Maximizing Speed and Sensitivity: Simultaneous High-throughput EDS-WDS Elemental Mapping in the SEM
Shangshang Mu[1], David Stowe[1]

[1]Gatan/EDAX, Pleasanton , United States

277 Fast and low dose EELS using compressive sensing

Alex Robinson[1], Jack Wells[1,2], Daniel Nicholls[1], Giuseppe Nicotra[3], Nigel Browning[1,4]
[1]SenseAI Innovations Ltd., Liverpool, United Kingdom, [2]Distributed Algorithms Centre for Doctoral Training, Liverpool, United Kingdom, [3]CNR-IMM, Catania, Italy, [4]University of Liverpool, Liverpool, United Kingdom

354 Quantification and denoising of atomic-resolution EDX spectrum images using a Multiscale Bayesian Approach

Pau Torruella-Besa[1], Abderrahim Halimi[2], Duncan T. L. Alexander[1], Cécile Hébert[1]
[1]Electron Spectrometry and Microscopy Laboratory (LSME), Institute of Physics (IPHYS), Ecole Polytechnique Fédérale de Lausanne (EPFL), Lausanne, Switzerland, [2]School of Engineering and Physical Sciences, Heriot-Watt University, Edinburgh, United Kingdom

372 Reducing user-interaction in the processing of electron energy-loss spectra

Mr. Daen Jannis[1,2], Dr. Wouter Van den Broek[3], Mr. Jo Verbeeck[1,2]
[1]University of Antwerp, Electron Microscopy for Materials Research (EMAT), Antwerp, Belgium, [2]University of Antwerp, Nanolab Center of Excellence, Antwerp, Belgium, [3]Thermo Fisher Scientific, Eindhoven, Netherlands

374 Relativisitic EELS cross-sections for all elements

Dr Zezhong Zhang[1,2,3], Dr. Ivan Lobato[4], Dr. Hamish G. Brown[5], Dr. Daen Jannis[1,2], Prof. Johan Verbeeck[1,2], Prof. Dirk Lamoen[1,2], Prof. Sandra Van Aert[1,2], Prof Peter D. Nellist[3]
[1]EMAT, University of Antwerp, Antwerp, Belgium, [2]NANOlab Center of Excellence, University of Antwerp, Antwerp, Belgium, [3]Department of Materials, University of Oxford, Oxford, United Kingdom, [4]Rosalind Franklin Institute, Oxfordshire , United Kingdom, [5]Ian Holmes Imaging Centre, Bio21 Molecular Science and Biotechnology Institute, University of Melbourne, Victoria, Australia

396 Molecular Microscopy by Thermo-Fisher-Scientific: FTIR-Imaging of a Tintoretto-Fresco and Raman-Imaging of the Strain-Distribution in Semiconductors

Dr. Maximilian Ries[1,2], Barbara Bravo[1], Eleonora Balliana[3], Fabian Heisinger[2], Imad Limame[2]
[1]Thermo Fisher Scientific, , Germany/Italy, [2]Technische Universität Berlin, , Germany, [3]Ca' Foscari University of Venice, , Italy

416 WhatEELS upgrade: the software tool based in Python for EELS analysis

Vanessa Costa-Ledesma[1], Daniel del-Pozo-Bueno[1], Francesca Peiró[1], Sònia Estradé[1]
[1]LENS-MIND, Dept. d'Enginyeria Electrònica i Biomèdica and Institute of Nanoscience and Nanotechnology (IN2UB), Universitat de Barcelona, Barcelona, Spain

512 Atom-counting for heterogeneous nanostructures using multimodal STEM

Dr Annick De Backer[1], Dr Zezhong Zhang[1], Dr Ana Sánchez-Iglesias[2], Prof Luis M. Liz-Marzán[2,3], Prof Peter D. Nellist[4], Prof Sara Bals[1], Duygu G. Şentürk[1], Dr Yansong Hao[1], Prof Scott Findlay[5], Prof Sandra Van Aert[1]
[1]EMAT & NANOlab Center of Excellence, University of Antwerp, Antwerp, Belgium, [2]CIC biomaGUNE, Basque Research and Technology Alliance (BRTA), Donostia-San Sebastián, Spain, [3]Ikerbasque, Basque Foundation for Science, Bilbao, Spain, [4]Department of Materials, University of Oxford, Oxford, United Kingdom, [5]School of Physics and Astronomy, Monash University, Melbourne, Australia

591 Development and applications of backscattered electron and X-ray detector

Dr Katherine Macarthur[1], Haithem Mansour[1], John Zhang[1], Anthony Hyde[1], Simon Burgess[1], Philippe Pinard[1]
[1]Oxford Instruments NanoAnalysis, High Wycombe, United Kingdom

592 Uranium reduction by magnetite and mechanism of UO2 formation monitored by low-dose STEM-EELS

Dr. Barbora Bártová[1,2], Thomas LaGrange[3], Zezhen Pan[1,4], Gregory Leinders[5], René Bes[6], Nicolas Jacquemin[1], Katharina Reinhold[1], Jacopo Carbone[1], Rizlan Bernier-Latmani[1]
[1]Environmental Microbiology Laboratory (EML), École polytechnique fédérale de Lausanne (EPFL), Lausanne, Switzerland, [2]Interdisciplinary Center for Electron Microscopy (CIME), EPFL, Lausanne,

Switzerland, [3]Laboratory for Ultrafast Microscopy and Electron Scattering (LUMES), EPFL, Lausanne, Switzerland, [4]Department of Environmental Science and Engineering, Fudan University, Shanghai, China, [5]Institute for Nuclear Materials Science, Belgian Nuclear Research Centre (SCK CEN), Mol, Belgium, [6]Center for X-ray Spectroscopy, University of Helsinki, Helsinki, Finland

709 The significance of the phonon polarization vector in vibrational EELS

Paul Zeiger[1], Jan Rusz[1]
[1]Uppsala University, Uppsala, Sweden

795 Application of secondary electron hyperspectral imaging to the analysis of pharmaceutical materials

Stuart Micklethwaite[1], Rastra Basnet[1], Joseph Ma[1], Daniel Hopper[1], James Nohl[2], Nicholas Farr[2], Cornelia Rodenburg[2], Dr Nicole Hondow[1]
[1]University of Leeds, Leeds, UK, [2]University of Sheffield, Sheffield, UK

804 Denoising 4D STEM datasets with PCA

Leonid Potapov[1], Mingjian Wu[2]
[1]temDM, Dresden, Germany, [2]IMN&CENEM, Friedrich-Alexander Universität, Erlangen-Nürnberg, Germany

834 Sub-nanometer mapping of strain-induced band structure variations in different semiconductor device configurations

Marc Botifoll[1], Dr. Sara Martí-Sánchez[1], Dr. Eitan Oksenberg[2], MSc. Christian Koch[1], MSc. Carla Borja[1], Dr. Maria Chiara Spadaro[1], Dr. Valerio Di Giulio[3], Prof. Quentin Ramasse[4,5], Prof. F. Javier García de Abajo[3,6], Prof. Ernesto Joselevich2[2], Prof. Jordi Arbiol[1,6]
[1]Catalan Institute of Nanoscience and Nanotechnology (ICN2), CSIC and BIST, Bellaterra, 08193 Barcelona, Spain, [2]Department of Molecular Chemistry and Materials Science, Weizmann Institute of Science, Rehovot 76100, Israel, [3]ICFO-Institut de Ciencies Fotoniques, The Barcelona Institute of Science and Technology, 08860 Castelldefels, Barcelona, Spain, [4]SuperSTEM Laboratory, STFC Daresbury Campus, Daresbury WA4 4AD, United Kingdom, [5]School of Chemical and Process Engineering & School of Physics and Astronomy, University of Leeds, Leeds LS2 9JT, United Kingdom, [6]ICREA, Passeig Lluís Companys 23, 08010 Barcelona, Spain

852 Nanoscale structural and spectroscopic characterization of hard carbons for Na-ion batteries

Tatiana Kormilina[1], Harald Fitzek[1], Daniel Knez[2], Ilie Hanzu[3], Gerald Kothleitner[1,2], Georg Haberfehlner[2]
[1]Graz Centre for Electron Microscopy, Graz, Austria, [2]Institute of Electron Microscopy and Nanoanalysis, Graz University of Technology, Graz, Austria, [3]Institute for Chemistry and Technology of Materials, Graz University of Technology , Graz, Austria

879 FTIR-Imaging of a Tintoretto-Fresco

Dr. Maximilian Ries[1], Barbara Bravo[1], Eleonora Balliana[2]
[1]Thermo Fisher Scientific, , Germany/Italy/USA, [2]Ca' Foscari University of Venice, Venice, Italy

880 Raman-Imaging of the Strain-Distribution in Semiconductors

Dr. Maximilian Ries[1,2], Fabian Heisinger[2], Dr. Imad Limame[2]
[1]Thermo Fisher Scientific, , Germany/USA, [2]Technische Universität Berlin, Berlin, Germany

933 Annular silicon drift detector for advanced EDS on SEM applications

Dr. Igor Németh[1], Dr. Yang Yang
[1]Bruker Nano GmbH, Berlin, Germany

968 Electron energy loss spectroscopy for differentiating of minerals polymorphs

Dr Vladimir Roddatis[1], Dr Elizaveta Kovaleva[1,2], Dr Marcin Syczewski[1], Anja Schreiber[1], Dr Richard Wirth[1], Prof Monica Koch-Müller[1]
[1]GFZ German Research Centre for Geosciences, Potsdam, Germany, [2]Department of Earth Sciences, University of the Western Cape, , South Africa

996 2D and 3D Oxidation State Mapping in FeO/Fe3O4 Nanocubes Using the Fe-M2,3 EELS Edge

Dr Mario Pelaez-Fernandez[1,2,3], Daniel del-Pozo-Bueno[4,5], Dr Maya Marinova[6], Dr Adrien Teurtrie[1], Prof. Hugues Leroux[1], Prof. Francesca Peiró[4,5], Prof. Sonia Estradé[4,5], Dr Francisco De la Peña[1]

[1]Unité Matériaux et Transformations (UMET UMR 8207), Université de Lille, Bâtiment C6, Cité Scientifique, Villeneuve d'Ascq, France, [2] Instituto de Nanociencia y Materiales de Aragon (INMA), CSIC-U. de Zaragoza, Zaragoza, Spain, [3]Laboratorio de Microscopias Avanzadas, Universidad de Zaragoza, Zaragoza, Spain, [4]LENS-MIND, Departament d'Enginyeria Electrònica i Biomèdica, Universitat de Barcelona, Barcelona, Spain, [5]Institute of Nanoscience and Nanotechnology (IN2UB), Universitat de Barcelona, , Spain, [6]Univ. Lille, FR 2638-IMEC-Institut Michel-Eugène Chevreul, , France

1039 Resolving short-range order in Carbon Nitride-based catalysts using EELS

Mr. Teodor Jianu[1], Mr. Horațiu Szalad[1], Dr. Baile Wu[1], Dr. Vladimir Rodatis[2], Prof. Dr. Dr. h.c. Markus Antonietti[1], Dr. habil. Nadezda V Tarakina[1]

[1]Department of Colloid Chemistry, Max Planck Institute of Colloids and Interfaces, Potsdam, Germany, [2]German Research Centre for Geosciences GFZ, Helmholtz Centre Potsdam, Potsdam, Germany

1069 WDS-supported Bayesian Peak Deconvolution for optimized Standardless EDS-Quantification

Jörg Nissen[1], Frank Eggert[2], Dirk Berger[1], Ulrich Gernert[1]

[1]Technische Universität Berlin, Center for Electron Microscopy (ZELMI) , Berlin, Germany, [2]Microanalyst.net, Berlin, Germany

1075 Measurement of EELS standards and application on oxidation state determination of a MeOH catalyst

Dr. Daniela Ramermann[1], Dr. Elisabeth H. Wolf[1], Dr. Michael Poschmann[1], Dr. Christoph Göbel[1], Dr. Lukas Pielsticker[1], Dr. Holger Ruland[1], Dr. Walid Hetaba[1]

[1]Max Planck Institute for Chemical Energy Conversion, Department of Heterogeneous Reactions, Mülheim an der Ruhr, Germany

1076 Numerical Analysis of Temperature Calibration using Plasmon Energy Expansion Thermometry

Lucas Pedersen[1], Yi-Chieh Yang[2], Mads Sørensen[3], Joerg Jinschek[4]

[1]Department of Applied Mathematics and Computer Science, Technical University of Denmark (DTU), Kgs. Lyngby, Denmark, Kgs. Lyngby, Denmark, [2]National Center for Nano Fabrication and Characterization, Technical University of Denmark (DTU), Kgs. Lyngby, Denmark, , , [3]Department of Applied Mathematics and Computer Science, Technical University of Denmark (DTU), Kgs. Lyngby, Denmark, , , [4]National Center for Nano Fabrication and Characterization, Technical University of Denmark (DTU), Kgs. Lyngby, Denmark, ,

1120 Multimodal imaging accelerates the analysis of composition in bone implant sites

Joshua Lea[1], Pedro Machado[1], Zhidao Xia[2], Dr Louise Hughes[1]

[1]Oxford Instruments NanoAnalysis, High Wycombe, United Kingdom, [2]Centre for Nanohealth, Institute of Life Science, Swansea University Medical School, Swansea , United Kingdom

Late Poster Presentation

1271 Atomic Structure and Electron Magnetic Circular Dichroism of Individual Rock-Salt Structure Antiphase-Boundaries in Spinel Ferrites

Associate Professor Xiaoyan Zhong[1]

[1]TRACE EM Unit and Department of Materials Science and Engineering, City University of Hong Kong, Kowloon, Hong Kong SAR, China, [2]City University of Hong Kong Matter Science Research Institute (Futian), , Shenzhen, China, [3]Nanomanufacturing Laboratory (NML), City University of Hong Kong Shenzhen Research Institute, Shenzhen , China

35

Electron and x-ray spectroscopy for real-space electronic structure mapping in superconducting nickelates

Berit Goodge[1]
[1]Max Planck Institute for Chemical Physics of Solids, Dresden, Germany

IM-05 (1), Lecture Theater 3, august 26, 2024, 10:30 - 12:30

Background and aims: The recently discovered superconducting nickelates are an archetypal example of how exotic or functional properties can be realized by careful materials synthesis and engineering. While many fundamental aspects of these materials remain under active investigation, it is clear that (as with many quantum materials) they are rooted in strong interactions between atomic structure, orbitals, and electronic charge. The unique sample geometry and complicated synthesis of the so-called infinite-layer nickelates, however, have not only raised questions about the origin of superconductivity in thin film specimens and generally hindered the use of many common “field-standard” spectroscopic probes. Here, I will focus on two advanced core-level spectroscopic techniques, both of which provide unique access to real-space electronic information.
Methods: At the atomic scale, highly local spectroscopic measurements are conducted by electron energy loss spectroscopy (EELS) in the scanning transmission electron microscope (STEM) with a sub-Ångström probe to enable location-specific measurements across the doping-dependent superconducting dome in nickelate thin films. Leveraging hard x-rays at high-brilliance synchrotron facilities, we harness beyond-dipole and dipole-forbidden transitions with s-orbital non-resonant inelastic x-ray scattering (sNIXS) to directly map the complete charge density [1] in bulk undoped infinite-layer nickelates.
Results: Area-selective STEM-EELS measurements reveal a distinct electronic landscape in the superconducting nickelate, particularly in regards to nickel hybridization, and it’s doping evolution across the superconducting dome which point to multi-band superconductivity [2]. Elemental and electronic investigation across the atomic substrate-film interface provide definitive evidence against the picture of possible interfacial superconductivity hosted at a strongly polar oxide interface [3]. The quantitative precision offered by bulk sNIXS measurements are used to investigate questions of nickelate “self-doping” in chemically undoped compounds through strong interactions with rare-earth states.
Conclusions: The insights offered by hyperspectral techniques, particularly those with real-space sensitivity, are crucial for building fundamental understanding of many quantum, biological, and functional materials. Both techniques described here can be further extended to in situ or operando conditions, opening the door to study phase evolution driven by temperature, pressure, fields, etc., some challenges and promising developments of which I will also mention [4,5].

Keywords:

STEM-EELS, sNIXS, quantum, superconductivity, spectroscopy

Reference:

[1] Yavas, et al. Nature Physics 15, 559–562 (2019).
[2] Goodge, et al. PNAS 118(2), e2007683118 (2021).
[3] Goodge, et al. Nature Materials 22, 466–473 (2023).
[4] Goodge, Baek, Kourkoutis. arXiv:2007.09747 (2020).
[5] Goodge, et al. Microscopy and Microanalysis 26(3), 439–446 (2020).

549

Simulations of phonon and magnon EELS/EEGS including dynamical effects and multiple inelastic excitations

José Ángel Castellanos-Reyes[1], Paul Zeiger[1], Jan Rusz[1]
[1]Department of Physics and Astronomy, Uppsala University, Uppsala, Sweden

IM-05 (2), Lecture Theater 3, august 26, 2024, 14:00 - 16:00

Background incl. aims
Phonons and magnons play important roles in various technological applications. Phonons are essential for understanding heat flow at the nanoscale, while magnons hold promise as an information carrier (quasi-)particle for a new generation of hardware in information technologies. Instrumental advances, bringing high spatial resolution offered by scanning transmission electron microscopes (STEMs) together with high energy resolution and high dynamic range offered by direct electron detectors, offer an exciting route for studying these quasiparticles down to atomic scale [1-2].
However, the strong interaction between the electron beam and the sample, resulting in multiple elastic and inelastic scattering events, complicates the interpretation of experimental data and reliable theoretical predictions are thus of high importance.

Methods
We extend the quantum excitation of phonons method [3] to the spectroscopic domain. This is achieved by deriving a time-autocorrelation function of the so-called auxiliary wave-function and showing that it represents the desired spectral information. The exact quantum-mechanical evolution of the auxiliary wave-functions is approximated by scattering on a structure model with the atomic coordinates (or magnetic moment directions in the case of magnon EELS) evolving classically. Motion of atoms or precession of magnetic moments is simulated by molecular dynamics or atomistic spin dynamics, respectively.

Results
We present a derivation of a new theoretical framework that treats elastic and inelastic scattering on equal footing, including energy loss and gain processes, and effects of multiple elastic and inelastic scattering events [4]. The resulting simulation method remains flexible and efficient, and in comparison with recently introduced frequency-resolved frozen phonon multislice method (FRFPMS; [5]) it includes multiple inelastic scattering, doesn't require knowledge of Debye-Waller factors, and effectively includes anisotropic vibrations (or precession of magnetic moments) and non-local absorption effects of the elastic channel. We present the method on simulations of phonon EELS/EEGS on crystalline silicon and magnon EELS/EEGS for bcc iron and compare them to available data.

Conclusion
A new approach to simulations of phonon and magnon EELS has been presented. Comparison with FRFPMS and adiabatic magnon spectra from spin dynamics shows good agreement.

Keywords:

phonon, magnon, EELS, EEGS, STEM

Reference:

1. M J Lagos et al., Microscopy 71 (2022), p. i174.
2. A Barman et al., J. Phys.: Condens. Matter 33 (2021), 413001.
3. B D Forbes, A V Martin, S D Findlay, A J D'Alfonso, and L J Allen, Phys. Rev. B 82 (2010), 104103.
4. J Á Castellanos-Reyes et al., arXiv:2401.15599.
5. P M Zeiger and J Rusz, Physical Review Letters 124 (2020), 025501.

164

Structure Prediction using Data Derived Potentials and EELS

Thomas Ginnis[1], Professor Rebecca J Nicholls[1], Professor David Armstrong[1]
[1]Department of Materials, University of Oxford, Oxford, United Kingdom

IM-05 (1), Lecture Theater 3, august 26, 2024, 10:30 - 12:30

Background

(Scanning) Transmission Electron Microscopy ((S)TEM) coupled with Electron Energy Loss Spectroscopy (EELS) is a powerful and information rich technique capable of providing information about composition and local bonding environments at a high spatial resolution. However, the Energy Loss Near Edge Structure (ELNES) of core-loss EELS peaks can be difficult to interpret due to the large number of factors which can influence the ELNES shape. Traditionally, spectra collected from known standards have been used to interpret ELNES, or spectra have been simulated from structures obtained from databases such as the Materials Project or the Inorganic Crystal Structure Database. This work presents a workflow for using Ab-Initio Random Structure Searching (AIRSS) accelerated by Ephemeral Data Derived Potentials (EDDP) to predict the structures of compounds after measuring their composition using quantitative EELS, then using CASTEP and OPTADOS to predict the ELNES of these structures. The workflow has been tested on silicised boron nitride, a system important in high temperature ceramic matrix composites.

Methods

TEM lamella were prepared from single crystal SiC and silicised BN. A TEM sample of commercially pure BN was obtained by dispersing the BN nanopowder on a carbon grid. The TEM samples were analysed using STEM-EELS, and elemental maps, thickness information, and ELNES datasets were obtained.

These EELS datasets were fitted with the model fitting functionality of Hyperspy, and these models were used to calculate the compostitions of the samples.

After calculating the composition of the silicised BN sample, a unit cell of this composition was generated containing multiple formula units. The cell was then used to train a data derived potential, capable of calculating the energy of an arrangement of atoms given their coordinates. This was performed with the EDDP code, which generates random sensible structures and calculates their energy using the plane wave pseudopotential Density Functional Theory (DFT) code CASTEP with the Regularised Strongly Constrained and Appropriately Normed (rSCAN) functional and the Many Body Dispersion (MBD) semi-empirical dispersion correction to account for long range van der Waals forces. These atomic coordinates and energies are used as the training data for an ensemble neural network.

The initial potential learned by the system will have a large error, but is sufficiently robust enough to allow for structure searching, by generating a random sensible structure and relaxing it to a local minimum using the learned potential. DFT is then used to calculate the actual energies of the minima of this initial structure search, and expand the training data for the learned potential. The network is retrained on the expanded training dataset.

This process is repeated 5 times until a robust and accurate potential is formed. This potential can then be used for rapid random structure searching and can predict low energy structures of the unit cell defined by the measured composition.

The lowest energy structures are then relaxed further using DFT to ensure they are at true energy minima, and the ELNES spectra for each of the atomic environments present are calculated using CASTEP and OPTADOS.

These calculated spectra can be used as reference spectra in a library and can be compared directly with ELNES measured in STEM-EELS experiments.

Results

The validity of the model fitting functionality in Hyperspy for determining the composition of silicised BN was tested using the pure BN nanopowder and semiconductor grade SiC, and the method could predict the compositions of these known compounds, proving that the quantification method is suitable for systems containing Si, C, B and N.

Initial EDDP calculations involved the Si-B-N system. A unit cell containing 3 Si, 6 N and 5 N atoms was created, and this composition was chosen based on literature values of the typical composition of silicised BN. An ensemble neural network containing a single layer with 5 nodes was produced, and this resulted in a potential with an error of less than 30 meV / atom on the testing set.

This data derived potential was used for a random structure search of over 10,000 structures. The lowest energy structures were selected, and a stricter geometry relaxation was performed using DFT. The EELS spectra for these low energy structures were calculated with CASTEP and OPTADOS before being compared with experimental spectra from silicised boron nitride. This allowed for information about the local bonding environment to be understood.

Conclusions

The EDDP method has enabled rapid random structure searching of systems which were previously too large to search efficiently. This has opened up a workflow in which EELS can be used on a wider range of materials, including those which do not have high quality reference standards or even known crystal structures in large databases.

The usefulness of this workflow was demonstrated on silicised BN, and further work could use a similar workflow to understand how the composition and ELNES of these materials changes as a result of environmental degradation.

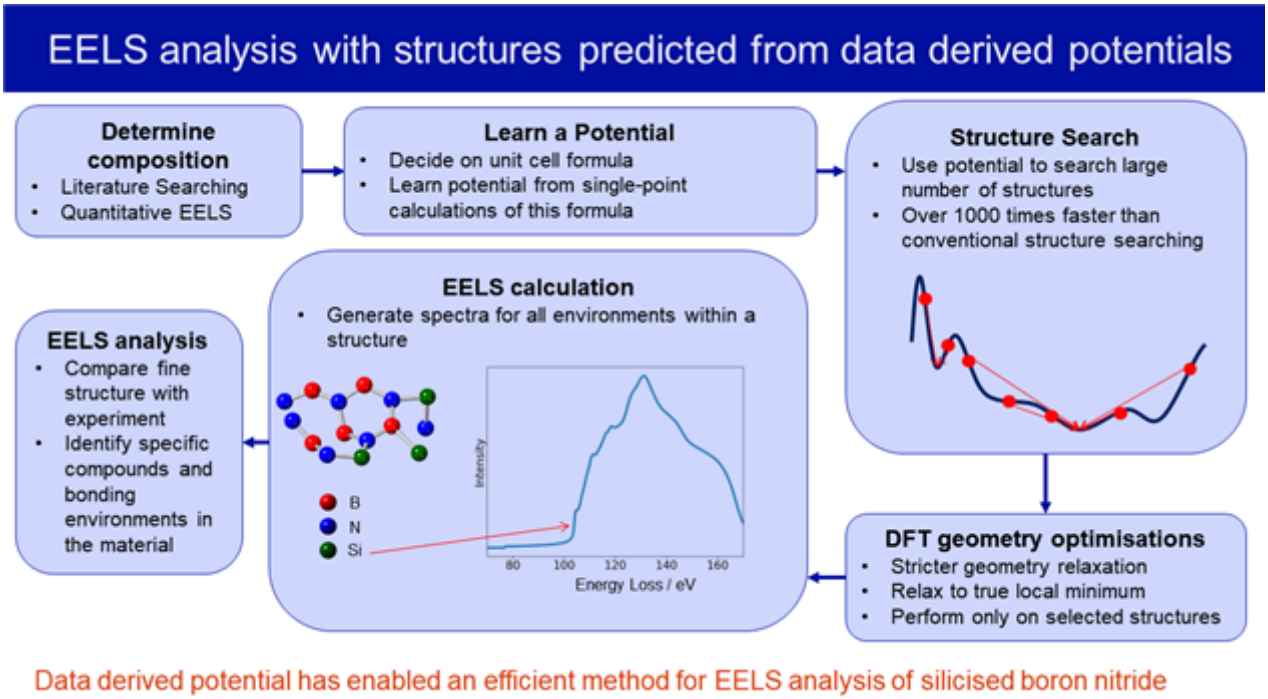

Keywords:

EELS, DFT, ML, Structure Prediction

Reference:

Pickard, C. J. Phys. Rev. B 106, (2022)

Pickard, C. J. et al. Journal of Physics Condensed Matter 23, (2011)

Clark, S. J. et al. Zeitschrift fur Krist. 220, (2005)

Morris, A. J. et al. Comput. Phys. Commun. 185, (2014)

Zhang, S. et al. J. Eur. Ceram. Soc. 42, (2022)

393

Atomic Imaging of Lattice and Electron Ordering in Tensile-Strained LaCoO3 Films

Dr. Hongguang Wang[1], Dr. Bonan Zhu[2], Prof. David O. Scanlon[2], Prof. Peter A. van Aken[1]
[1]Max Planck Institute for Solid State Research, Heisenbergstr. 1, 70569, Stuttgart, Germany,
[2]Department of Chemistry, University College London, London WC1H 0AJ, United Kingdom

IM-05 (1), Lecture Theater 3, august 26, 2024, 10:30 - 12:30

Background

Strong multiple interactions between degrees of freedom (spin, orbital, charge, and lattice) in complex oxides give rise to rich electronic phase diagrams and thus to intriguing macroscopic functionalities, such as ferromagnetism, superconductivity, and multiferroicity [1, 2]. A famous example is LaCoO3 (LCO), in which unexpected ferromagnetism occurs in tensile-strained epitaxial LCO thin films, in contrast to paramagnetism in bulk LCO [3]. However, the underlying mechanism of emergent ferromagnetism and spin-state transitions remains controversial, with the tensile strain-induced ferroelastic deformation and oxygen vacancy ordering are known as two possible driving forces. Previous density functional theory (DFT) calculations on the ferromagnetism of tensile-strained LCO have shown that the tensile strain-induced changes in lattice constants are insufficient to stabilize the long-range ferromagnetic order [4]. Suppression of CoO6 octahedral rotations should be considered to modify the eg orbital order configuration and induce a spin-state transition to a ferromagnetic state. To date, no direct experimental evidence has been reported to support this theoretical prediction.

Methods

In this work, we systematically investigate the atomic and electronic structures, and their correlation with the spin-state transition and the ferromagnetic insulating state of high-quality LCO epitaxial films grown by pulsed laser deposition.

Results

Scanning transmission electron microscopy (STEM) and electron energy-loss spectroscopy (EELS) were used to examine the 6 uc and 25 uc thick LCO films for comparison. High-angle annular dark-field STEM results support the appearance of dark stripes only in the 25-uc thick LCO film, showing well-ordered dark stripes with a period of ~ 3 uc in the interior part of the film (Fig. 1). EELS maps of the interface region show a sharp interface between LCO and STO without the formation of any misfit dislocations. Energy-loss near-edge structure analysis was performed to investigate the electronic structures of the LCO films at the atomic scale. In the dark stripes, the pre-peak of the O-K edge almost disappears, and the intensity of the O-K edge peaks is significantly reduced. Meanwhile, the peak positions of the Co-L2,3 edges shift to lower energies, and the Co-L3/L2 ratio is larger in the dark stripes than in the bright regions. These features fingerprint a reduction of the Co valence state in dark stripes due to the formation of oxygen vacancies. Quantitative analysis of annular bright-field STEM results reveals previously unreported long-range suppression of CoO6 octahedral rotations throughout 25-uc thick LCO epitaxial films, inducing an increase in the angle βCo-O-Co from bulk 163.5o to 172.5o. DFT calculations further unravel the underlying physical mechanism of the spin-state transition to induce an emergent and robust ferromagnetic insulating state.

Conclusion

This work provides new insights into how the interplay between degrees of freedom drives the ferromagnetic insulating state in tensile-strained ferroelastic LCO epitaxial films [5].

Fig. 1 STEM images of the LCO films with thicknesses of 6 uc and 25 uc, respectively.

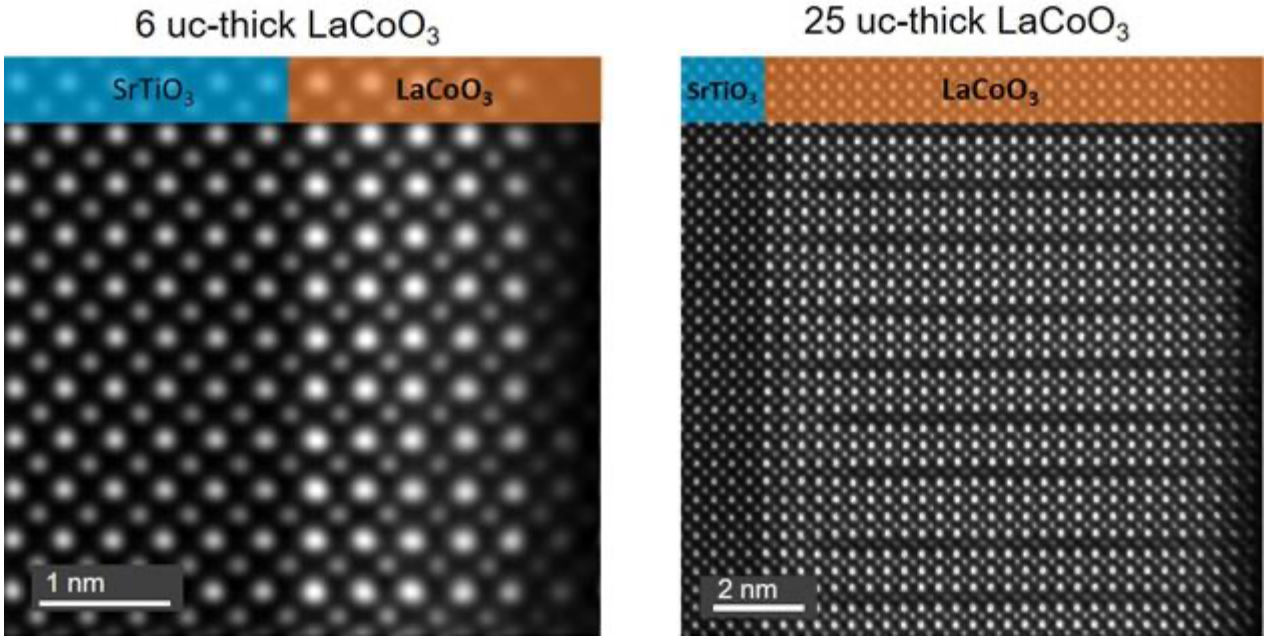

Keywords:

EELS, STEM, LaCoO3, octahedral rotation

Reference:

1. R. Zhao et al. Nat. Commun. 13 (2022), 2364.
2. H. Wang et al. ACS Nano 14 (2020), 12697-12707.
3. N. Biskup et al. Phys. Rev. Lett. 112 (2014), 087202.
4. J.M. Rondinelli & N.A. Spaldin, Phys. Rev. B 79 (2009), 054409.
5. D. Li, H. Wang et al. Nat. Commun. 14 (2023), 3638.

415

Seeking peak precision in atomic EELS mapping with counting mode direct electron detection

Dr Duncan Alexander[1], Dr Chih-Ying Hsu[1,2], Dr Pau Torruella[1], Sebastian Cozma[1], Lucia Varbaro[2], Prof. Jean-Marc Triscone[2], Prof. Cécile Hébert[1]
[1]Electron Spectrometry and Microscopy Laboratory (LSME), Institute of Physics (IPHYS), École Polytechnique Fédérale de Lausanne (EPFL), Lausanne, Switzerland, [2]Department of Quantum Matter Physics (DQMP), University of Geneva, Geneva, Switzerland

IM-05 (1), Lecture Theater 3, august 26, 2024, 10:30 - 12:30

Since the advent of aberration-corrected scanning transmission electron microscopy (STEM) with electron energy-loss spectroscopy (EELS) spectrum imaging capabilities, atomic resolution STEM-EELS has become a vital technique for probing both elemental compositions and bonding states across epitaxial thin films.[1] Nevertheless, data quality are often limited in terms of spatial and spectral precision. In large part, these limitations have derived from the charge-coupled devices (CCD) that, until recently, have been the primary sensors used for EELS, which are associated with a host of deficits: poor detective quantum efficiency (DQE) and point spread function (PSF); slow read out time and poor duty cycle; and correlated channel noise. Typical consequences for atomic resolution mapping include: spatial distortions from scan drift; strong trade-offs regarding the measurement of sharp spectral features versus large spectral range for measuring many elements; high beam currents and/or long dwell times for obtaining sufficient signal-to-noise; and a noise structure ill-suited to denoising using machine learning algorithms. In comparison, direct electron detection promises to address all of these deficiencies, at the same time. Here, we explore the benefits brought by direct electron detection using a large array monolithic active pixel sensor having ~3.4 k energy channels, coupled to a state-of-the-art EEL spectrometer, with the goal of seeking maximum precision for both spectral peaks (EELS fine structures) and spatial peaks (atomic columns).
As test objects, we take superlattices of perovskite rare-earth nickelates, which constitute both pure and alloyed layers.[2] Not only is it paramount to characterize their chemical nature for correctly interpreting their physical properties, these samples also provide interesting challenges for testing atomic-resolution STEM-EELS, such as the overlap of the rare-earth M edges with each other and with the Ni L edge. The STEM-EELS measurements are made using a Gatan Continuum ERS spectrometer equipped with a K3 detector operated in counting mode, installed on a double-aberration corrected and monochromated FEI Titan Themis 60-300, run at 200 (or 300) kV. Different acquisition strategies are tested: single-EELS, dual-EELS, single frame, multi-frame with on-line drift correction, multi-frame with off-line rigid and non-rigid registration.
The figure shows example results from a superlattice of layers with target compositions of alloy $(0.7Nd,0.3La)NiO_3$ and pure $SmNiO_3$, grown on $LaAlO_3$. The spectrum image was acquired using the detector's maximum speed of 0.34 ms per pixel, with 0.25 Å pixel size, a beam current of 100 pA, 20 and 47 mrad convergence and collection semi-angles, for a total of 5 integrated frames, with frame-by-frame drift correction. The right-hand side of the figure shows background-subtracted raw spectra integrated from regions of $SmNiO_3$ (top), $(Nd,La)NiO_3$ (middle) and $LaAlO_3$ (bottom). Despite the broad spectral range covering all major elemental edges of O K (532 eV), Al K (1560 eV), Ni L (855 eV), La M (832 eV), Nd M (978 eV) and Sm M (1080 eV) from the 0.45 eV/channel dispersion, because of the good PSF, the L and M edge white lines are remarkably sharp. This can be seen in the right-hand insets showing zooms of the La M–Ni L overlap region, where the shapes of both edges can be seen in the $(Nd,La)NiO_3$ alloy. The left-hand insets show the O K-edge onset. Both nickelate layers show a prepeak at ~528 eV, that derives from hybridization of the O 2p with the Ni 3d, rare earth 5d, and Ni 4sp electronic states. The narrow prepeak is distinctly visible. Further, it acts a sensitive marker of electron flux-induced damage.[3] Its undiminished magnitude in the data show that, because of the

detector speed, sensitivity and 100% duty cycle, we were able to stay below the flux damage threshold even with the small 0.25 Å pixel size; an order of magnitude improvement compared to the previous results taken with a CCD-based spectrometer. After denoising the spectrum image using principal component analysis (PCA), a standards-based approach was used to generate the displayed elemental maps, where the O K edge is fitted as either nickelate (O_nick) or $LaAlO_3$ (O_LAO). A clear atomic resolution is attained in all maps; even for Al whose K edge shows very small signal intensity. Fourier transform analysis indicates that the summed denoised spectrum image signal attains a spatial resolution of 1.2 Å. In the single-element Sm map of an $SmNiO_3$ layer, displayed at the bottom right, a resolution of 1.7 Å is achieved. More impressively, the spatial precision is such that this map clearly shows the characteristic ± 20 pm up-down antipolar displacements of the Sm cations in this orthorhombic phase.

In conclusion, a latest-generation counting mode detector shows a step-change improvement for atomic resolution mapping of perovskite oxide heterostructures. While ideal acquisition strategies are still being refined, current results already demonstrate the potential for high precision mapping, both spectrally and spatially. Although PCA-denoised maps are superficially correct, we note that this processing systematically generates spectral artefacts, as shown in the pixel-by-pixel sequence of 3 reconstructed spectra across a Sm column in the bottom right of the figure. Potentially this can be understood as the decomposition identifying the spectral structure of a phase, which however does not properly represent the sharp spatial modulations of the chemically-different atomic columns. Work is in progress to identify other denoising approaches that leverage the Poisson noise structure of the counting mode EELS data while generating a physically-correct output.

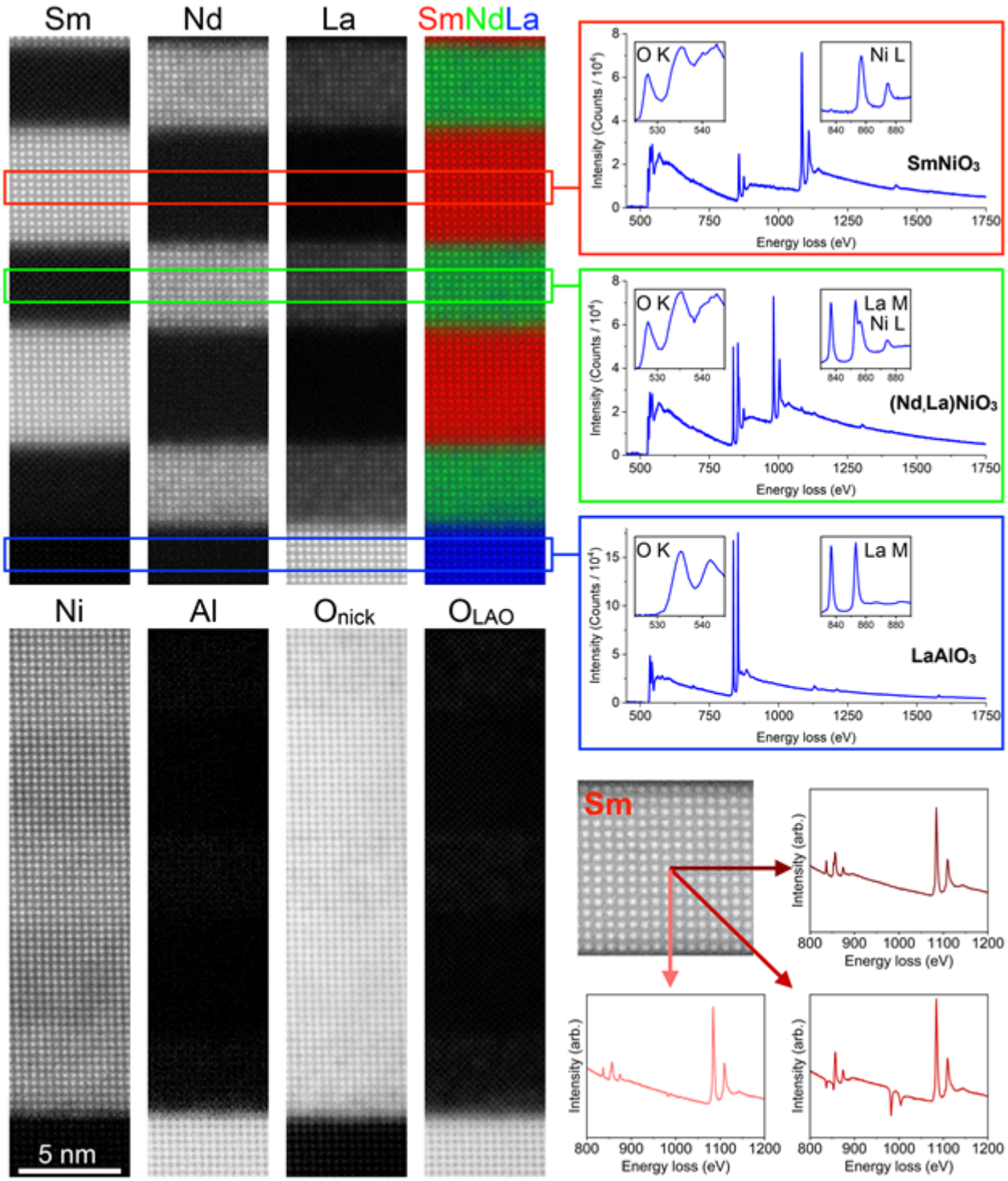

Keywords:

direct electron detection; EELS; atomic-mapping

Reference:

[1] D.A. Muller et al., Science 319 (2008) 1073–1076
[2] L. Varbaro et al., Adv. Electron. Mater. 9 (2023) 2201291
[3] B. Mundet et al., Nano Lett. 21 (2021) 2436–2443

463

Analytical electron tomography, fine structure EELS and nanoscale X-ray CT of nanoporous Copper materials

Tatiana Kormilina[1], Georg Haberfehlner[2], Samuel Graf[3], Eva-Maria Steyskal[3], Erdmann Spiecker[4], Gerald Kothleitner[1,2]
[1]Graz Centre for Electron Microscopy, Graz, Austria, [2]Institute of Electron Microscopy and Nanoanalysis, Graz University of Technology, Graz, Austria, [3]Institute of Materials Physics, Graz University of Technology, Graz, Austria, [4]Institute of Micro- and Nanostructure Research and Center for Nanoanalysis and Electron Microscopy, Friedrich-Alexander University, Erlangen, Germany

IM-05 (1), Lecture Theater 3, august 26, 2024, 10:30 - 12:30

Background incl. aims
For systems with a complex morphology, 2D information can be insufficient, which requires tomographic approaches. Together, electron tomography and nanoscale X-ray CT cover the range from 3D sub-nanometer resolution for small sample volumes, up to samples sized several tens of micrometers, and in the electron microscope this information can be coupled with analytical information from associated spectroscopy techniques.
Among advanced modern materials, nanoporous metals (usually represented by nanoporous gold or other noble metals) can form the backbone for various applications, such as catalysis or supercapacitors. Copper is a promising alternative to rare and expensive noble metals due to its cost, redundancy and scalability. Nanoporous Cu materials can be made by electrochemical dealloying[1] where the size of resulting pores is tailored to fit the intended application. Due to its less noble nature, Cu is more prone to oxidation, and oxide chemistry on the pore surfaces plays a significant role for intended applications. It is therefore imperative to know the morphology and inner surface chemistry of the nanoporous material as well as to be able to assess pore parameters, such as size distribution or local curvatures for scalable pore sizes ranging from 20 to 500 nm, which requires adapting available characterization methods.
Methods
Nanoporous Cu structures, dealloyed from either Cu-Mn or Cu-Al alloys with different dealloying conditions and optional subsequent coarsening, were investigated with following methods: high-angle annular dark field scanning transmission electron tomography (electron tomography), energy-dispersive x-ray spectroscopy (EDXS), electron energy loss spectroscopy (EELS), Zernike phase contrast laboratory nanoscale x-ray computed tomography (nano-CT). Samples for electron tomography were prepared as 100-300 nm thin pillars via focused ion beam milling (FIB). Samples for nano-CT (60 µm thick) were formed by laser ablation with a finishing touch of FIB.
Results
We use electron tomography to capture in detail the nanoporous Cu network morphology from HAADF data, while also reconstructing 3D elemental distributions from EDXS. Implementing multimodal joint reconstruction of all channels (EDXS and HAADF) with total generalized variation regularization (TGV)[2] algorithm we can capture the surface oxidation of Cu in 3D, as well as local residuals of Mn after dealloying. We use EELS fine structure to self-reference multiple linear least squares fitting (MLLS) segmentation to classify and map present Cu and Mn oxide species. We further implement Zernike phase contrast laboratory nano-CT for statistical pore parameter analysis of coarsened samples.
Conclusion
In nanoporous copper samples dealloyed from Cu-Mn alloy we were able to identify and map Cu and Mn oxide species. Based on Mn oxides present we suppose a different reaction path on the dealloying stage to the one suggested in literature.[1] We have reconstructed and segmented 3D distributions of present elements and overall nanoporous Cu morphology to quantify porosity as well

as pore size, distribution and connectivity. With statistically-rich nano-CT segmentation we show that at the testing stage coarsening procedure works differently on np-Cu dealloyed from Cu-Mn or Cu-Al alloys likely because of the complexity of phase diagram of Cu-Al. We report that pore coarsening on Cu-Al has good scalability but suffers from residual presence of unreacted mother alloy bubbles. [3]

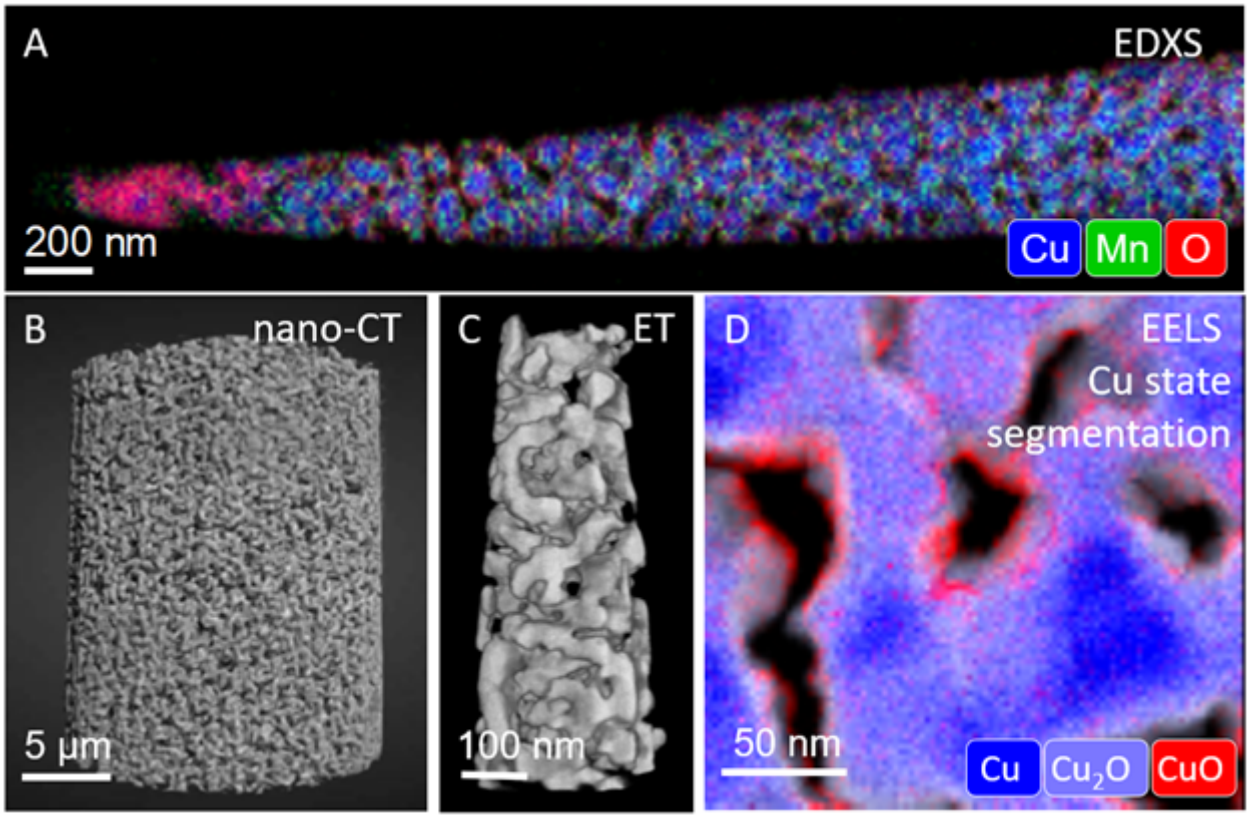

Keywords:

nanoporous metal, electron tomography, EELS

Reference:

[1] E. Hengge J. Ihrenberger, E. M. Steyskal, R. Buzolin, M. Luckabauer, C. Sommitsch, R. Würschum, Nanoscale Adv. 5, 393–404 (2023).
[2] R. Huber G. Haberfehlner, M. Holler, G. Kothleitner, K. Bredies, Nanoscale 11, 5617–5632 (2019).
[3] TK acknowledges ACR-BMK 2024 scholarship for financial support.

651

Multi Element ELNES Mapping of Compounds

Daen Jannis[1,2], Mr. Nicolas Gauquelin[1,2], Ms. Maria Meledina[3], Mr. Yuchen Zhao[4], Mr. Yunzhong Chen[4], Mr. Jo Verbeeck[1,2]
[1]EMAT, Universiteit Antwerpen, Antwerpen, Belgium, [2]NANOlab, Universiteit Antwerpen, Antwerpen, Belgium, [3]Thermo Fisher Scientific, Eindhoven, Netherlands, [4]Beijing National Laboratory of Condensed Matter Physics, Chinese Academy of Sciences, Beijing, China

IM-05 (1), Lecture Theater 3, august 26, 2024, 10:30 - 12:30

Scanning transmission electron microscopy in combination with electron energy loss spectroscopy is a powerful method which provides very local spectroscopic information[1]. The local spectroscopic data contains elemental and electronic information. However, the elemental quantification needs a rather large energy window to have simultaneous quantification on multiple elements. Whereas the electronic information needs high energy resolution which limits the size of the energy window due to the limited amount of pixels in an electron detector. This makes the simultaneous elemental quantification and fine structure analysis almost impossible when multiple elements are of interest. One possible solution would be to scan multiple STEM-EELS map and changing the drift tube or magnetic prism between each frame. The difficulty is that sample drift, damage and real time user interaction, such as refocusing, make this procedure very cumbersome. Another solution is doing DualEELS which applies two drift tube voltages at each probe position which solves the problems discussed above[2]. However only two snippets are available which is still insufficient for most materials where multiple edges occur.
A novel method was developed which overcomes these challenges by applying any number of offsets to the drift tube without adding dead time of the detector. Moreover, the defocus for the different drift tube voltages is corrected for to maintain a good energy resolution. This methodology provides easy correlation of elemental abundances with the fine structure for multiple edges in a sample.
In this work, the methodology is applied to multiple samples providing new insights into solving materials science questions. For example in Fig. 1, the core-loss edges of K-L, Ti-L, O-K, Eu-L and Ta-M together with the low loss are mapped quasi-simultaneously on the interface of EuTiO3 (ETO) and KTaO3 (KTO) which are interesting in the research on 2D electron gas systems[3]. At the top of ETO (purple box), a different oxidation state is observed from the fine structure of Ti, O and Eu simultaneously when comparing it to the fine structure of the ETO layer (red box). With this example we show the power of the new approach for quality, speed and ease of use in ELNES applications.

Figure 1. A series of 2d spectrum image maps converted into a 1d line maps across an interface between ETO (top) and KTO (bottom) where the low loss and different fine structures are shown for different positions with respect to the interface. The information from the different ELNES profiles can be directly correlated since they are acquired quasi-instantaneous.

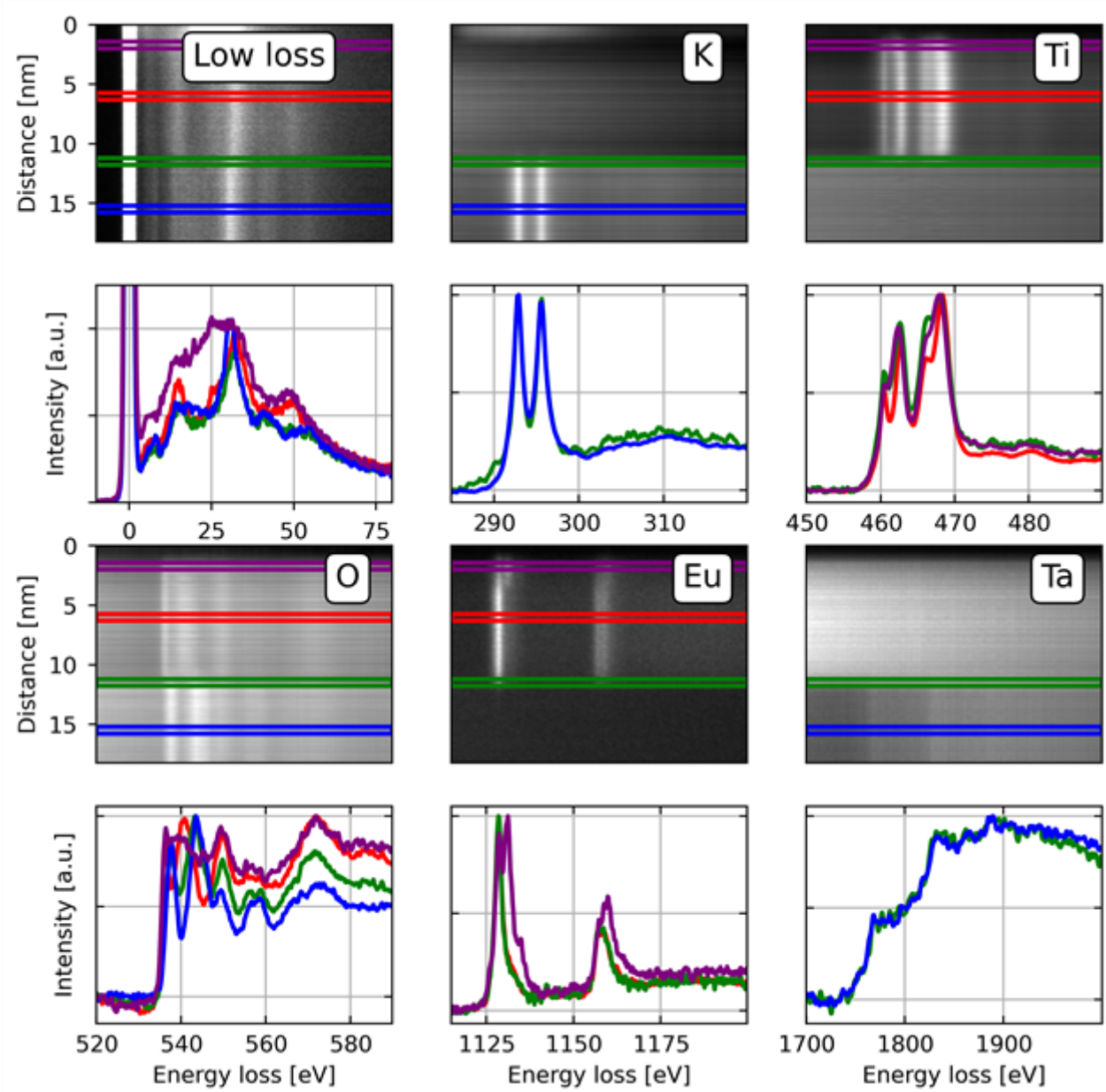

Keywords:

EELS, Elemental quantification, Fine structure

Reference:

[1]Botton G., Phys.Rev. B, 54 (3) 1682-1691
[2] Scott J. et al, Ultramicroscopy 108 (2008) 1586-1595
[3] Xu et al. Advanced Materials (2024), 2313297.
[4] This project has received funding from the European Union's Horizon Research and Innovation Program under grant agreement NO 823717 ESTEEM3.

1000

PolSpec – broadband cost-effective hyperspectral imaging

Huihui Liu[1], Sunil Kumar[1,2], Edwin A Garcia Castano[1], Paul French[1,2]
[1]Physics Department, Imperial College London, SW7 2AZ, , UK, [2]Francis Crick Institute, 1 Midland Road, NW1 1AT, , UK

IM-05 (1), Lecture Theater 3, august 26, 2024, 10:30 - 12:30

Background incl. aims
Spectrally-resolved imaging is implemented in almost every optical imaging modality – from endoscopy through microscopy, tomography, and remote sensing. It is typically used to provide spectroscopic contrast, e.g., between different species or states of molecules or different “colour” labels, e.g., for pathology, spatial proteomics, etc., as well as diverse applications outside biomedicine. Increasingly, it is used with machine learning, e.g., to increase performance or automated identification/classification tasks. Spectrally resolved imaging can be classified as multispectral imaging, where detected photons are assigned to a relatively small number of discrete spectral bins, or hyperspectral imaging where photons are allocated to part of a continuous a wavelength range. Spectrally resolved imaging techniques based on filters that reject “out-of-band” photons are inefficient and techniques that acquire the full (x-y-λ) hyperspectral image data cube, e.g., using spectrographs, tend to be slow since at least one dimension requires sequentially acquisition. Where photons are “sorted” into multiple spectral bins for wide—field imaging, e.g., using (cascades of) dichroic beam splitters, multispectral imaging can be fast and efficient at the cost of complexity and limited flexibility. Here we present a new low-cost approach to flexible wide-field hyperspectral imaging using polarization optics instead of dielectric coatings or dispersive devices, including a demonstration of single-shot full-field hyperspectral imaging.
Methods
Our approach we describe as “PolSpec” is to use a Lyot filter to provide continuously varying loss modulation across the desired spectral range to generate orthogonal “spectral modulation vectors” (SMV) that can represent specific spectral components, as indicated in figure 1(a). If the modulation functions are contrived to be sinusoidal and cosinusoidal, then these SMV correspond to spectral phasors, but other orthogonal (or near orthogonal) modulation functions can be used. Direct acquisition of spectral phasor images (as opposed to lossy calculation of spectral phasors from hyperspectral image data) has recently been demonstrated [1,2] utilising specific (fixed) sinusoidal spectral filters with sequential image acquisition [1] or using a cascade of image splitters for single-shot acquisition [2]. We have implemented single-shot full-field hyperspectral imaging using SMV with $\cos(\theta)/\sin^2(\theta)$ spectral modulation with the configuration depicted in figure 1(b) for a system component cost of <€2500 using low-cost polymer films to provide the required polarisation and retardance components. The spectral range and discrimination of this approach can be easily tuned using different retarders (typically half-wave plates) or can be made electronically tuneable using a liquid crystal retarder (LCR). Single-shot operation can be achieved using a polarisation-resolving camera (“Polarsens™”) [3].
Results
Figure 1(c) shows a demonstration of single-shot full-field hyperspectral imaging using the system depicted in figure 1 to image a colour test chart displayed on a computer screen. The SMV plot clearly separates the different spectral components and by filtering in the SMV plane, we can generate colour images in object space.
Conclusion
We have demonstrated a flexible approach to full-field “hyperspectral” imaging using SMV and implemented a singe-shot version with low-cost polarisation optics components and a Polarsens™ camera. Most implementations of PolSpec begin with a polariser that will present up to 50% loss,

e.g., when imaging fluorescence. In addition, the Polarsens™ camera also presents a 50% loss. For fluorescence imaging, it is desirable to use a cooled camera with which PolSpec can be implemented using a polarisation image splitter. If the retardance required for the SMV is provided using an LCR, the full SMV data set can be acquired in two (rapid) sequential photon efficient polarisation-resolved camera acquisitions. Many other PolSpec configurations are possible, including ~lossless polarisation-resolved hyperspectral imaging with some increased system complexity.

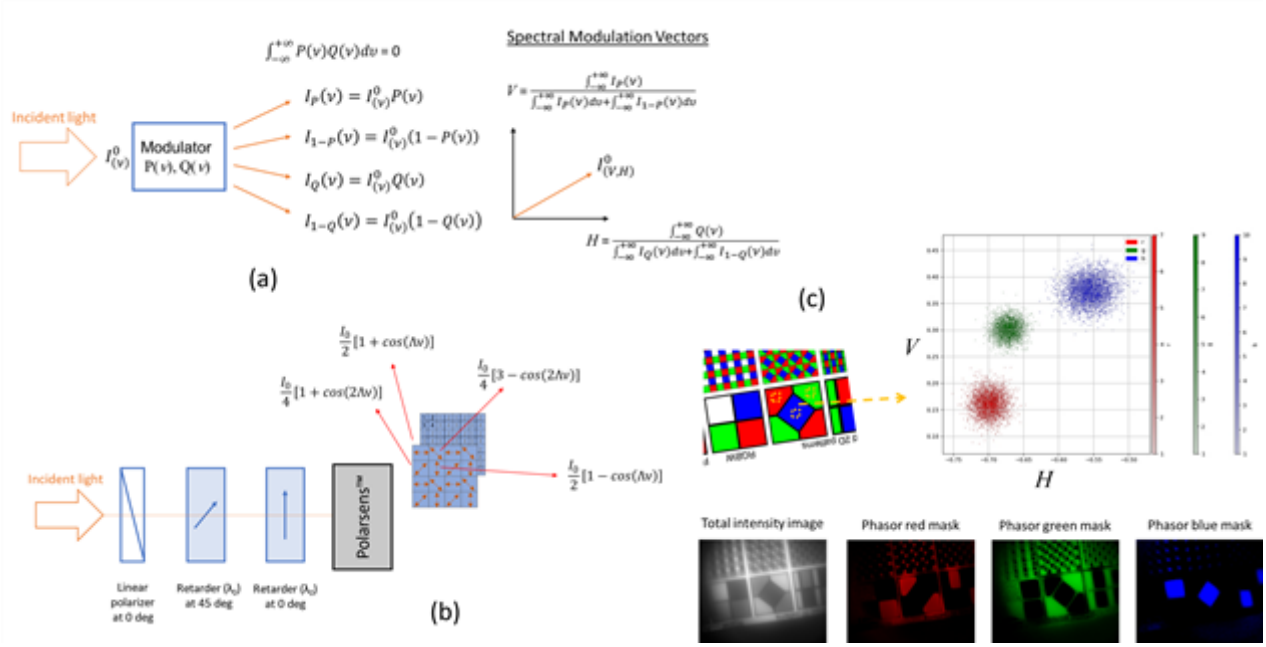

Keywords:

Spectrally resolved imaging, hyperspectral, polarization

Reference:

[1] A. Dvornikov and E. Gratton, Biomed. Opt. Express 9 (2018) 3503; https://doi.org/10.1364/BOE.9.003503
[2] Wang et al, Cell Reports Methods 3 (2023) 100441; https://doi.org/10.1016/j.crmeth.2023.100441
[3] https://www.sony-semicon.com/en/technology/industry/polarsens.html

119

Unveiling Metal-Insulator Transitions in (V1-xCrx)2O3 through in situ Monochromatized STEM/EELS

Dr. Abdelali Khelfa[1], Mr. Jean-Denis Blazit[1], Mr. Luiw H. G. Tizei[1], Mr. Etienne Janod[2], Mr. Julien Tranchant[2], Mr. Benoît Corraze[2], Mr. Laurent Cario[2], Mrs. Odile Stephan[1], Mrs. Laura Bocher[1]
[1]Laboratoire de Physique des Solides - Université Paris Saclay - CNRS, Orsay (91405), France, [2]Institut des Matériaux Jean Rouxel - Université de Nantes - CNRS, Nantes (44322), France

IM-05 (2), Lecture Theater 3, august 26, 2024, 14:00 - 16:00

Background incl. aims
The exploration of insulator-to-metal transitions (IMTs) in Mott insulators and strongly correlated systems has revealed intriguing phenomena induced by various stimuli such as temperature, pressure, doping, or electric fields [1,2]. Despite significant advancements, the mechanisms governing electronic phase separation at the nanoscale remain elusive. Addressing this knowledge gap requires a comprehensive approach, considering structural and electronic degrees of freedom. In this context, our study aims to investigate the temperature-driven IMT in (V0.988Cr0.012)2O3 (see Figure a), employing advanced techniques capable of probing multiple features simultaneously. The Cr-doping enables us to explore transitions from the paramagnetic insulator (PI) phase to the paramagnetic metallic (PM) phase around 200 K and also from the PM phase to the antiferromagnetic insulator (AFI) phase below 180 K. Interestingly, the PI/PM transition is isostructural of the hexagonal structure (space group R-3c) while the PM/AFI transition is associated with a crystallographic symmetry breaking into a monoclinic structure (space group I2/a). There is, therefore, a strong interest in investigating both spectroscopically and structurally this material using the same in situ tool.
Methods
To achieve our objectives, we employ in situ monochromatized EELS [2] and 4DSTEM micro/nano-diffraction [3] techniques. These experiments are conducted using a state-of-the-art NION Ultra-HERMES 200 microscope, equipped with a Medipix direct detector and a HennyZ double tilt cryo-holder. This cutting-edge instrumentation allows us to unravel intricate details associated with the IMT process.
Results
Specifically, we focus on identifying variations in low-loss spectra, highlighting fingerprints of the PI, PM, and AFI phases (Figure b). By comparing structural information acquired by 4DSTEM with such spectroscopic signatures, we probe a phase coexistence at low temperatures, as depicted in Figure c [4].
Conclusion
Overall, our results highlight the instrumental capabilities of high-energy resolution EELS as a valuable tool for unraveling the intricate dynamics of IMTs, offering new perspectives on the underlying physics of these fascinating phenomena.

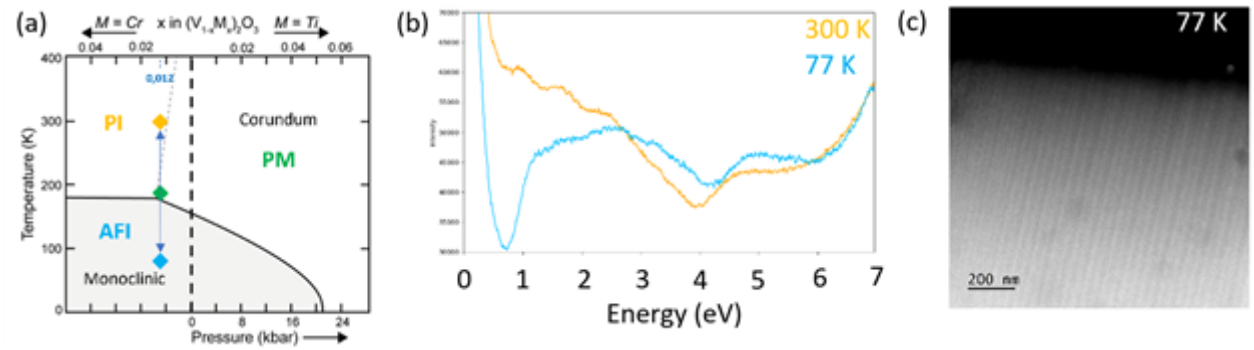

Keywords:

Mott-Insulators, IMT, In-Situ, EELS, 4DSTEM

Reference:

[1] E. Janod et al., Adv. Funct. Mater., 25 (2015), p. 6287-6305.
[2] H. A. H. Abe et al., Jpn. J. Appl. Phys., 37 (1998), p. 584.
[3] I. Koita et al., Microscopy and Microanalysis 29 (2023), p. 1691-1692.
[4] J. Zhang et al., Phys. Rev. X, 9 (2019), 011032.

136

An accessible Secondary Electron Hyperspectral Imaging approach to draw meaningful insights from scanning electron microscopy

James Nohl[1,2], Jingqiong Zhang[1], Lyudmila Mihaylova[1], Serena Cussen[3], Cornelia Rodenburg[1]
[1]Department of Materials Science and Engineering, The University of Sheffield, Mappin Street, Sheffield, UK, [2]The Faraday Institution, Quad One, Becquerel Avenue, Harwell Campus, Didcot, UK, [3]School of Chemistry, University College Dublin, Belfield, Dublin 4, Ireland

IM-05 (2), Lecture Theater 3, august 26, 2024, 14:00 - 16:00

Background
Hyperspectral imaging in the scanning electron microscope (SEM) commonly uses the energy dispersive X-ray (EDS/EDX) signal. The colour maps produced have become a staple part of analysis for visualising elemental heterogeneity and quantifying bulk elemental composition of hard materials. Now, automated collection and analysis routines have extended to secondary electron hyperspectral imaging (SEHI) and the ability to produce colour maps of surface chemical heterogeneity down to the nanoscale [1].
SEHI, combined with an accessible and automated data analysis tool, has yielded maps of surface chemical bonding, such as the surface functionalisation of soft materials, compounds of light elements, and crystallinity by cross-linking. As well as offering complimentary information to elemental composition, the emission characteristics of SEs offer improved surface sensitivity and spatial localisation versus X-ray imaging in SEM, particularly for softer materials.

Methods
In this implementation, SEHI data volumes are built by sequentially imaging with the through-lens-detector (TLD) with a mirror electrode which steps through a series applied voltage biases to act as a variable low-pass energy filter. Automated data collection routines control the cutoff energy of the low pass filter to acquire images quickly. Imaging is done at 1 kV accelerating voltage and < 50pA beam current to produce suitable signal to noise and SE yield close to 1, as well as to reduce SE2 background emissions, and to limit the beam dose received by the material.
The data volume is differentiated with respect to energy to plot local SE spectra and slices of energy ranges (Figure 1a) are summed to create maps which relate a colour to a chemical feature in the SE spectrum (Figure 1b-d).
The energy ranges for each colour channel can be identified without prior knowledge by a blind-source separation using a non-negative matrix factorisation (NNMF) method. The program for creating colour-SEHI images has been packaged and redistributed as a portable MATLAB application.

Results
The first demonstration of the colouring method is on a lithium metal anode used in lithium metal, lithium-sulphur and lithium-air batteries. The surface ‘platelets’ are heterogenous features in red which measure 250 nm across. Whereas lithium oxide morphologies were imaged over a 25 µm horizontal field width by windowless EDS. Ranking of surface chemical species by comparison to theoretical models was used to identify contributions from lithium hydroxide, nitride and carbon containing species and found the red regions to have a higher proportion of lithium nitrides and hydroxides while the blue range included more lithium-carbon compounds.
Applying the analysis to a spider dragline silk fibre reveals domains of nanoscale ordering due to cross-linking, which measure 45 nm across (coloured green, Figure1c). A higher proportion of cross-linking is indicated by more intense SE emissions at 1.1 eV denoting di-sulphide bridging.
At a length scale of 25 µm horizontal field width, the approach is applied to a perovskite solar cell material, which is a mix of organic methylammonium and inorganic lead iodide (ie. hard and soft)

material. The automated approach to colouring identifies a two-phase material, to identify regions of lead iodide (PbI2) within an organic-inorganic perovskite.

Conclusions

This advance in SEHI analysis is an important extension of LV-SEM capability to map and identify regions of surface chemical bonding. This is achieved through an accessible data collection and analysis routine that applies hyperspectral imaging to the SE signal.

Characterisation of surface chemical bonding heterogeneity on bulk functional materials becomes accessible down to nanoscale even for soft matter, as demonstrated by mapping 45 nm wide cross-linked regions in spider silk where di-sulphide bridges are more prevalent. Light element compound distribution is identified on a lithium metal anode material as well as phase separation in an organic-inorganic perovskite solar cell material.

Having demonstrated the technique can be applied to characterise both organic and inorganic material, future studies will include the lithium metal anode post electrochemical cycling and growth of the solid-electrolyte interphase layer.

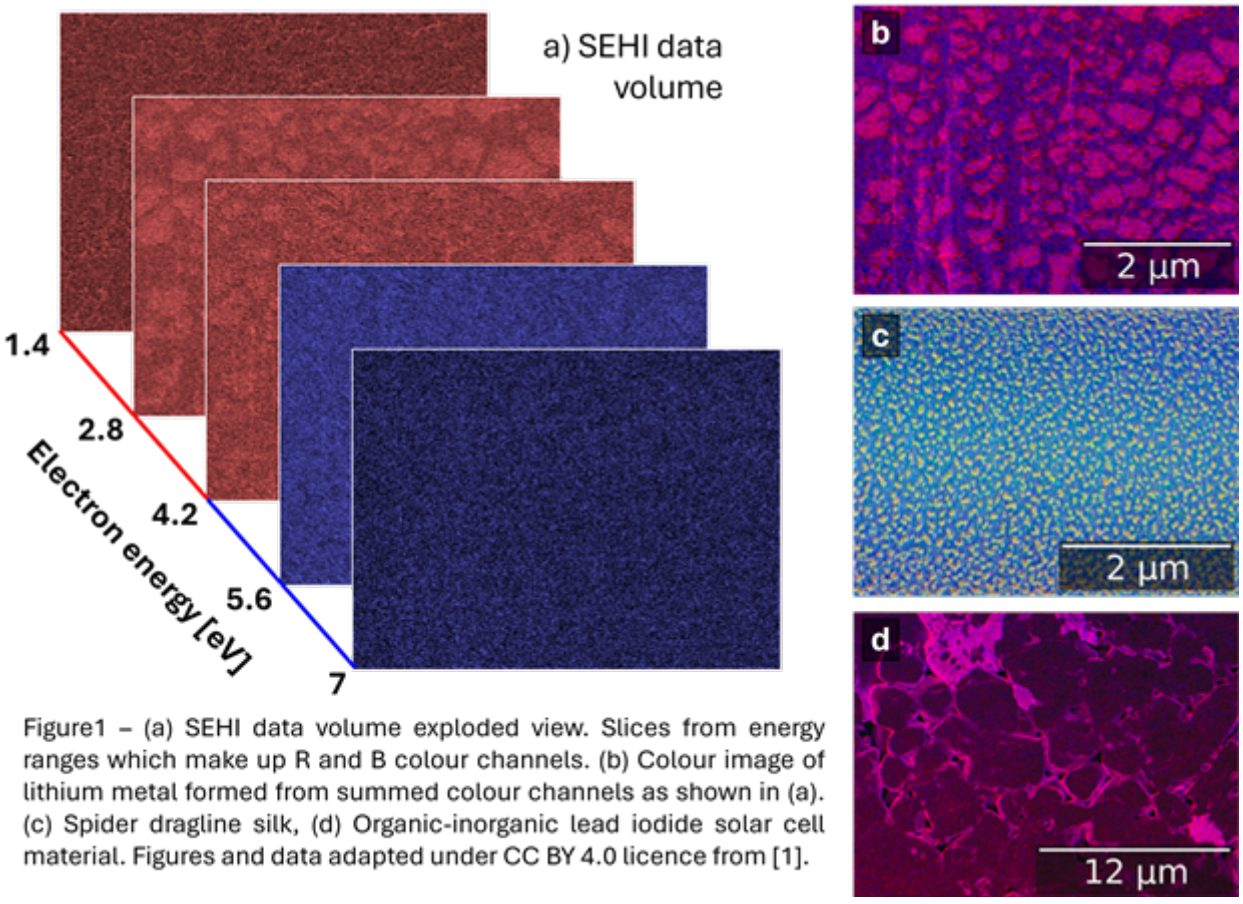

Figure1 – (a) SEHI data volume exploded view. Slices from energy ranges which make up R and B colour channels. (b) Colour image of lithium metal formed from summed colour channels as shown in (a). (c) Spider dragline silk, (d) Organic-inorganic lead iodide solar cell material. Figures and data adapted under CC BY 4.0 licence from [1].

Keywords:

SEHI, SEM, surface chemistry, nanoscale

Reference:

[1] J.F. Nohl, N.T.H. Farr, Y. Sun, G.M. Hughes, N. Stehling, J. Zhang, F. Longman, G. Ives, Z. Pokorná, F. Mika, V. Kumar, L. Mihaylova, C. Holland, S.A. Cussen, C. Rodenburg, Materials Today Advances, 19, 2023, 100413, DOI:10.1016/j.mtadv.2023.100413.

272

Measuring hybridisation in Van der Waals heterostructures using momentum-resolved EELS

Hannah Nerl[1], Dr Ana Valencia[2], Mr Khairi Elyas[3], Juan Pablo Guerrero Felipe[1], Dr Katja Höflich[3], Prof Caterina Cocchi[1,2], Prof Christoph Koch[1]
[1]Department of Physics and IRIS Adlershof, Humboldt Universität zu Berlin, Berlin, Germany, [2]Institute of Physics and Center for Nanoscale Dynamics (CeNaD), Carl-von-Ossietzy Universität Oldenburg, Oldenburg, Germany, [3]Ferdinand-Braun-Institut gGmbH, Leibniz-Institut für Höchstfrequenztechnik, Berlin, Germany

IM-05 (2), Lecture Theater 3, august 26, 2024, 14:00 - 16:00

Background
Van der Waals heterostructures have become omnipresent in materials research today as they offer sheer endless opportunities to tune properties by stacking [1]. In a Lego-like fashion, researchers combine a range of two-dimensional (2D) materials to create ever-more complex structures. However, regarding the properties of stacked 2D materials, the question arises: do we make something new or do we have a simple sum of its parts? We are still often lacking a means to study these complex stacked materials. One particular challenge that is frequently faced is that the phenomena under investigation might lie in an energy-momentum space that is impossible to access using optical methods.

Methods
Here, we show that using modern electron microscopy (EM), the energy-momentum space that becomes available can cover several Brillouin zones (BZ) in the momentum direction and several electron-volts in the energy direction. EM therefore represents an excellent opportunity to study stacked heterostructures. We combine the resolving power of the Nion HERMES instrument with the detection capabilities of a direct detector camera (Dectris ELA) to map phenomena across the BZ. Using this approach, the behaviour of phonons, excitons and plasmons can be mapped across the entire BZ. Results were compared to time-dependent density functional theory (TD DFT). To demonstrate this technique, we present the findings from a heterostructure commonly used in nanoscience research today. Hexagonal boron nitride (hBN) is the most common encapsulant for nanoelectronics and nanodevice fabrication as it is thought to not affect the properties of the TMDCs, due to its insulating character. It is known to even enhance the excitonic intensities and to decrease the excitonic bandwidth of TMDCs [2].

Results and Conclusions
Momentum-resolved EELS (q-EELS) was employed to obtain ωq maps of hBN, WSe2 and a hBN – WSe2 heterostructure along the high symmetry directions ΓM and ΓK of the crystal structure and the results are presented here.[3] Figure 1, a shows q-EELS as acquired of the hBN – WSe2 heterostructure. The spectra are shown for steps in q= 0.0106 x |Γ-K-M'-Γ'| to cover the |q| distance from 1.6 to 2.2 of |Γ-K-M'-Γ|. This partially shows the detection challenge at hand. There is a significant difference in intensities at q=0 at Γ and Γ' of excitonic and plasmonic peaks compared to the finite q intensities between the Γ points. Figure 1, b shows the peak evolution between the Γ points. This time the spectra of the same data set are shown for steps in q= 0.0106 x |Γ-K-M'-Γ| for |q| from 0.01 to 0.85 of |Γ-K-M'-Γ|. Both, excitons and plasmons and their hybridisation were studied using this approach. When comparing the energy-momentum dispersion of the main plasmon peaks, clear signs of hybridisation in the hBN – WSe2 heterostructure were observed when compared to the individual components of the heterostructure. The π- π* and the π- σ plasmon peaks were found to shift to energies that matched neither WSe2 nor hBN. Aside from the plasmon

peaks, hybridisation in excitons was also investigated. hBN represents a particular challenge due to the presence of excitons that have a highly directional q dependence and lie at high q and high in energy. The presence of the fine structure at the M point as shown in Figure,b is originating from the hBN itself and is also found in hBN alone. The peak at the M point is thought to originate from vertical e-h transitions between the k points belonging to the ML line in the band structure.[4] This fine structure is absent in the ΓM direction. These findings are in excellent agreement with BSE calculations [4] as well as non-resonant inelastic x-ray scattering data from a synchrotron facility [5]. It shows that EM combined with modern direct detector technology can at least rival the results from x-ray facilities with the added benefit that the EM brings improved spatial resolution. Our results regarding the plasmon hybridisation also show that great care has to be taken when predicting properties of Van der Waals heterostructures.

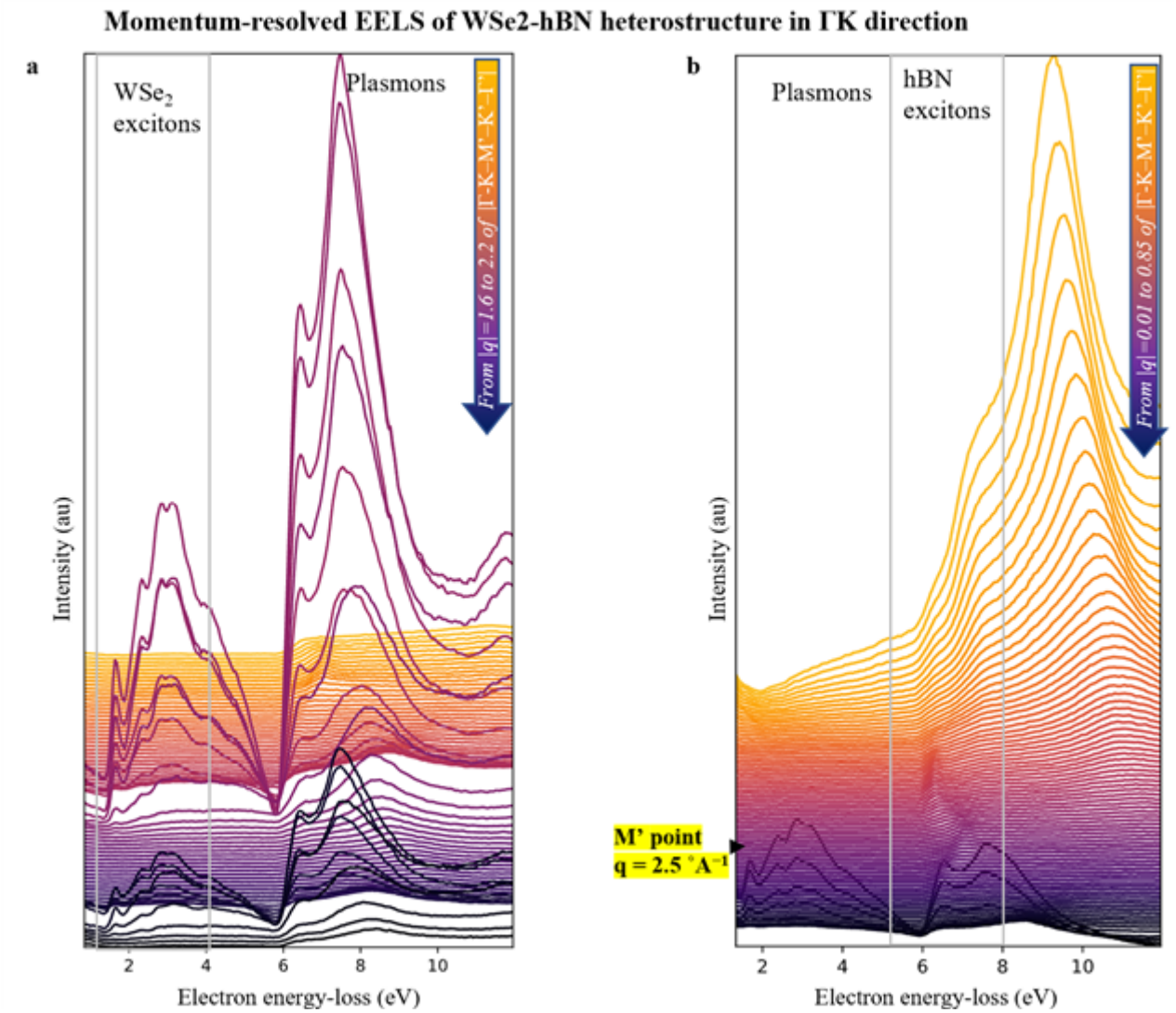

Keywords:

momentum-resolved-EELS, excitons, plasmons, TMDC, hBN

Reference:

[1] Geim, A. K. & Grigorieva, I. V. Van der waals heterostructures. Nature 499, 419–425 (2013).
[2] Wierzbowski, J. et al. Direct exciton emission from atomically thin transition metal dichalcogenide heterostructures near the lifetime limit. Sci Rep 7, 12383 (2017).
[3] to be submitted.
[4] Fugallo, G. et al. Exciton energy-momentum map of hexagonal boron nitride. Phys. Rev. B 92, 165122 (2015).

[5] Galambosi, S. et al. Anisotropic excitonic effects in the energy loss function of hexagonal boron nitride. Phys. Rev. B 83, 081413 (2011).

303

Phonon dispersion surfaces from the electron microscope compared with calculations including dynamical diffraction

Dr. Benedikt Haas[1], Steven Quillin[2], Tracy Lovejoy[2], Niklas Dellby[2], Ondrej Krivanek[2,3], Adnan Hammud[4], Tim Schröder[1], Christoph Koch[1], Peter Rez[2]
[1]Department of Physics & Center for the Science of Materials Berlin, Humboldt-Universität zu Berlin, Berlin, Germany, [2]Bruker AXS (formerly Nion Co. R&D), Kirkland, USA, [3]Department of Physics, Arizona State University, Tempe, USA, [4]Department of Inorganic Chemistry, Fritz-Haber Institute of the Max-Planck Society, Berlin, Germany

IM-05 (2), Lecture Theater 3, august 26, 2024, 14:00 - 16:00

Background
Thermodynamic properties such as heat capacity or thermal conductivity depend critically on phonon dispersion. Determining these properties from nanometer sized regions would enable significant advances in nanoscience. Measuring phonon dispersions in the electron microscope with spatial resolution of a few nm was demonstrated in 2016 [1] and later optimized for parallel acquisition [2-3]. We have now extended this technique to sample two momentum directions, thus obtaining phonon dispersion surfaces in 3D momentum-energy space. To study the influence of Umklapp scattering (scattering into higher Brillouin zones) and dynamical diffraction on the measured dispersion, we compare experimental results to electron-phonon scattering simulations that include dynamical diffraction.

Methods
A FIB lamella from diamond in the [110] zone axis was cut from a single crystal and polished to about 80 nm thickness. We used a Nion HERMES microscope operated at 80 kV with a convergence semi-angle of 1.6 mrad and equipped with a Dectris ELA direct detector to acquire phonon dispersions in parallel acquisition mode utilizing a slot as the EELS entrance aperture to define a line in momentum space. The diffraction pattern was consecutively displaced over the slot aperture by 4.1 mrad per step with a slot width of 6.6 mrad to obtain individual slices of 3D energy-momentum space. The data from each position was post-processed by registration and integration of the 120 frames of 1 s acquisition time (26 min total acquisition time for the 13 positions). The zero-loss lines were straightened and other processing steps applied before stacking the slices in 3D to reconstruct the diffraction plane. The data was then visualized using tomviz [4].
To simulate electron scattering from the diamond sample including phonon scattering and dynamical diffraction, a Bloch wave-based method developed by Rez and Singh was used [5]. This method applies operators for dynamical diffraction, phonon scattering followed by further dynamical diffraction to evaluate the phonon scattered intensity. The experimentally determined sample thickness of 76 nm was used in the calculations.

Results
Fig. 1a shows the phonon dispersion from diamond spanning multiple Brillouin zones. While the diffraction intensities fade quickly with increasing scattering angle, the phonon branches first become more intense and then decrease only slowly. This clearly demonstrates that Umklapp scattering dominates the interaction between the fast beam electrons and phonons in the sample. Fig. 1b shows the experimental phonon dispersion surfaces and the results from the calculation are given in Fig. 1c. We will quantitatively compare the experimental and calculated results. We also investigate the influence of high-angle phonon scattering, which should be a multi-phonon process known as thermal diffuse scattering, by comparing experiment with calculations for large scattering angles.

Conclusion

We have demonstrated the experimental reconstruction of phonon dispersion surfaces in momentum-momentum-energy space using electron microscopy. The comparison of such rich data sets with Bloch wave-based electron-phonon scattering simulations that include dynamical diffraction makes it possible to understand the fundamental processes of electron-phonon interactions. This paves the way to obtain quantitative phonon densities of state at nanometric spatial resolution, which can be used to determine thermodynamic properties such as heat capacity or thermal conductivity.

FIGURE 1: a) Experimental diamond phonon dispersion covering multiple Brillouin Zones (BZ). b) Experimental phonon dispersion surface volume of diamond. c) Calculated phonon dispersion volume including dynamical diffraction.

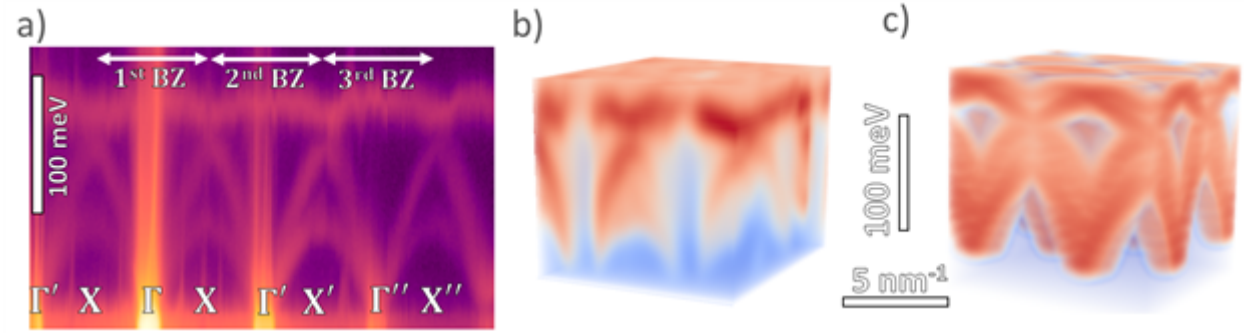

Keywords:

Monochromated EELS, phonons, DFT

Reference:

[1] F.S. Hage et al., Sci. Adv. 4 (2018), 1. doi: 10.1126/sciadv.aar749
[2] T.C. Lovejoy et al., Microsc. Microanal. 26 (2020), 964. doi: 10.1017/S1431927620016505
[3] Plotkin-Swing et al., Ultramicroscopy 217 (2020), 113067. doi: 10.1016/j.ultramic.2020.113067
[4] B. Levin et al., Microsc. Today 26 (2018), 12. doi: 10.1017/S1551929517001213
[5] P. Rez and A. Singh, Ultramicroscopy 220 (2021), 113162. doi: 10.1016/j.ultramic.2020.113162

397

Assessing the Precision of Local Temperature Measurement by Plasmon Energy in In-Situ Heating Electron Microscopy

Yi-Chieh Yang[1], Luca Serafini[2], Nicolas Gauquelin[2], Johan Verbeeck[2], Joerg Jinschek[1]
[1]Nanolab, Technical University of Denmark (DTU) , Kongens Lyngby, Denmark, [2]EMAT, University of Antwerp, Antwerp, Belgium

IM-05 (2), Lecture Theater 3, august 26, 2024, 14:00 - 16:00

Background incl. aims
In-situ transmission electron microscopy (TEM) has become increasingly important in the characterization of microstructures in functional and structural materials when real-time observation under application conditions is required to reveal underlying structure-property relationships [1]. With the advancement of microelectromechanical systems (MEMS) technology for the application of stimuli on the materials, the high sample stability and precise control of the stimuli, especially in elevating temperature with a local accuracy within 4% [2], enable atomic-scale resolution in such in situ TEM experiments. However, uncertainty remains regarding the exact temperature profile across a TEM sample itself, which limits the interpretation of observed structural phenomena in in-situ TEM heating experiments.
Methods
Here, we exploited plasmon energy expansion thermometry (PEET), detecting temperature-dependence of the bulk plasmon peak in an energy electron loss spectrum (EELS) [3] and testing its validity and accuracy using tungsten (W). The reasons to assign W as the model material come from the high melting temperature which is above 3000 °C and the sharp plasmon resonance in EELS, as shown in figure(a). These advantages benefit PEET through improved precise EELS peak determination over a wide implementation temperature range.
For sample preparation, W lamellas with varying sample thickness of 30 to 70 nm were prepared using a ThermoFischer Hydra Plasma FIB (Xe plasma at 30 kV) and were mounted on a DENS Wildfire heating chip [2] using W-gas assisted deposition. Two types of FIB-cut W lamellas were prepared: One is placed at the center of the spiral heater where we expect a homogeneous temperature distribution, as shown in figure(b). The other one is placed at an off-central position where we expect a thermal gradient [4].
Ex-situ temperature measurements were conducted using Raman spectroscopy with a 532 nm laser of beam size less than 1 µm. Si particles of 45 nm diameter were drop-casted on the heating chips. Exploiting the temperature dependence of the bonding vibration, the local temperature can be obtained by the Raman frequency of the Si-Si bond, which shifts with temperature at approximately 0.0232 cm-1 per °C.
For the in-situ heating experiments, both a ThermoFischer Themis (at EMAT) and Spectra (at DTU) S/TEM equipped with X-FEG mono have been operated at an accelerating voltage of 300 kV. For our PEET experiments, the monochromator was excited to achieve an energy resolution of 0.12eV. The effect of the STEM convergence semi-angle (3.6 to 18 mrad) as well as of the EELS collection semi-angle (6 to 70 mrad) was investigated in the PEET mapping experiments. The bulk plasmon peak was collected using Quantum 966 Gatan Image Filter with a dispersion of 0.01 eV per pixel and dwell time of 0.1 second per pixel.
Results
PEET mapping on the W lamella at the center of the spiral heater (figure(a)) reveals a temperature-dependent plasmon energy shift of 1.8 eV as the temperature progressively increases from room temperature (figure(c)) to 1100 °C (figure(d)). Correspondingly, the standard deviation when measuring at multiple positions also considerably increases, from 0.027 eV at room temperature (figure(c)) to 0.471 eV at 1100 °C (figure(d)), respectively. To understand this variation in plasmon

peak energy, we attempt to correlate the PEET mapping and the local estimated sample thickness (using the log-ratio method in EELS) and find a noticeable correlation as one factor responsible for this large deviation.
Leveraging these findings as calibration data, we further extended the application of PEET for detecting the temperature difference over space. The profound temperature gradient of the off-central W lamella was predicted by COMSOL simulation and verified by ex-situ Raman measurements. The results show that the thermal gradient can reach approximately 106 °C /m (from 667 to 772 °C within a 10 µm length) at a set temperature of 1000 °C. Interestingly, on the PEET map of the off-central W lamella at the same set temperature of 1000 °C, the plasmon energy shifts to higher values as the position moves farther away from the spiral center. By using the calibration data for correlating the plasmon energy to the local temperature, the data from the PEET map closely matched the thermal gradient observed in the ex-situ Raman measurement and simulation results.
Conclusion
Our study demonstrates that PEET is capable of obtaining quantitative temperature measurement results with the consideration of the sample thickness. Moreover, it effectively identifies pronounced thermal gradients within the sample. The improvement of the temperature determination in PEET provides a more reliable analysis of structure-properties correlation under various thermal conditions.

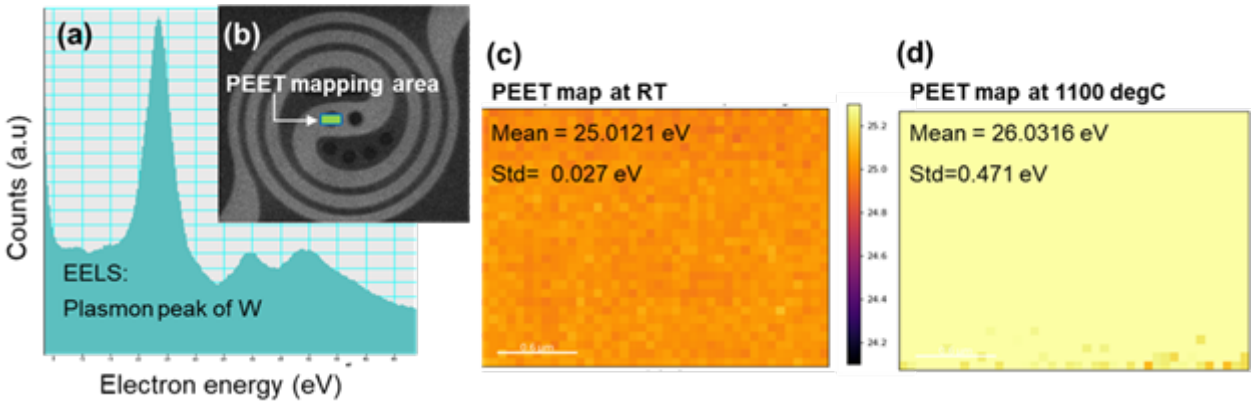

Keywords:

plasmon energy expansion thermometry

Reference:

[1] K. Jungjohann et al., Transmission Electron Microscopy: Diffraction, Imaging, and Spectrometry (2016), p. 17-80. doi:10.1007/978-3-319-26651-0_2
[2] J. Tijn van Omme et al., Ultramicroscopy, 192 (2018), p. 14-20. doi:10.1016/j.ultramic.2018.05.005
[3] M. Mecklenburg et L., Physical Review Applied, 9, 014005 (2018). doi: 10.1103/PhysRevApplied.9.014005
[4] S. Vijayan et al., Microscopy Research and Technique, 85.4 (2022) p. 1527-1537. doi:10.1002/jemt.24015
[5] LS and JV acknowledge funding from the eBEAM project which is supported by the European Union's Horizon 2020 research and innovation programme FETPROACT-EIC-07-2020: emerging paradigms and communities

728

Unravelling the collagen mineralization using multiscale in situ X-ray-scattering/Raman spectroscopy and ex situ electron microscopy/nano-Xray-fluorescence

Prof. Dr Roland Kröger[1], Dr Julia Parker[2], Ms Emma Tong[1]
[1]University of York, York, United Kingdom, [2]Diamond Light Source, Harwell, United Kingdom
IM-05 (2), Lecture Theater 3, august 26, 2024, 14:00 - 16:00

Background
The process of collagen mineralization is key to numerous biological processes including bone and tooth formation, arteriosclerosis as well as tendon and cartilage calcification and other forms of ectopic calcification. Therefore, understanding the processes that govern the formation of a hard inorganic calcium phosphate phase (usually hydroxyapatite) within a soft matrix of collagen is central to identify the physico-chemical processes involved in collagen calcification, which occurs in close interaction with the collagen template. E.g. for bone it is known that the hydroxyapatite mineral is organized, like collagen, in a hierarchical fractal-like fashion [1]. A key problem in this context is the dynamics of the mineralization and the possible presence of intermediate phases before a full mineralization with hydroxyapatite occurs. Using the polymer-induced liquid precursor (PILP) method for in vitro collagen mineralization [2], we employed state-of-the art characterization techniques, a combination of in situ X-ray scattering, in situ Raman spectroscopy, nano X-ray fluorescence (nXRF) with 50 nm resolution and transmission electron microscopy (TEM) to monitor the mineralization process at different length scales. In our studies we focused on the impact of mineralization on the collagen response and the possible occurrence of intermediate phosphate phases apart from hydroxyapatite.

Methods
A combination of in situ characterization with Raman spectroscopy and small and wide-angle X-ray scattering (SAXS, WAXS) was used with the same flow cell, which was heatable and kept at 37 ˚ C during the mineralization process. We applied PILP using osteopontin, fetuin-A and poly aspartic acid as active protein polymers to mimic this process in vitro using rat-tail derived collagen type I fibers. Raman spectroscopy enables a molecular level analysis of the mineralizing collagen, SAXS provides information on the particle evolution and impact of mineral growth on the collagen D-banding (a periodic pattern caused by repeat sequences of overlap and gap regions in the staggered collagen molecule organization) and WAXS permits the study of the time dependent evolution of crystallinity monitoring the {002} lattice planes in the hydroxyapatite mineral phase. The resulting mineralized collagen fibers were subsequently analyzed using nano - XRF microscopy to map the distribution of Ca and P within the fibers and TEM and electron diffraction for microstructural investigations and analysis of the mineral phases.

Results
In situ Raman spectroscopy reveals intermediate phosphate phases during the initial mineralization stage confirmed by electron diffraction in TEM. In accordance with these findings, we observe three stages of mineralization with SAXS showing an initial expansion of the collagen D-spacing, associated with the infiltration phase, a subsequent contraction of the D-spacing, associated with the beginning of nucleation and crystallization and finally a continuous growth phase, correlated with an expansion of the D-spacing. Analyses of the mineralized collagen ex situ using TEM and nXRF indicates the presence of two morphological features, which we associate with octa calcium phosphate and hydroxyapatite, respectively, and an inhomogeneous pattern of tessellation in accordance with reported patterns for bone mineralization [3].

Conclusion

Our in vitro studies of collagen mineralization shows a remarkable resemblance of observations made in biological systems indicating that the PILP process is an excellent proxy to study relevant physico-chemical processes e.g. in bone formation. The joint application of multiscale and multiplatform methods to monitor the progression of mineralization as well as the resulting mineralization patterns allows for unique insights into the evolution of the mineral phase and the interaction between the hard mineral phase with the soft collagen template.

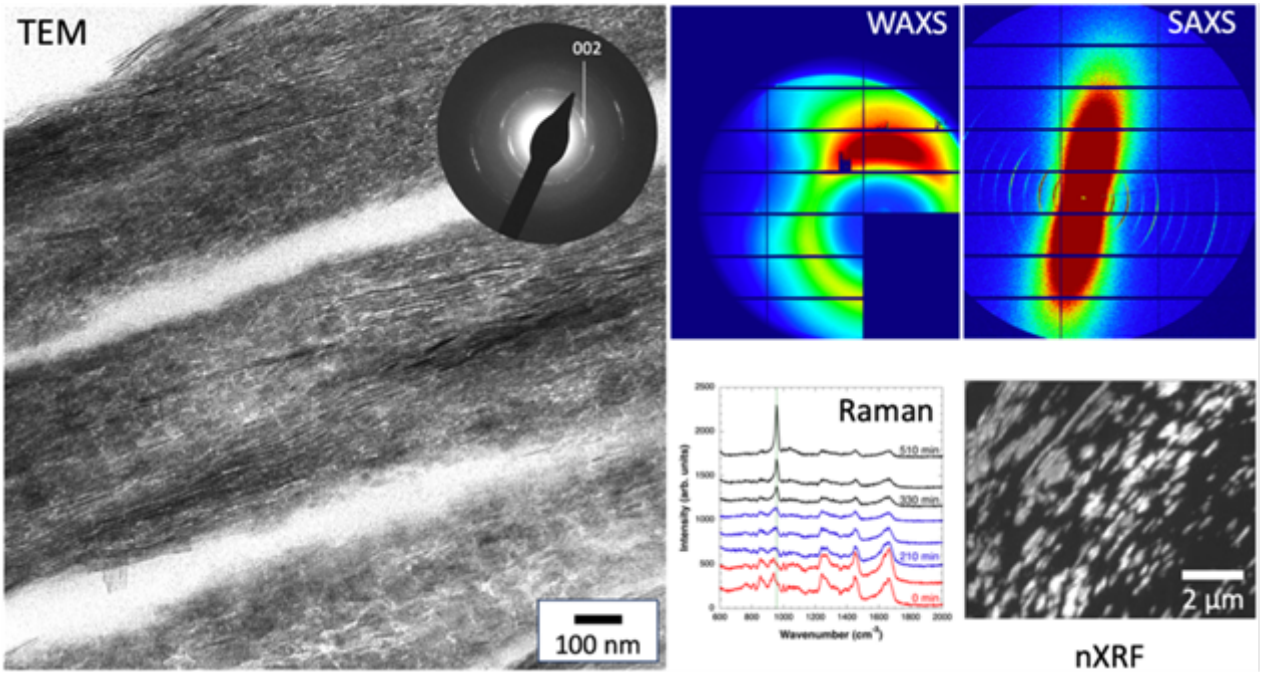

Keywords:

SAXS/WAXS, nano-XRF, Raman, TEM/STEM, Collagen-Mineralization

Reference:

[1] N. Reznikov, M. Bilton, L. Lari, M. Stevens, and R. Kröger, Fractal-like hierarchical organization of bone begins at the nanoscale, Science 360, science.aao2189 (2018).
[2] M.J. Olszta, D.J. Odom, E.P. Douglas, L.B. Gower, A new paradigm for biomineral formation: mineralization via an amorphous liquid-phase precursor, Connective Tissue Research 44 (1), 326 (2003).
[3] D. Buss, N. Reznikov, M. McKee, Crossfibrillar mineral tessellation in normal and Hyp mouse bone as revealed by 3D FIB-SEM microscopy, J. Struct. Biol. 212 107603 (2020).

123

Quantitative chemical analysis by STEM-EDS and machine learning: Are AgAu alloyed at the nanoscale?

Dr Murilo Moreira[1,2], Dr. Emmanuel Cottancin[1], Dr. Michel Pellarin[1], Dr. Lucian Roiban[3], Dr. Karine Massenelli-Varlot[3], Dr. Daniel Ugarte[2], Dr. Varlei Rodrigues[2], Dr. Matthias Hillenkamp[1,2]
[1]Institute of Light and Matter, University Lyon, University Claude Bernard Lyon 1, CNRS, UMR5306, Villeurbanne F-69622, France, [2]Institute of Physics Gleb Wataghin, State University of Campinas, Campinas, 13083-970, Brazil, [3]INSA Lyon, Universite Claude Bernard Lyon 1, CNRS, MATEIS, UMR5510, Villeurbanne , France

IM-05 (3), Lecture Theater 3, august 27, 2024, 10:30 - 12:30

Background incl. aims:
Bimetallic nanoparticles (BNPs) have attracted increasing attention in fundamental and applied sciences in recent decades. They are expected to play a central role in the energetic and ecological transition of our societies. Combining two or more metals on the nanoscale opens up a whole playground for the investigation and the fine-tuning of physicochemical properties and applications in nanoparticle-based devices. The BNP properties depend on size, shape, environment, chemical composition and spatial elemental distribution. Different chemical configurations (alloyed vs. segregated, chemically ordered, etc.) can change considerably the optical, magnetic, or catalytic properties via the electronic structure [1]. One of the most intensely studied bimetallic systems is the gold-silver alloy. Its nanoparticles have attracted much attention for their catalytic, plasmonic surface-enhanced sensing and photocatalytic properties. In the bulk, the two metals are completely miscible across the entire composition range, and their atomic radii, crystal structure, valence, and electronegativity are very similar. On the nanoscale, however, additional degrees of freedom have to be considered, namely the particle surface, as well as possible segregation and chemical ordering into structures not possible in bulk. Despite the high number of experimental and theoretical articles published on AgAu nanoparticles, the controversy about whether intrinsically one of the two metals preferentially segregates at the surface or not is still unresolved, both on the experimental as on the theoretical side [2,3]. In this context, we aim to contribute to this discussion by providing quantitative and statistically reliable chemical profiles of AgAu BNPs in the chemical ground state and thermodynamic equilibrium, using high signal-to-noise ratio and resolution hyperspectral images (HSI) obtained by Energy Dispersive X-ray Spectroscopy (EDS).

Methods:
The performance of EDS combined with Scanning Transmission Electron Microscope (STEM) has been significantly enhanced, permitting the analysis of chemical composition in nanometric objects, including bimetallic nanoparticles (BNPs) with diameters smaller than 10 nm. This breakthrough is crucial for the in-depth distinction between different chemical structures (random, gradient, or core-shell, etc.) of individual particles on a quantitative level. High-quality SNR are difficult to attain for such very small volumes, below 10 nm; besides, data acquisition and treatment methodologies, followed by rigorous error analysis, are essential. In this context, we have measured the chemical composition variations inside AgAu BNPs using EDS-STEM in a Titan-Themis Cubed and a Cold-FEG JEOL NeoARM operated at 80 kV with high solid angle X-ray detectors (≈1 sr). We have used unsupervised machine learning methods (Principal Component Analysis-PCA and Nonnegative Matrix Factorization-NMF) to verify the existence of latent information on radial composition variations in our data. This analysis provides direct, solid statistical verification that the estimated radial composition changes represent accurate information provided by the EDS spectra [4,5]. In addition, PCA and NMF components are used for the reconstruction of the dataset for denoising and background removal, respectively.

Results:
To guarantee that the BNPs are analyzed in the chemical ground state, we protect them by a thin layer of amorphous carbon and anneal them at 300°C. Analyzing the HSIs using PCA and NMF, we are able to retrieve denoised information for quantitative analysis, but we can also evidence the Ag segregation of hundreds of BNPs by analyzing the components and abundance maps obtained by PCA/NMF, both showing compelling complementarity to EDS-HSI datasets. Using unsupervised machine learning to provide statistical validation for the information extraction, we further analyze quantitative profiles by azimuthal averaging (to attain better SNR) of isotropic BNPs in the HSI for both raw and NMF reconstructed data. Here, our results demonstrate the possibility of quantifying the chemical composition within bimetallic nanoparticles in 4-10 nm in diameter range. These findings represent a significant improvement over the widely used qualitative chemical mapping (see Fig 1.), providing essential insights into understanding the elemental distribution within small volumes. Our results reveal chemical gradients with Ag enrichment towards the surface of the BNPs.

Conclusion:
Finally, by combining well-defined model samples, robust and quantitative EDS-TEM analysis and machine learning for statistical validation we contribute to the comprehension of nanoalloy physics. We not only demonstrate the feasibility of the method but settle the ongoing controversy about nanoscale miscibility in the AgAu system. While Au and Ag are miscible in in the core of BNPs as small as 4 nm in diameter, with a core of 2 nm (<400 atoms), a slight enrichment of silver at the surface of the order of 10% is consistently evidenced. Our work furthermore paves the way for its extension to environmental and tomographic studies of multimetallic nanostructures.

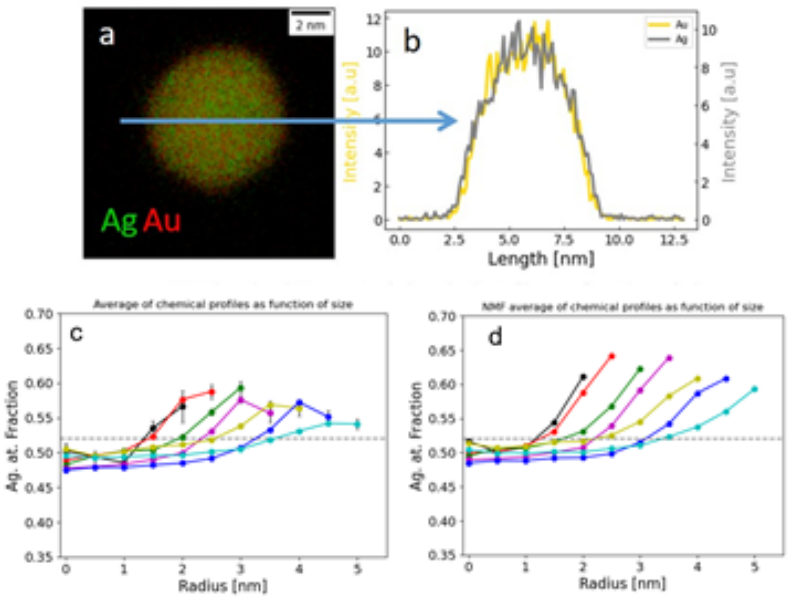

Figure 1: Derivation of chemical gradients. a) EDS elemental mapping and b) its respective qualitative line profile. C) Chemical profiles obtained for Ag atomic fraction of NMF reconstructed HSIs, here the profiles are obtained by the averaging of 118 BNPs profiles dispersed in sizes from 2-5 nanometers in radius. The single BNP profiles are calculated from the summing of pixel intensity of concentric rings; the origin of the graph defines the center of the BNPs. The outermost points repeesenting information from BNPs surface are not reliable due to high error bars/low SNR compared to background which decreases the detection/quantification limit. d) Chemical profiles obtained for Ag atomic fraction of NMF reconstructed HSIs. The outermost points here suggest an increase on the detection limit after NMF reconstruction due to denoising and background removal. There is no protocol well-established for uncertainty determination for NMF reconstructed profiles.

Keywords:

EDS-STEM, Chemical Gradients, Bimetallic nanoparticles

Reference:

1-Alloyeau, D. et al. editors. Nanoalloys: Synthesis, Structure and Properties. Springer-Verlag London, (2012).
2-Lasserus, M., et al., Nanoscale 10, 2017–2024 (2018).
3-Gromoff, Q., et al., Nanoscale 16, 384 (2023).
4-Moreira, M., et al., Microsc. Microanal. 28, 338 (2022).
5-Moreira, M., et al., ACS Appl. Nano Mater. 7, 1369–1378 (2024)

291

5D-ToF-STIM Hyperspectral Imaging with a keV He+ Focused Ion Beam

Dr. Dustin Andersen[1], Michael Mousley[1], Saba Tabean[1], Radek Holeňák[2], Eleni Ntemou[2], Gerhard Hobler[3], Tom Wirtz[1], Daniel Primetzhofer[2], Santhana Eswara[1]
[1]Advanced Instrumentation for Nano-Analytics (AINA), MRT Department, Luxembourg Institute of Science and Technology (LIST), Belvaux, Luxembourg, [2]Department of Physics and Astronomy, Uppsala University, Uppsala, Sweden, [3]Institute of Solid-State Electronics, TU Wien, Vienna, Austria

IM-05 (3), Lecture Theater 3, august 27, 2024, 10:30 - 12:30

Scanning ion microscopy in combination with transmission ion energy-loss spectroscopy (IELS) for low-energy ions is a promising field of study, which seeks to provide complementary information to that of more conventional techniques like electron energy-loss spectroscopy (EELS) in scanning transmission electron microscopy (STEM). In contrast to electrons, ions are capable of both capturing and losing charge, allowing for charge exchange and neutralization processes [1]. In addition, while primary electrons are capable of exciting plasmonic and electronic states, as well as ejecting core-shell electrons, ions are further capable of temporarily merging their electron orbitals with those of the sample's atoms (potentially ejecting ion-induced Auger electrons), as well as ejecting sample atoms (measurable using mass spectrometry), creating unique signals not available to electron beams. The energy lost by the ions during these sample interactions can be measured as an increase in the time-of-flight (ToF) from the sample to the detector. Furthermore, the scattering pattern seen on the detector contains detailed information not only about the crystal structure, but also the trajectories of the ions within that structure [2]. By combining spatially resolved ion energy-loss and scattering information, we can thus create a rich 5D dataset: 2D position on the sample plane, 2D position on the detector plane, and finally ToF information for each ion or neutral collected. He+ ions are chosen for this work as they are particularly well suited to low-energy transmission ion microscopy due to their relatively small scattering cross-section (allowing for thicker samples) and their relatively low damage to the sample.
Our work at LIST focuses on low-energy (up to 30 keV) scanning transmission helium ion microscopy (STIM) coupled with ToF to analyze the angular and energy distribution of the transmitted helium ions and neutrals. Two prototype instruments are being developed: one based on a commercially available gas-field ion source (GFIS), which can achieve sub-nm probe sizes, and a second based on a commercially available DuoPlasmatron source with a probe size of <300 nm. Each prototype is equipped with a high-sensitivity microchannel plate (MCP) with a delay-line-detector (DLD), capable of measuring the exact location and timing of single ion or neutral impacts. However, due to the complexity of modifying the GFIS column to perform beam pulsing, it is not yet capable of TOF measurements (i.e. only capable of 4D datasets), while the DuoPlasmatron source comes with pulsing/blanking plates. The DuoPlasmatron based prototype also has a high flexibility in the instrument configuration, allowing for post sample ion deflection to determine the fraction of ions neutralized within the sample, as well as the ability to vary the post-sample flight distance.
Using a previous iteration of the DuoPlasmatron system, we have been able to create images by generating contrast from the total counts, the ratio of neutrals to ions, the scattering angle, and the energy loss (other criteria could also be envisioned with such a rich dataset). As each pixel in the sample image contains a full ToF spectrum and a scattering pattern, we have developed python software based on matplotlib and pandas with a graphical user interface for interactive plotting of sample images, detector images, and ToF spectra based on flexible combinations of ROI selections, in order to intuitively explore the 5D dataset. We have also compared our experimental scattering angle and energy-loss results from this instrument to SRIM simulations [3].
In parallel with the development of these instruments, we have also performed stationary-beam transmission ion experiments at the mature time-of-flight medium energy ion scattering (ToF-MEIS)

beam line at Uppsala University, where extremely fast blanking speeds (below 1 ns) and higher accelerating voltages (up to 350 kV) are possible (Rev. Sci. Instrum. 83, 095107). Here we have seen differences in both the scattering pattern and ion energy distribution based on the direction of the beam passing through a thin single-crystal Si film with an amorphized layer on one side. In the case where the ions pass through the amorphous layer and then the crystalline layer, we observe a distinct crystalline scattering pattern, but a relatively broader energy distribution. For the inverted sample, where the ions instead pass through the crystalline layer first, we observe an apparently random scattering pattern, but a relatively narrower energy distribution. Ion channeling simulations performed with IMSIL [4] at TU Wien corroborate the dependence of both the energy and scattering distributions on the orientation of the sample with respect to the beam. These results are also in agreement with the simulation and experimental results of Holenak et al. demonstrating that a disordered surface layer can redirect incident ions into planes and channels, instead of randomizing their trajectories [5].

The authors acknowledge funding from the Luxembourg National Research Fund (FNR) AIMSTHIM2 (C21/MS/16215748) and STHIM (C16/MS/11354626), for the experimental work performed at LIST, as well as funding from the EU Horizon 2020 programme through the RADIATE project for the experimental work performed at Uppsala University.

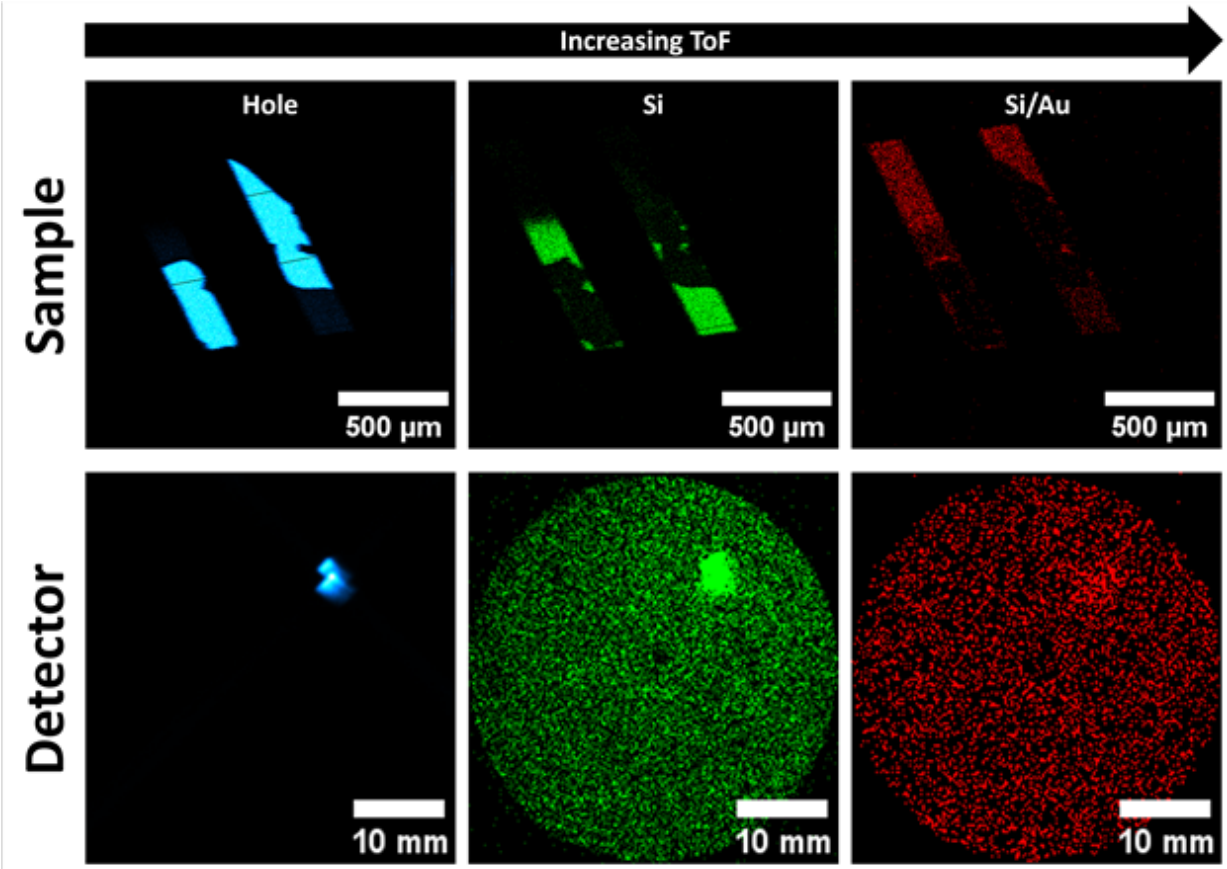

Transmitted ion/neutral intensities in the sample and detector planes with increasing time-of-flight (ToF) for 20 keV He^+ ions on a perforated thin Si membrane partially coated with Au.

Keywords:

Time-of-Flight, Ion Beams, Energy-Loss Spectroscopy

Reference:

[1] R Holeňák et al., Vacuum 185, 109988 (2021).
[2] H Krause et al., Phys. Rev. A 49, 283 (1994).
[3] M Mousley et al., Microsc. Microanal. 29, 563 (2023).
[4] G Hobler, Nucl. Instrum. Meth. B 96, 155 (1995).
[5] R Holeňák et al., Phys. Rev. Applied 21, 024048 (2024).

373

Atomic Lensing Model for Atomic Scale Multi-Elemental Quantification in STEM

Dr Zezhong Zhang[1,2,3], Dr. Annick De Backer[1,2], Dr. Ivan Lobato[4], Prof. Sandra Van Aert[1,2], Prof. Peter Nellist[3]
[1]EMAT, University of Antwerp, Antwerp, Belgium, [2]NANOlab Center of Excellence, University of Antwerp, Antwerp, Belgium, [3]Department of Materials, University of Oxford, Oxford, United Kingdom, [4]Rosalind Franklin Institute, Harwell Research Campus , United Kingdom

IM-05 (3), Lecture Theater 3, august 27, 2024, 10:30 - 12:30

Background incl. aims
To understand the structure-property relationship in nanostructured materials, we need to probe their crystal structures and compositions at the atomic scale. Advanced materials typically consist of multiple elements in a complicated structure. Significant challenges remain to disentangle the contributions of composition and thickness in STEM due to dynamic scattering, necessitating detailed simulations. However, the combination of the computational cost of the multislice calculation and the enormous ordering possibilities for a given composition makes the quantification of mixed columns almost impossible. To address these challenges, we here report the development of the atomic lensing model for the fast prediction of ADF-EDX scattering cross-sections of mixed columns [1].

Methods
The channelling effect originates from the fact that a fast negatively charged electron will be attracted by the positively charged atomic nuclei. As a consequence, an atomic column with periodically spaced atoms along the beam direction acts as a waveguide dynamically focusing the electrons. This leads to a non-linear signal as a function of depth for atomic resolution ADF and EDX, which significantly complicates elemental quantification. Based on the channelling theory of incoherent imaging, the so-called atomic lensing model was therefore developed to take the ordering of multiple elements into account [2]. In the atomic lensing model, dynamical scattering is treated as a superposition of individual atoms focusing the incident electrons. This model predicts the ADF scattering cross-section of a mixed column from the libraries of pure elements. Based on the incoherent imaging of ADF and EDX signals, this model has been shown to work for EDX as well and allows us to predict mixed column cross-sections with any atomic ordering efficiently. The validity of the atomic lensing model was verified numerically with frozen phonon multislice simulations. The speed and accuracy of the atomic lensing model were compared against multisclice and PRISM algorithms. For instance, the atomic lensing model is the only feasible approach that can explore all the ordering possibilities for a 20-atom-thick binary alloy column, taking 30 s to loop over 1 million orderings with an accuracy of ± 1 atom.

Results
We explained the linear dependence between ADF and EDX cross-sections from scattering theory and examined it numerically with multislice simulations, which is the basis for the extension of the atomic lensing model to both signals under the incoherent imaging mode. As shown in Fig.1 for a Au@Pt nanorod, one cannot distinguish the elements with adjacent atomic numbers from an ADF image but can fingerprint them with EDX. The predictions, based on the atomic lensing model, are in good agreement with multislice simulations and significantly deviate from the linear model in which a simple scaling with the number of atoms is assumed. Based on the atomic lensing model and the correlation between ADF-EDX due to signal incoherence, we are able to count the number of atoms from an experimental ADF-EDX dataset of a Au@Ag core-shell nanoparticle [2]. We also

demonstrated that this model can reliably predict EDX values for an Al-Ag-Pt-Au high entropy alloy up to 10 nm. Beyond this thickness, the contribution of neighbouring columns becomes significant.

Conclusion

The atomic lensing model significantly accelerates the prediction of ADF-EDX scattering cross-sections. It enables exploring atomic arrangements in multi-elemental materials with high throughput and opens new avenues for quantitative analysis in materials science.

Figure 1. (a) Atomic model of a Au@Pt core–shell nanoparticle. (b) Comparison of the scattering cross-sections (SCS) quantified from multislice simulations, the atomic lensing model (ALM), and a linear incoherent model.

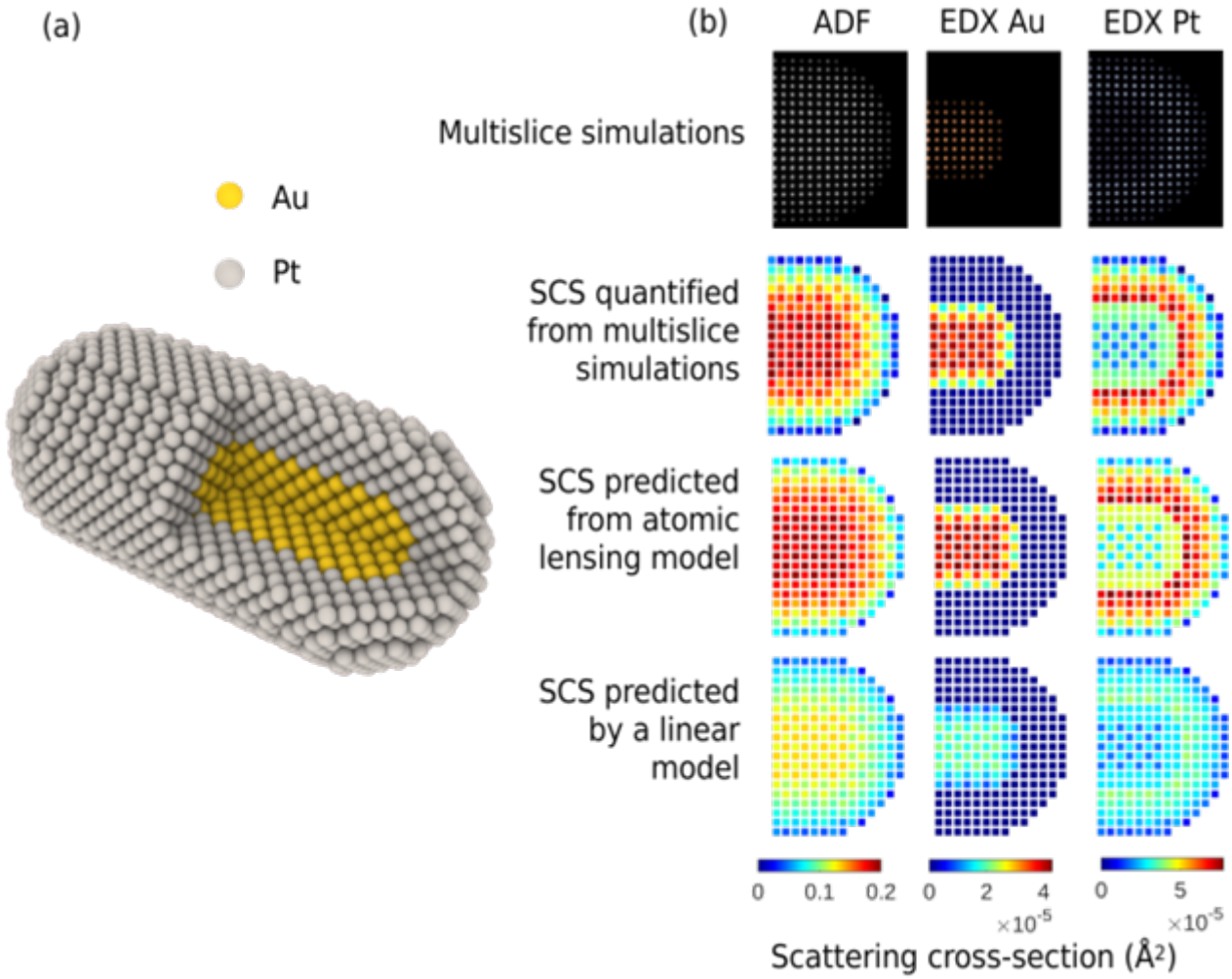

Keywords:

Quantitative STEM-EDX, Scattering cross-section

Reference:

[1]Zhang, Z., Lobato, I., De Backer, A., Van Aert, S., & Nellist, P.D. (2023) Ultramicroscopy, 246, 113671.
[2]van den Bos, K.H.W., De Backer, A., Martinez, G.T., Winckelmans, N., Bals, S., Nellist, P.D., & Van Aert, S. (2016) Rev. Lett. 116(24), 1-6.
[3]De Backer, A., Zhang, Z., van den Bos, K.H.W., Bladt, E., Sánchez-Iglesias, A., Liz-Marzán, L.M., Nellist, P.D., Bals, S. &Van Aert, S. (2022) Small Methods, 6(11), 2200875.
The authors acknowledge financial support from the Research Foundation Flanders (FWO, Belgium) through Project No. G.0502.18N and a post-doctoral grant to ADB. This project has received funding from the European Research Council ((Grant Agreement No. 770887 PICOMETRICS).

417

Use of prior knowlege and physics-guided NMF for improved phase segmentation of EDX datasets.

Prof. Cécile Hébert[1], Dr. Adrien Teurtrie[1,2], Dr. Pau Torruella-Besa[1], M. Sebastian Cozma[1], Dr. Hui Chen[1], Dr. James Badro[3], Dr. Duncan T.L. Alexander[1]
[1]EPFL-IPHYS-LSME, Lausanne, Switzerland, [2]Unité Matériaux et Transformations, UMR-CNRS 820, Lille, France, [3]Institut de Physique du Globe, Paris, France

IM-05 (3), Lecture Theater 3, august 27, 2024, 10:30 - 12:30

While modern analytical transmission electron microscopes fitted with an energy-dispersive X-ray (EDX) detector can acquire a huge amount of data at an ever-increasing speed, there is still a need to improve processing tools. Machine learning algorithms based on multivariate statistical analysis are widely used to reduce the dimensionality of datasets and perform denoising. On the other hand, to perform quantification, one needs to fit the EDX spectrum with Gaussians for the X-ray lines and a mathematical model taking into account the Bremsstrahlung background. Usually, those two steps are performed independently: first the statistical decomposition and denoising; and then the fitting and quantification.

With a new Python package named espm, that provides a new algorithm entitled ESpM-NMF, we propose to perform the two steps jointly, where the machine learning algorithm directly learns the parameter characterizing the model of the spectrum. We have, in addition, implemented an advanced regularization procedure to take into account the relatively smooth nature of the spatial distribution of components.
Our method has many advantages:
- It is much more resilient to noise and enables analysis and quantification of datasets with much lower signal than conventional methods.
- It allows prior knowledge to be easily taken into account, such as the fact that some regions of the image may contain only one phase or that some of the phases do/do not contain certain chemical elements. With this, we drastically improve the chances that the results of the decomposition have an actual physical meaning.
- The results of the decomposition naturally contain the information needed for quantification, as we directly learn the height of the Gaussian peaks modelling the X-ray lines. There is therefore no need for a further step of fitting the spectra to obtain relative abundances of elements.

In the following paper, we will demonstrate how we can easily use reasonable a priori knowledge on a sample to guide a decomposition. The sample is a synthetic mineral assemblage used to study Earth's mantle. It has a homogenous starting composition with major elements Si and Mg (besides O), minor elements Fe, Ca & Al, and some dopants. The sample is synthesized in a diamond anvil cell at pressure of 55 GPa, and heated with a laser to around 3200-3500 K, resulting in a complex microstructure of a matrix phase (bridgemanite) containing inclusions (ferropericlase and calcium perovkites). The overall composition of the main phases has, in addition, a gradient towards the center of the heated spot, that is of particular scientific interest. Small regions of the datasets are excluded from the analysis via a mask because they contain an iron-rich core which is not of interest (top right) and a hole due to the FIB preparation (bottom).

An unguided decomposition with two components leads to a nearly realistic result with two phases: a matrix (a), with inclusions (b). However, a close analysis shows that the intensity of the image of the component #2 never goes to 0, indicating an imperfect unmixing. Moreover, the Si content obtained in the matrix phase (panel (a)) is 52 at. %, which is above the expected maximum of 50%. Using a

Mask (c), it is possible to force the inclusion component to be 0 in the yellow areas. This is a very reasonable constraint based on evidence from the general structure of the specimen. By doing so, we obtain a more realistic composition of the matrix phase with 48 at. % Si. This finding further supports the supposition that the mask selects a pure phase region containing only the matrix.

A further investigation can be performed using a decomposition with 4 components, of which 2 are forced to represent the matrix by setting the same mask on the other 2 components. This will allow for variations inside each of the 2 main phases. Indeed, as seen in the lower 4 panels of the figure, with this 4-component decomposition, one sees a compositional gradient from top right (close to the central laser spot) to bottom left. In general, both the matrix phase and the inclusions contain more iron as they approach the iron-enriched core.

While not shown in the figure, with our algorithm, it is also possible to constrain the chemical composition of some of the components. The use of well-chosen constraints can be both a way to reach a more realistic segmentation in the actual phases composing the specimen, but is also a powerful method to explore and better understand a complex specimen. As such, ESpM-NMF both redefines the standard pipeline for EDX dataset processing, and offers strong versatility for tailoring the analysis to the specific nature and characteristics of a sample.

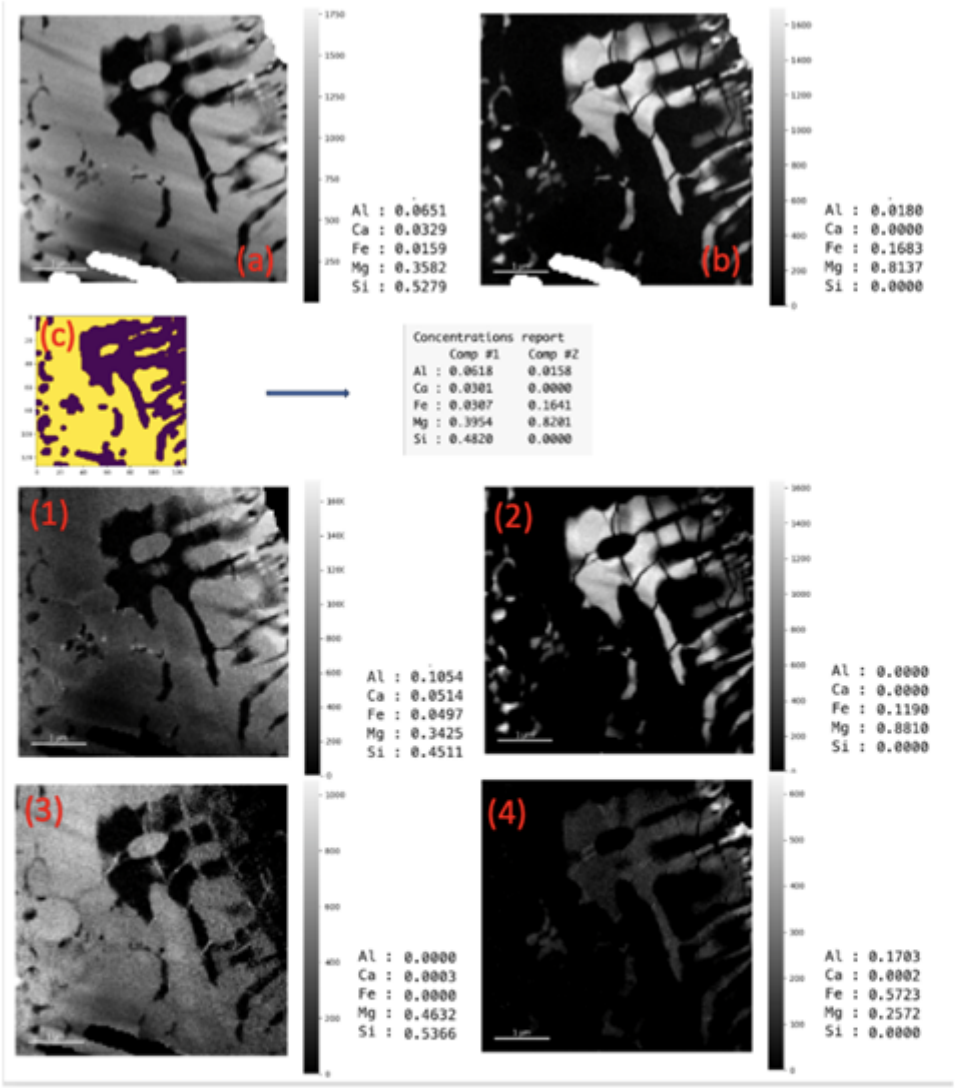

(a) and (b) results of a 2-components decomposition using *ESpM-NMF* without constraints, together with the quantification result. (c) mask used to force component #2 to be exactly 0 in the yellow area, ensuring that component #1 is closer to the matrix phase, and resulting atomic percentages of the two components. (1)-(4) result of a 4-components decomposition where the mask (c) has been applied on components (2) and (4).

Keywords:

EDX NMF pysics guided ML

Reference:

[1] Adrien Teurtrie et al., From STEM-EDXS data to phase separation and quantification using physics-guided NMF, to be published.
[2] Adrien Teurtrie, Nathanaël Perraudin, Thomas Holvoet, Hui Chen, Duncan T.L. Alexander, Guillaume Obozinski and Cécile Hébert, “espm: A Python library for the simulation of STEM-EDXS Datasets”, Ultramicroscopy 249, 113719, 2023, https://doi.org/10.1016/j.ultramic.2023.113719.

734

Direct visualization of chemical transport in solid-state chemical reactions by time-of-flight secondary ion mass spectrometry

Sang Pham[1], Sean Collins[1,2]
[1]Bragg Centre for Materials Research & School of Chemical and Process Engineering, University of Leeds, Leeds, United Kingdom, [2]School of Chemistry, University of Leeds, Leeds, United Kingdom
IM-05 (3), Lecture Theater 3, august 27, 2024, 10:30 - 12:30

Background incl. aims
Systematic control and design of solid-state chemical reactions are essential for modifying material properties and pioneering novel synthesis techniques. Enhanced chemical transport and accelerated kinetics of active elements and compounds across interfaces are known to drive solid-state chemical reactions [1]. Monitoring temperature-dependent chemical dynamics at micro- to nanometer length scales in real-time is crucial for providing valuable feedback to tailor the properties, performance, and stability of multi-material structures. Conventional methods for studying solid-state reactions, such as in-situ TEM heating, can identify formed phases and their relative weights but may overlook transient and minor phases [2, 3]. Time-of-flight secondary ion mass spectrometry (TOF-SIMS) at nanometer resolution offers a solution to these challenges. This technique provides information about element distribution and bonding encoded in multiatom ions from the near-surface region of solids [4], making it ideal for studying complex chemical processes in energy storage and hot corrosion. In this study, we combine focused ion beam–scanning electron microscopy (FIB-SEM) and TOF-SIMS to track the migration of active chemical elements from a glass coating to the oxide scale during in-situ hot corrosion experiments. Our findings demonstrate the distinct potential of TOF-SIMS in exploring nano-scale chemical dynamics of materials in response to temperature, optical, or electromagnetic stimulations.

Methods
TOF-SIMS analysis was performed using a Ga primary ion beam at an accelerating voltage of 30 kV and a current of 0.23 nA, scanned continuously across the sample surface throughout in-situ heating using MEMS heating chip. The lateral resolution of the resulting images was estimated as better than 290 nm at an abrupt step in the 23Na+ signal (20%–80% of the maximum intensity). Isochronal heating was applied from 50 to 850 °C (1 °C/s), producing a Z-direction (direction of successive two-dimensional scans) that directly tracks the temperature. Each frame's acquisition time was 1.4 s, allowing for real-time observation of chemical dynamics. The examined sample comprises a sodium borate coating as the uppermost layer, followed by the intermediate oxide layers with the dendritic iron oxide grown above the continuous iron–chromium oxide layer. The sample was cross-sectioned using FIB, and the cross-sectioned specimen was lifted out and deposited on a MEMS heating chip (flat on the chip, perpendicular to the ion beam).

Results
This advance in nanoscale chemical analysis with TOF-SIMS reveals corrosion induced by sodium diffusion below the coating's glass transition. These findings unveil sodium diffusion decoupled from boron at much lower temperatures than previously known. Moreover, selective dissolution of iron oxides in solid-state corrosion was observed, with iron moving into the borate coating while chromium remains in the steel oxide, elucidating a part of the nanoscale electrochemical mechanism. Additionally, this technique enables the detection of transient phases and impurities during hot corrosion reactions between sodium ion and oxide layers, allowing us to track the formation of early-stage corrosion reaction products and lithium impurities in the oxide layers. Ultimately, we can employ image-based determination of the sodium diffusion coefficient by combining our established

Fickian diffusion model with microscopic measurements of the moving sodium front, extracting the activation energy for diffusion and the temperature-dependent diffusion coefficient through FIB-based TOF-SIMS analysis.

Conclusion

In summary, the developed in-situ TOF-SIMS experiments provide valuable inputs for the study of chemical dynamics occurring in the hot corrosion processes of inorganic glasses with complex compositions, offering insights for mitigating corrosion reactivity at high temperatures. More widely, the developed TOF-SIMS techniques open the exploration of chemical dynamics at high temperatures in applications from metal-forming and engine lubricants to nuclear reactor components to advance the understanding of performance degradation through to new materials synthesis routes.

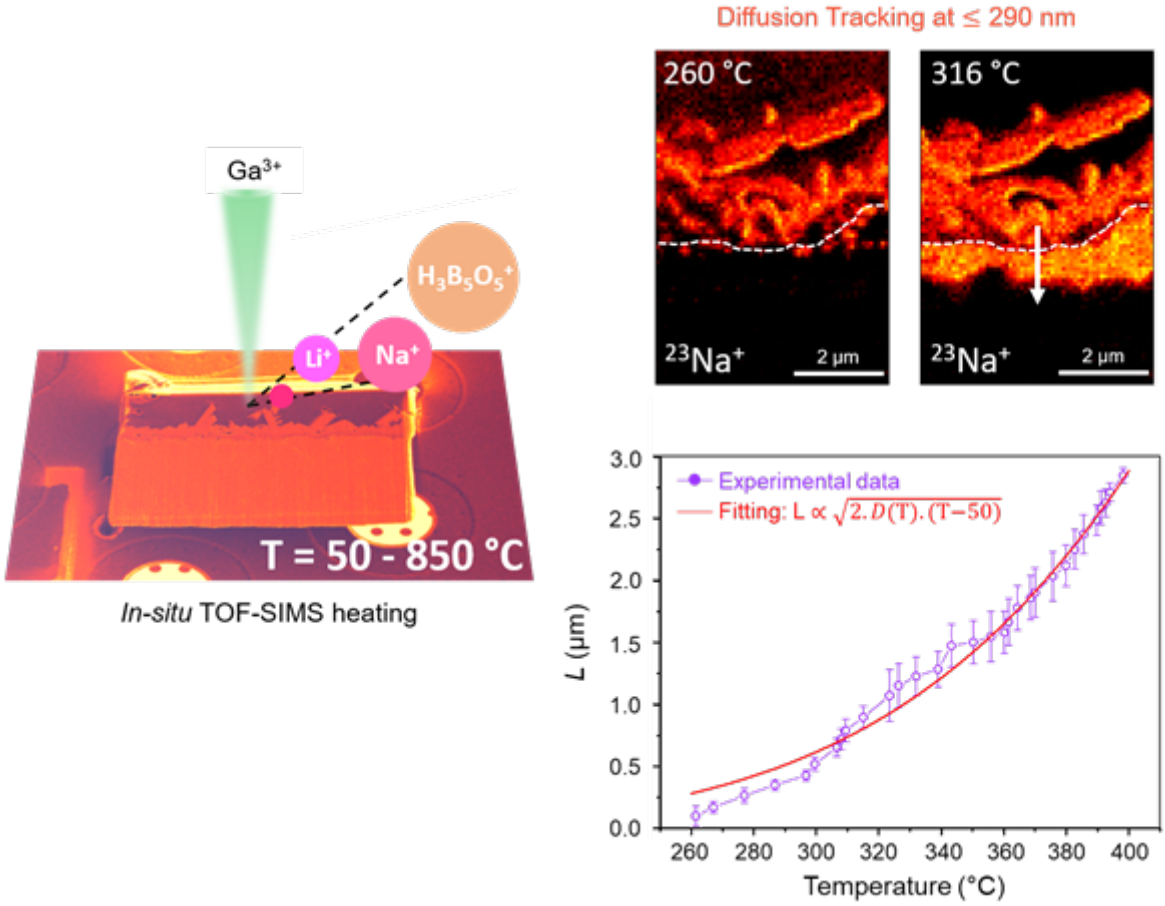

Keywords:

Coatings, TOF-SIMS, Sodium, Borate, Corrosion

Reference:

[1] Cohn, G. Chem. Rev. 1948, 42 (3), 527– 579; [2] Sindorf, D. W. et al., J. Am. Chem. Soc. 1983, 105 (12), 3767– 3776; [3] Wang, Z. et al., Nano Lett. 2012, 12 (12), 6126– 6132; [4] Smentkowski, V. S. et al., Surf. Sci. 2016, 652, 39– 45; [5] Pham, S. et al., Nano Lett. 2024, 24, 12, 3702–3709.

755

Electron beam propagation impact on high-resolution quantitative chemical analysis of GaN/AlGaN 1 nm-thick quantum wells

Florian Castioni[1,2], Sergi Cuesta[3], Patrick Quéméré[2], Eric Robin[3], Vincent Delaye[2], Eva Monroy[3], Pascale Bayle-Guillemaud[3], Nicolas Bernier[2]
[1]Université Paris-Saclay, CNRS, Laboratoire de Physique des Solides, Paris, France, [2]Université Grenoble Alpes, CEA, LETI, Grenoble , France, [3]Université Grenoble Alpes, CEA, IRIG, Grenoble, France
IM-05 (3), Lecture Theater 3, august 27, 2024, 10:30 - 12:30

Background: High-resolution energy dispersive x-ray spectroscopy (HR-EDX) in STEM is a technique of choice for conducting chemical analyses of III-nitride materials quantum wells (QWs) used as UV sources [1]. When travelling through a crystalline material, the phenomenon of “cross-talk” – the interaction of the electron beam (EB) with surrounding atomic columns - can significantly affect the quantitative results. Although the phenomenon was widely studied [2], there is still a lack of experimental works showing the possibility to quantify the impact of these effects on chemical analyses. The present contribution aims to show how to correlate HR-EDX mappings with inelastic multislice simulations [3] to determine the aluminum content in such devices.
Methods: Two GaN QWs with respective widths of 1.5 and 10 nm (Figure 1a) are studied, both surrounded by Al0.1Ga0.9N barriers. Both structures are grown by plasma assisted molecular beam epitaxy (MBE), and the samples are prepared with a Ga+ focused ion beam scanning electron microscopy (FIB-SEM) based on the standard lift-out method. STEM-EDX analyses are conducted using a probe-corrected TFS Titan Themis microscope operating at 200 kV and equipped with a Super-X detector system. Spectroscopic high-resolution data are acquired through a multi-frame spectrum-imaging approach, with thousands of frames rapidly acquired at high-resolution and automatically realigned thereafter. EDX quantification analyses are conducted using the ζ factors approach [4], and considers the inhomogeneity of the sample in the x-rays absorption correction process. Finally, beam propagation and EDX intensity maps were simulated using the µSTEM software [3].
Results: Figure 1b highlights the significant difference of EDX Al K emission observed between the two structures studied, when the probe is positioned at the middle of the respective QWs. The simulation of the probe propagation (Figure 1c) reveals that, for the 1.5 nm width layer, the electron wave is quickly delocalized into the adjacent barriers even for thin samples (~30 nm), explaining the disparity in intensity measured between the two structures. Quantification of this signal using the ζ factor method [4] estimates the Al content inside the 1.5 nm width QW around 1 at.%, significantly impacting the structure’s band properties. To understand the effect of such beam broadening on EDX quantification, we compare the experimental results with a simulated HR-EDX profile of Al K obtained from a given theoretical structure (Figure 1d). The chemical properties of this hypothetical structure, considering interfaces chemical gradient and well aluminum content, were adjusted until achieving optimal agreement between experimental and simulated profiles (Figure 1e). If a significant chemical gradient at the interfaces is confirmed, the results reveal that most of the Al K emission detected within the QW can be attributed by the propagation of EB in the surrounding layers.
Conclusion: This study aims to present a clear methodology to detect the effect of beam broadening on HR-EDX quantitative analyses. The demonstration is done on a regular heterostructure and conventionally (FIB) prepared sample, showcasing its potential application on various systems. In this presentation, we will particularly focus on which conditions this comparison between experimental data and simulations can be carried out to quantitatively detect these slight changes in chemical compositions at high spatial resolution. This work, performed on the Platform for NanoCharacterisation (PFNC) of CEA, was supported by the “Recherche Technologique de Base” Program of the French Ministry of Research.

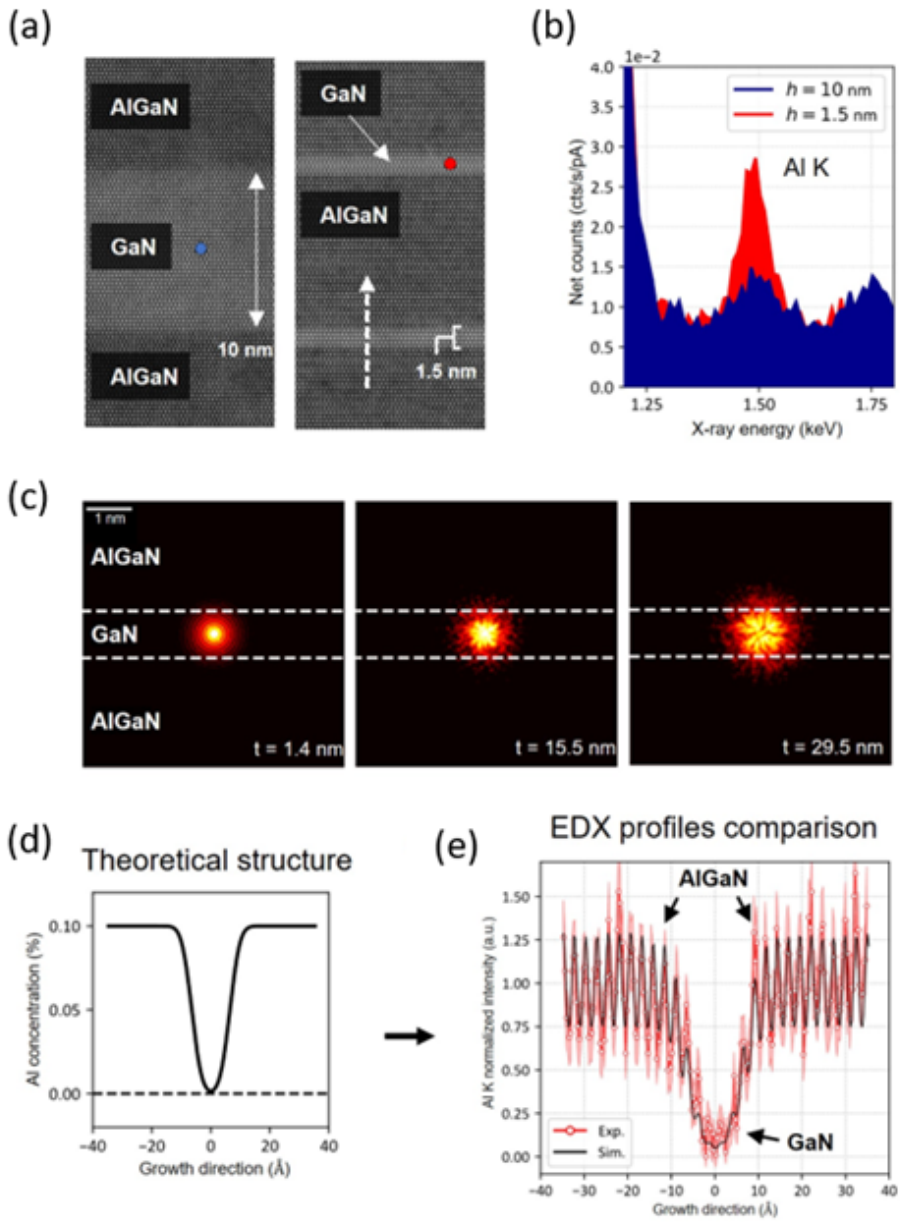

Figure 1. (a) High-resolution STEM-HAADF images of the two QW layers studied, indicating the electron beam position when performing EDX analysis. (b) Comparison of EDX Al K emission detected within the two QW layers, showing a clear increase of the peak intensity for the thinnest (1.5 nm width) layer. (c) Inelastic multislice simulation of the probe propagation in 1.5 nm width QW, showing the evolution of electron wave probability of presence at 3 different crystal thicknesses *t*. (d) Theoretical composition profile of the 1.5 nm thick QW used for the simulation of the x-ray production. (e) Comparison of the experimental and simulated high-resolution EDX Al K intensity profiles.

Keywords:

HR-EDX, chemical quantification, e-beam propagation

Reference:

[1] M. Asif Khan et al., Jpn. J. Appl. Phys. 44 (2005) 7191–7206.
[2] N.R. Lugg et al., Ultramicroscopy. 151 (2015) 150–159.
[3] L.J. Allen, A.J. D'Alfonso, S.D. Findlay, Ultramicroscopy. 151 (2015) 11–22.
[4] Watanabe, M. & Williams, D. B. J Microsc. 221 (2006) 89–109.

994

SEM-Cathodoluminescence Imaging and Spectroscopy - Applications in Archeology and Life Science

Dr. Ifat Kaplan-Ashiri[1]
[1]Electron Microscopy Unit, Department of Chemical Research Support, Weizmann Institute of Science, Rehovot, Israel

IM-05 (3), Lecture Theater 3, august 27, 2024, 10:30 - 12:30

Scanning electron microscopes (SEMs) are widely used as an imaging technique for any solid materials found on Earth. Newly synthesized materials, frozen biological samples, and geological and ancient materials can all be studied by SEMs. SEM-based spectroscopies, such as energy dispersive X-ray spectroscopy (EDS) and cathodoluminescence (CL), are applied to study the composition and structure of various samples. SEM-CL imaging and spectroscopy detect the emitted photons in the visual range. The luminescence results from band transitions can be related to different material properties, such as band gap, crystallinity, impurities, and defects in the structure.
We have been using SEM-CL as an imaging and spectroscopy tool in different fields, including less-studied ones such as archeology and life science. CL spectral measurements of $CaCO_3$ samples were performed as part of research in archeology, and the CL imaging of cholesterol crystals was implemented as part of a complete workflow to study their 3D structure.
Materials such as calcium carbonates ($CaCO_3$) found in archeological excavations can be studied with SEM-CL as their intrinsic defects and dopants create luminescent centers that can be detected. The various forms of $CaCO_3$ have unique defects that can be revealed by detecting the luminescence of the crystals. SEM-CL was used to study $CaCO_3$ in different forms: calcite and aragonite, which nucleate through geogenic and biogenic pathways, and pyrogenic lime plaster. The structural variations in $CaCO_3$ from various origins were measured by SEM-CL and correlated with radiocarbon dating (1-3). Using SEM-CL and complementing it with other analytical techniques, we formed a database of $CaCO_3$ samples from different sources. This database is of great importance in identifying the form of $CaCO_3$ when sorting materials from archeological excavations and increasing the accuracy of age determination by carbon dating.
SEM-CL of organic materials is quite challenging as their luminescence decay very fast under the irradiation of the electron beam. Cholesterol crystals are CL active and stable enough to be detected and imaged. Cryo SEM-CL was used as a first step in a correlative workflow that was developed to study atherosclerotic lesions in three dimensions at the nanometer scale. The cholesterol crystals and lipid droplets, both luminescence active, were identified by CL imaging. Following the CL imaging, the crystals were identified using SEM and moved to the FIB-SEM for volume imaging, all done under cryo conditions. The results of this workflow show that thin crystals appear to be associated with intracellular or extracellular lipid droplets and multilamellar bodies. The large crystals are independently positioned in the tissue and are not associated with specific cellular components (4).
In summary, SEM-CL studies of $CaCO_3$ samples and cholesterol crystals revealed the opportunity to use this method to explore materials and systems in fields such as life science or archeology.

Keywords:

Cathodoluminescence, SEM, Cryo, $CaCO_3$, Cholesterol

Reference:

1- Michael B. Toffolo, Giulia Ricci, Luisa Caneve, Ifat Kaplan-Ashiri. Luminescence reveals variations in local structural order of calcium carbonate polymorphs formed by different mechanisms. Scientific Reports, 9(1), 16170, 2019.

2- Michael B. Toffolo, Giulia Ricci, Rémy Chapoulie, Luisa Caneve, Ifat Kaplan-Ashiri. Cathodoluminescence and laser-induced fluorescence of calcium carbonate: A review of screening methods for radiocarbon dating of ancient lime mortars. Radiocarbon 62(3), 545-564, 2020.
3- Michael B. Toffolo, Lior Regev, Eugenia Mintz, Ifat Kaplan-Ashiri, Francesco Berna, Stéphan Dubernet, Xin Yan, Johanna Regev, Elisabetta Boaretto. Structural characterization and thermal decomposition of lime binders allow accurate radiocarbon age determinations of aerial lime plaster. Radiocarbon, 62(3), 633-655, 2020.
4- Jenny Capua-Shenkar, Neta Varsano, Noya-Ruth Itzhak, Ifat Kaplan-Ashiri, Katya Rechav, Xueting Jin, Manabu Niimi, Jianglin Fan, Howard S Kruth, Lia Addadi. Examining atherosclerotic lesions in three dimensions at the nanometer scale with cryo-FIB-SEM. Proceedings of the National Academy of Sciences, 119(34), e2205475119, 2022.

1005

Hyperspectral CT allows for non-destructive elemental imaging in museum specimen

Henrik Lauridsen[1], Daniel Klingberg Johansson[2], Christina Carøe Ejlskov Pedersen[3], Kasper Hansen[3], Michiel Krols[4], Kristian Murphy Gregersen[5], Julie Nogel Jæger[5], Catherine Jane Alexandra Williams[6], Ditte-Mari Sandgreen[7], Aage Kristian Olsen Alstrup[1,8], Mads Frost Bertelsen[9,10], Peter Rask Møller[2]
[1]Department of Clinical Medicine, Aarhus University, , Denmark, [2]Natural History Museum of Denmark, University of Copenhagen, , Denmark, [3]Department of Forensic Medicine, Aarhus University, , Denmark, [4]TESCAN XRE, , Belgium, [5]Institute of Conservation, Royal Danish Academy, , Denmark, [6]Department of Animal and Veterinary Sciences, Aarhus University, , Denmark, [7]Givskud Zoo-Zootopia, , Denmark, [8]Department of Nuclear Medicine & PET, Aarhus University Hospital, , Denmark, [9]Center for Zoo and Wild Animal Health, Copenhagen Zoo, , Denmark, [10]Department of Veterinary Clinical Sciences, University of Copenhagen, , Denmark

IM-05 (3), Lecture Theater 3, august 27, 2024, 10:30 - 12:30

Background incl. aims
Fluid preserved animal specimens in the collections of natural history museums around the world constitute an invaluable archive of past and present animal diversity. Many researchers rely on these collections for e.g. anatomical, taxonomical and genetic studies. In recent years, non-invasive imaging techniques such as x-ray computed tomography (CT) and magnetic resonance imaging (MRI) are increasingly being used to extract anatomical information from preserved specimens without harm. Although conventional CT allows for precise measurement of radiodensity (often corresponding to physical density) and MRI can be weighted to highlight contents of interest (e.g. water, fat, bone, etc.), these techniques generally do not allow for high resolution element specific mapping i.e. only showing contrast agents or foreign objects made of a certain element.
In museum specimens, sometimes foreign objects have been introduced perimortem or postmortem e.g. projectile residues from the collection process or objects used for mounting the specimen. These foreign objects often consist of heavy metals and thus severely impact imaging and related measurements such as the estimation of bone mineral content. Also, they may constitute a health issue for collection staff. Therefore, a non-destructive method to identify elemental contents deep within museum specimens is desirable. Here we aimed to use hyperspectral micro-CT imaging to non-destructively determine the elemental content of a prized platypus specimens in the vast collection of fluid preserved mammals at the Natural History Museum of Denmark. This was the Dana platypus from The Carlsberg Foundation's Oceanographical Expedition round the World 1928-30 (a.k.a. the fourth Dana expedition). This specimen contained large centimeter-sized nodules with an unknown content.
Methods
The neurocranium and part of the bill of the Dana platypus was imaged using a UniTOM XL Spectral system (TESCAN GROUP, Brno, Czech Republic) equipped with a hyperspectral detector (channel size of 1 keV) with the following parameters: x-ray tube voltage = 160 kVp, x-ray tube current = 94 µA, x-ray tube power = 20 W, integration time = 83 ms, field-of-view = 76.4 × 76.4 × 27.1 mm3, spatial resolution = 0.108197 mm, acquisition time = ~10 h. K-edge subtraction to highlight the lead (Pb) signal (K-edge at 88.0045 keV) was performed using 1 channels width and 3 channels separation (91 keV – 85 keV).
Results
Different elements have different x-ray attenuation signatures in function of the x-ray photon energy. Hyperspectral CT clearly detected a K-edge at 88 keV in regions of interest placed within the foreign objects of the Dana platypus, which was not observed within bone voxels. This allowed for K-edge subtraction (integrating and subtracting channels on either side of a K-edge to produce element

specific images) and the precise mapping of Pb in the neurocranium of the Dana platypus. In addition to confirming the presence of large concentrations of Pb in the foreign objects within the Dana platypus, hyperspectral imaging also showed that the widely distributed small dense particles within the fur of the specimen were not corroded lead residues nor another heavy element material e.g. arsenic or mercury residues from previous preservation methods.

Conclusion

In addition to widely used CT imaging and increasingly used MRI for museum specimen imaging, hyperspectral CT adds another dimension by providing element specific information. In this case demonstrating the content of heavily corroded lead shotgun pellets inside a >100 years old platypus specimen.

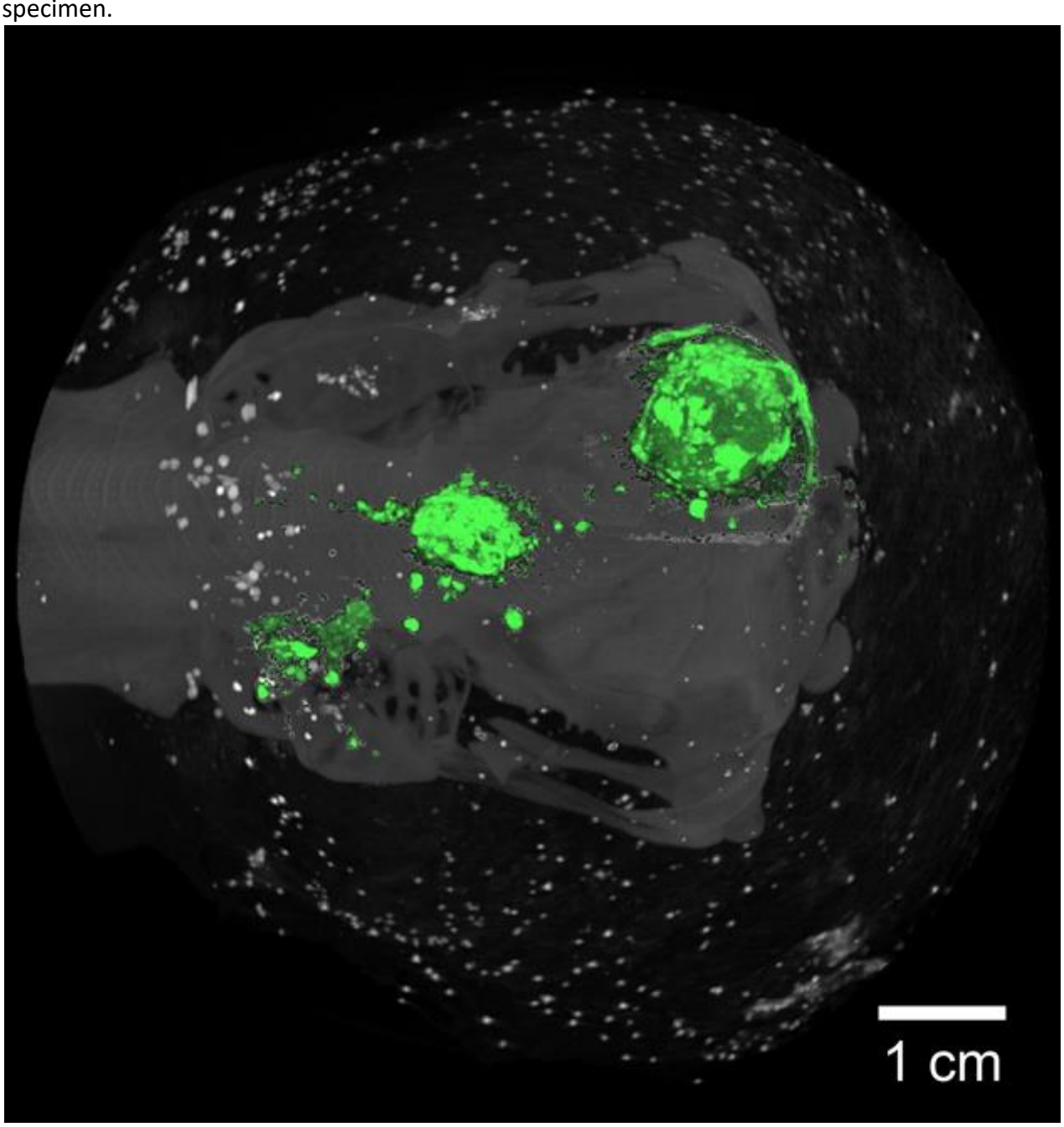

Keywords:

X-ray computed tomography, lead, non-invasive

121

Multidimensional Characterisation and Multivariate Analysis of Cu3P Nanocages for Catalysis

Dr. Andrea Griesi[1], Mr. Rundong Mao[2], Mr. Sirous Khabbazabkenar[1], Mr. Yurii Ivanov[1], Mr. Guohua Jia[2], Mr. Giorgio Divitini[1]
[1]Ististuto Italiano di Tecnologia, Genova, Italy, [2]Curtin University , Perth, Australia

Poster Group 1

"Multidimensional Characterisation and Multivariate Analysis of Cu3P Nanocages for Catalysis"
Dr. Andrea Griesi1, Mr. Rundong Mao2, Dr. Sirous Khabbazabkenar1, Dr. Yurii P Ivanov1, Dr. Guohua Jia2, Giorgio Divitini1.
1 Istituto Italiano di Tecnologia, Electron Spectroscopy and Nanoscopy, Genova 16163, Italy.
2 Curtin Institute of Functional Molecules and Interfaces School of Molecular and Life Sciences, Curtin University GPO Box U1987, Perth, WA 6845, Australia.

Background:
The use of nanomaterials in catalysis has consistently sparked significant scientific interest, primarily due to their high surface-to-volume ratio and the ability to finely control active sites. This study focuses on exploring the characteristics of Cu3P engineered in the shape of nanocages, with promise as a catalyst for CO2 reduction[1]. To achieve a comprehensive understanding of the system, we combined the 3D morphology obtained via electron tomography with compositional data from energy-dispersive X-ray spectroscopy (EDX), and local chemical states estimates from electron energy loss spectroscopy (EELS). The resulting understanding of the Cu3P nanocages will lead to optimal design of the structures and improvement of the catalytic performance.
Methods:
In our investigation of Cu3P nanocages, we utilised a probe-corrected ThermoFisher Spectra 300 transmission electron microscope (TEM) to define their morphological, structural, and elemental characteristics at high spatial resolution. We acquired several tilt series over a tilt range of at least 120° over isolated and assembled nanoparticles. STEM-EDX data were acquired using a Dual-X detector (collection angle ~1.7 sr), while EELS data were acquired in a Continuum GIF. Additionally, for a comprehensive examination of this nanosystem, we conducted an extensive compositional study by integrating machine learning algorithms[2] with hyperspectral EDX and EELS datasets.
Results:
Through the synergistic application of these different techniques, we gained a comprehensive understanding of structural and electronic properties of Cu3P nanocages, with an average size of 15 nm. Multivariate analysis played a crucial role in discerning compositional variations within these nanostructures. In particular, principal component analysis (PCA) and non-negative matrix factorisation (NMF) were employed on both compositional datasets (EDX and EELS core loss), allowing a deep understanding of the elemental distribution within the nanocages. This approach allowed us to uncover subtle differences in the elemental distribution of nanocages, shedding light on the intricate interplay between morphology, structure and elemental composition in these catalytic nanostructures. The analysis of the fine structure of EELS edges also enables the differentiation between oxidation states for copper through the structure. Such multidimensional analysis not only improves our understanding of Cu3P nanocages, but also shows the power of integrating microscopy techniques and advanced data analysis methods that enable comprehensive characterisation of nanomaterials. In addition, by combining electron tomography information with compositional information, we were able to visualise the three-dimensional morphology of nanocages, providing fundamental information about the nature of these catalysts.

Conclusion:
This research contributes to the advancement of nanocatalysis and underscores the paramount importance of microscopic investigations in comprehending and refining catalytic processes. The combination of various techniques, such as EELS, EDX, and electron tomography within a TEM, presents a complete approach to studying nanocatalysts like Cu3P nanocages for CO2 reduction. These methodologies enable an in-depth examination of the structural characteristics, elemental composition, and three-dimensional morphology of catalysts. Concurrently, this study serves as a demonstration of the role played by machine learning algorithms in processing microscopy data. The synergy between machine learning and the advanced capabilities of next-generation microscopes introduces novel avenues for researchers to efficiently optimise and refine the interpretation of generated data, thereby unlocking the full potential of advanced microscopy technologies.
Keywords:

Machine Learning, Catalysis, Electron Tomography, hyperspectral imaging

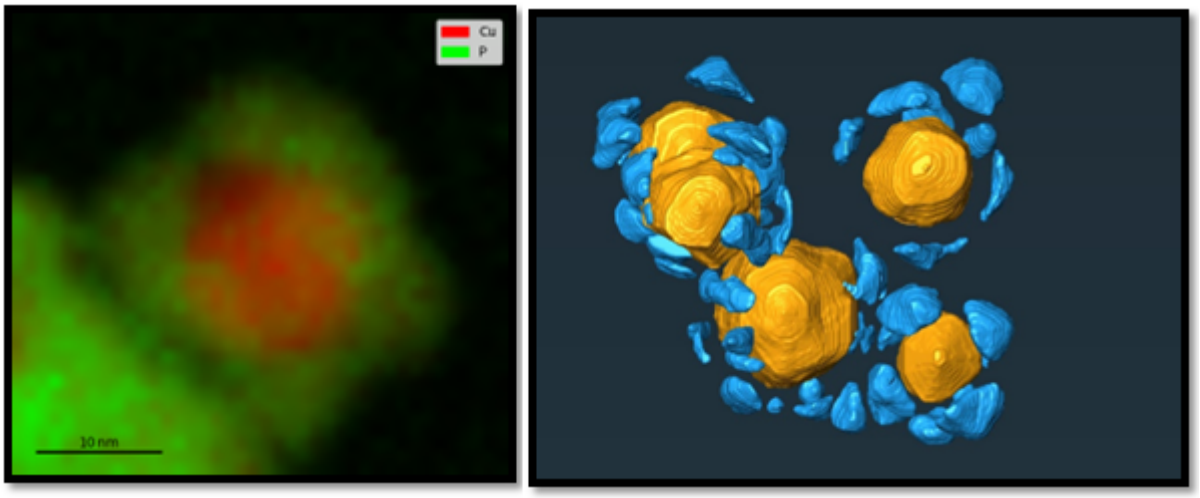

Keywords:

Machine Learning, Electron Tomography, hyperspectral

Reference:

C. A. Downes, N. Libretto, A. E. Harman-Ware, R. M. Happs, D. A. Ruddy, F. G. Baddour, J. R. Ferrell III, S. E. Habas, and J. A. Schaidle, ACS Appl. Energy Mater. 3, 10435 (2020).
2. S. Cacovich, F. Matteocci, M. Abdi-Jalebi, S. D. Stranks, A. Di Carlo, C. Ducati, and G. Divitini, ACS Appl. Energy Mater. 1, 7174 (2018).

163

EELS at Extreme Energy Losses; complementary Information to X-ray Absorption Spectroscopy (XAS) in a TEM

Dr Sorin Lazar[1], Mrs. Maria Meledina[1], Mrs. Claudia S. Schnohr[2], Mr. Thomas Hoeche[3], Mr. Peter Tiemeijer[1], Mr. Paolo Longo[1], Mr. Bert Freitag[1]
[1]Thermo Fisher Scientific, Eindhoven, Netherlands, [2]Felix Bloch Institute for Solid State Physics, Leipzig, Germany, [3]Fraunhofer-Institut für Mikrostruktur von Werkstoffen und Systemen IMWS, Halle (Saale), Germany

Poster Group 1

Energy electron loss spectroscopy is already an established technique to study structure and property relationship required to optimize materials and make break-through inventions in material science. So far EELS lacks performance at energy losses higher than 2 keV to obtain bonding or coordination state information via ELNES or EXELFS with high lateral resolution [1]. We used a new optical setup designed to optimize the coupling between spectrometer and post-specimen optics for high energy resolution and high collection efficiency. The new optical setup allows to minimize the acquisition time (minutes) and the beam current to avoid sample damage or drift artifacts and to achieve results beyond the earlier attempts reported in literature [2].
The real application benefit in EELS is its spatial resolution which is much better than the micron resolution that XAS can achieve. A challenge lays in analysis of elements in low concentration due to the signal strength. For this reason we have made a comparison between XAS and EELS data from a sub-micron size precipitate on the Zr_L23 edge in high-strength, translucent glass-ceramics in the system MgO-ZnO-Al2O3-SiO2-ZrO2 with only 5.8% Zirconia in the compound [3]. The comparison of ELNES with XANES reference data clearly reveals that the coordination is CN=8.
For a more quantitative comparison the setup was used to acquire Cu_K edge at 8.98 keV energy loss from metallic Cu, CuO and Cu2O. The EELS data is benchmarked against XAS data in XANES and EXELFS and relevant information is extracted from the EELS data using similar analysis as done for XAS data. It is noteworthy to mention that the results show an excellent match of EXELFS and EXAFS and the EELS data allows extracting the bond length with very good accuracy as it will be shown in this work.
In order to further assess the optimization of the entire EELS optics including the S/TEM column we have acquired a series of K-edges at extreme energy loses namely the Mo K-edge at 20 keV, Ag K-edge at 25.5 keV and Sb K-edge at 30.5 keV as presented in figure 1 (from left to right: Cu K-edge, Mo K-edge and Ag K-edge) and for some of the materials the bond length has been calculated from the EELS data.
With this work we will also discuss the limitations of the current technology and how they are mitigated by the deep integration of the filter in the optics on the new platform.
The integrated approach optimizing the entire EELS optics including the S/TEM column enables this increase in performance. The examples presented show the power of correlative studies involving X-ray absorption spectroscopy (XAS) and high loss EELS, which opens new applications to combine the advantages of both techniques.

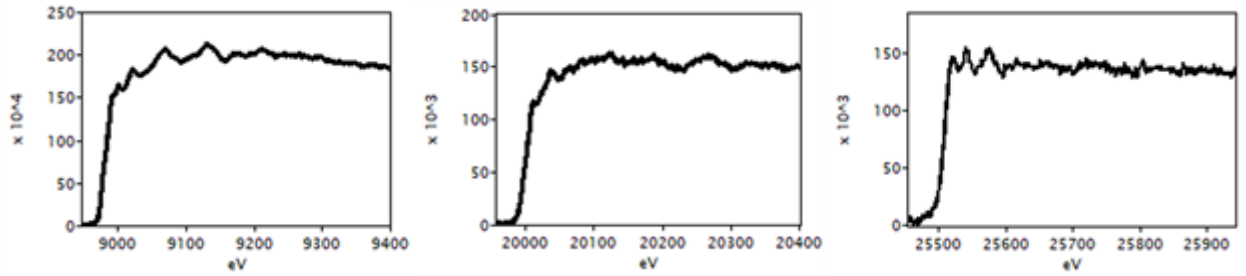

Keywords:

XAS, EELS, TEM

Reference:

[1] L M Brown (1997) In: J M Rodenburg (ed.) Electron Microscopy and Analysis 1997: pp. 17–22 (IOP Publishing Ltd, Bristol)
[2] Ian MacLaren, Kirsty J. Annand, Colin Black, and Alan J. Craven, Microscopy, Volume 67, Issue suppl_1, March 2018, pp78-85,2017
[3] Sabrina Seidel et. al. https://doi.org/10.1039/C6RA10353G

249

Maximizing Speed and Sensitivity: Simultaneous High-throughput EDS-WDS Elemental Mapping in the SEM

Shangshang Mu[1], David Stowe[1]
[1]Gatan/EDAX, Pleasanton , United States

Poster Group 1

Background incl. aims
High-throughput Scanning Electron Microscopy-Energy Dispersive X-ray Spectroscopy (SEM-EDS) elemental mapping ensures the acquisition of multiple elemental maps simultaneously (hyperspectral mapping) within minimal timeframes. This process requires a high beam current on the SEM side to generate high input of X-ray counts, coupled with fast electronics of the Silicon Drift Detector (SDD) to operate at short pulse processing times, thereby efficiently converting incoming X-rays into output X-ray counts. However, shorter pulse processing times may lead to a low energy cut-off, as the noise level becomes comparable to that of the signal from low energy X-rays, presenting a challenge for high-throughput EDS mapping of light elements. While Wavelength Dispersive X-ray Spectroscopy (WDS) exhibits lower throughput than EDS at equivalent beam currents, its superior sensitivity and higher peak-to-background ratio enable better detection of light elements that may be difficult to observe using EDS alone. Therefore, simultaneous WDS mapping of light elements and high-throughput EDS mapping of higher-Z elements can facilitate rapid and accurate determination of element distribution for both light and higher-Z elements.
Methods
To demonstrate this capability, a boron steel sample was mapped using an EDAX Octane Elite Super EDS detector and an EDAX Lambda Plus WDS detector (Gatan inc.) in a Field Emission SEM. The beam current was set at 75 nA to achieve approximately 250,000 counts per second (cps) on the EDS detector. Capitalizing on advancements in SDD efficiency [1], a pulse processing time of 0.48 µs was used, resulting in an output of approximately 190,000 cps. An 80 Å diffracting crystal combined with polycapillary optics in the WDS detector were utilized to map B K. The region of interest was simultaneously mapped using EDS and WDS for a duration of 2 hours in the EDAX APEX 3.0 software (Gatan inc.). Drift corrections by the software were applied to compensate for sample drift induced by the high beam current.
Results
The SEM image (Figure 1a) unveils grains clusters segregated by relatively large melt-like pockets ranging from 5 to 25 µm in size. Orientation contrast highlights individual grains approximately 5-10 µm in size, with melt-like features as small as 1 µm developed at triple junctions. The resulting elemental maps are 512x400 pixels. The Co K EDS map (Figure 1b) illustrates a higher Co concentration within the grains in comparison to the melt-like pockets, while the Fe distribution depicted by EDS (Figure 1c) displays an inverse correlation with Co levels. Leveraging the superior sensitivity and high peak-to-background ratio of WDS, the WDS map of B K (Figure 1d) distinctly reveals a significantly higher concentration within the melt-like pockets and a depletion within the grains. However, due to the superfast pulse processing time utilized, the EDS map of B K (Figure 1e) fails to show the pronounced concentration contrast between melt-like pockets and grains.
Conclusion
In summary, simultaneous EDS-WDS mapping at a high beam current successfully delineated the element distribution for both the light element boron and the transition metals in a boron steel sample. By harnessing the benefits of both techniques, simultaneous high-throughput EDS-WDS mapping enables the acquisition of high-quality X-ray map data within the shortest possible timeframe.

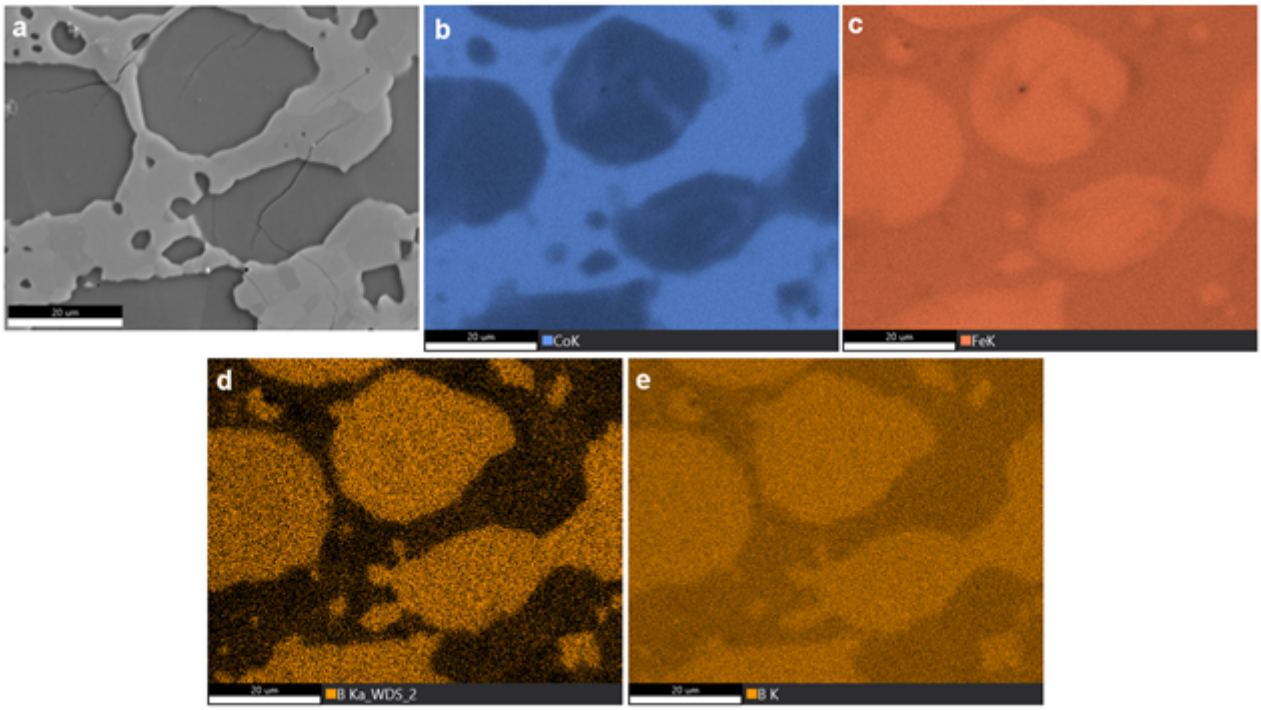

Keywords:

EDS-WDS, mapping, high-throughput, light elements

Reference:

[1] T Nylese and J Rafaelsen, Microscopy Today 25 (2017), p. 46. doi:10.1017/S1551929517000190

277

Fast and low dose EELS using compressive sensing

Alex Robinson[1], Jack Wells[1,2], Daniel Nicholls[1], Giuseppe Nicotra[3], Nigel Browning[1,4]
[1]SenseAI Innovations Ltd., Liverpool, United Kingdom, [2]Distributed Algorithms Centre for Doctoral Training, Liverpool, United Kingdom, [3]CNR-IMM, Catania, Italy, [4]University of Liverpool, Liverpool, United Kingdom

Poster Group 1

The scanning transmission electron microscope (STEM) can capture a multitude of signals corresponding to the structural and chemical properties of a material. Examples of these methods include bright/dark field imaging, energy dispersive x-ray spectroscopy (EDS), or electron energy loss spectroscopy (EELS) [1]. EELS is of particular interest due to its sensitivity to low-mass elements and ability to determine their oxidation states, chemical bonding, and spatial distribution. An EEL spectrum is challenging to acquire due to low signals, energy spread of the beam, and the sensitivity of the detector. Furthermore, the stability of the sample is compromised due to the acquisition speed, which is a combination of signal limitations and camera read-out speed. One solution to overcome these limitations is the use of probe sub-sampling, whereby only a subset of probe locations is acquired with respect to the typical scanning grid. This has been shown to work for various STEM techniques such as 2-D imaging, EDX, and 4-D STEM [2,3]. Our goal is to apply these same strategies to EELS acquisition to increase speed whilst maintaining the structural and chemical analysis of the material.

A focused electron probe is aligned and the scan coils are connected to a scan generator to allow for a customised scanning pattern. The electron probe is then positioned at the sub-sampled probe locations and the EELS spectra acquired. For real time imaging, a subset of energy losses can be inpainted using a GPU implementation of the Beta Process Factor Analysis (BPFA) algorithm [4] on-the-fly to allow for finer alignment of the probe. For offline analysis, the data is reshaped to form a 3-D dataset where the first two dimensions correspond to probe locations, and the final dimension is a specific energy loss. This data is then inpainted using the BPFA with a 3-D patch. This process is depicted in Fig. 1.

To test this method, we simulated a sub-sampled EELS experiment using a silicon carbine sample with graphene grown on the carbon face [5]. The dataset contains 17x104 probe locations with a scan step of 0.13nm, and an energy width on the camera of 0.25eV (2048 channels). The dataset was tested using only 25% of the original data. The results (given in Fig.1) show that the data can be recovered to achieve functionally identical results to that of the original, full-sampled dataset.

This work has shown that atomic resolution EELS can be achieved with far fewer measurements of the sampling grid. By employing these methods, STEM-EELS can be faster, lower dose, and importantly accessible for potentially beam sensitive or dynamic samples. In this talk, we will present experimentally acquired data using a JEOL GrandARM2, with the goal of demonstrating practical implementation of this method.

Figure 1: Method for acquiring probe sub-sampled EELS data (left). The PC determines the scanning pattern which is connected to a scan engine to change the scan coil voltages. The EELS spectra is formed by integrating the camera signal column-wise, an this spectra is then used to form energy filtered images which can be inpainted using SenseAI's inpainting algorithm. In this case, an example of reconstructed EELS data and corresponding spectra are given. EELS spectra with zoom in at carbon π* and σ* characteristic peaks (top right). Example of integrated EELS maps at 285-286 eV energy loss for 25% probe sub-sampled data (bottom right).

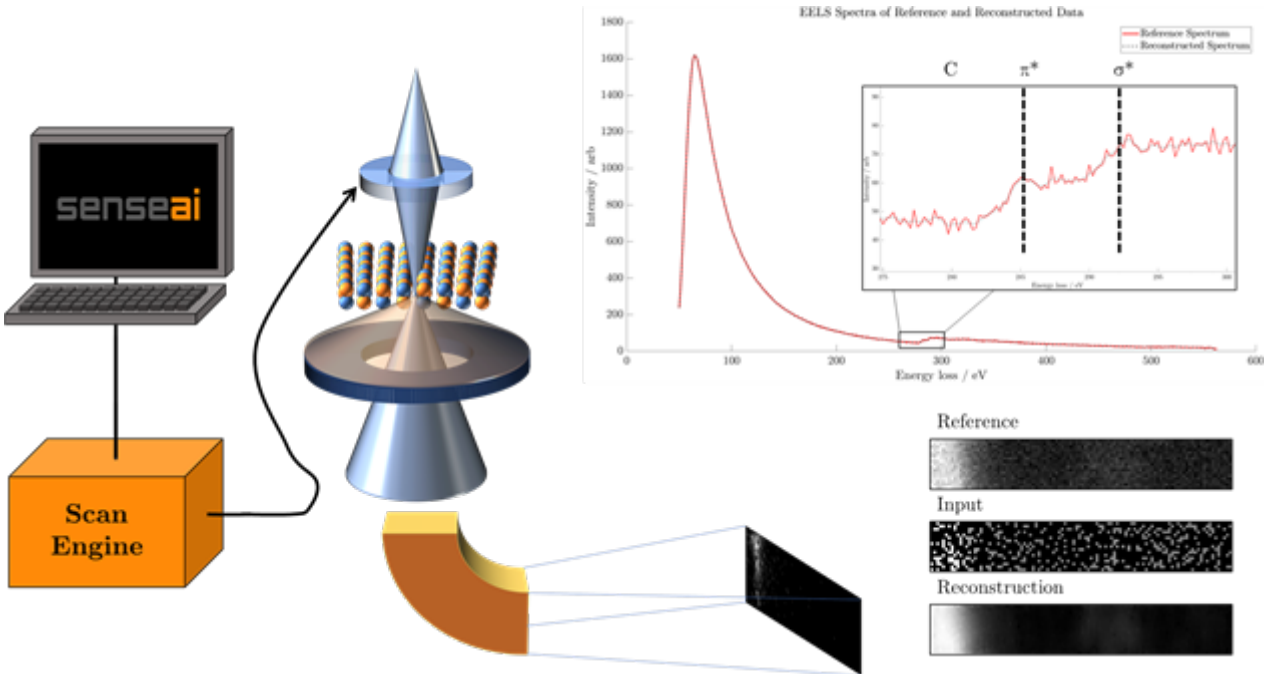

Keywords:

STEM, EELS, compressive sensing, sub-sampling

Reference:

[1] L.M. Brown, 1981, Journal of Physics F: Metal Physics, 11(1), p.1.

[2] D. Nicholls et. al., 2022, In ICASSP 2022-2022, (pp. 1586-1590). IEEE.

[3] A.W. Robinson, et. al., 2023, arXiv preprint arXiv:2309.14055.

[4] S. Sertoglu, and J. Paisley, 2015, in 23rd EUSIPCO, (pp. 2771-2775). IEEE.

[5] G. Nicotra et. al., 2015, Physical Review B, 91(15), p.155411.

354

Quantification and denoising of atomic-resolution EDX spectrum images using a Multiscale Bayesian Approach

Pau Torruella-Besa[1], Abderrahim Halimi[2], Duncan T. L. Alexander[1], Cécile Hébert[1]
[1]Electron Spectrometry and Microscopy Laboratory (LSME), Institute of Physics (IPHYS), Ecole Polytechnique Fédérale de Lausanne (EPFL), Lausanne, Switzerland, [2]School of Engineering and Physical Sciences, Heriot-Watt University, Edinburgh, United Kingdom

Poster Group 1

While latest generation aberration-corrected microscopes have enabled atomic-resolution scanning transmission electron microscopy (STEM) imaging to be relatively straightforward and accessible, atomic resolution spectroscopy, and in particular energy dispersive X-ray (EDX) spectroscopy, remains a challenge. Aside from having a suitable aberration-corrected probe, the relatively long of acquisition times necessary for achieving reasonable signal-to-noise ratios (SNR) impose tougher constraints on stage stability, optics and beam stability, and the resiliency of the sample to beam damage and contamination. To tackle this challenge, microscopists will often apply a simple directive: “acquire faster”. This is the motivation behind the development of EDX detectors with an increasingly large solid angle. However, there is a second way to approach the problem: using more sophisticated data analysis to be able to reduce acquisition times.

In this work, we propose the use of a multiscale Bayesian estimation strategy to deal with the extreme noise and signal sparsity observed in atomic-resolution EDX data. The method, originally developed for noisy LIDAR data[1], relies on two factors. First, it assumes pre-known contributions to the EDX spectrum from each chemical element. In the present work, the elemental contributions to the spectra are obtained from the espm library[2]. It should be noted that, since the espm-generated priors are themselves scaled by the corresponding k-factors, their corresponding abundance maps enable proper atomic percentage quantification. Secondly, it adopts a multiscale model that accounts for the Poisson statistics of the data and exploits spatial correlation between pixels to provide robust abundance estimates of each element in each pixel, even in the presence of high noise. The outputs of the algorithm are maps of the X-ray signal quantified in atomic percentage, which are considerably denoised, and corresponding Bayesian uncertainty maps.

The method has first been tested using (non-atomic) simulated EDX datasets generated using espm, which allow comparison to a ground truth (Figure 1 left). The plot shows the deviation from the ground truth abundance maps as a factor of SNR or, equivalently, virtual acquisition time. These outputs are compared to those made using a commercial analysis software: Velox from Thermo Fisher Scientific. As can be observed, the Bayesian multiscale (BMS) analysis demonstrates better accuracy, especially in low SNR situations, where it is shown to converge more quickly to the ground truth.
Next, the analysis method is tested on a wide range of experimental EDX spectrum images, acquired from several types of samples. Figure 1 right shows an example, where both Velox spatial filtering and BMS are applied to an atomic-resolution EDX spectrum image acquired from a film of $LaVO_3$ grown epitaxially on a $DyScO_3$ substrate (see reference 3 for details). Raw integrated counts maps are also included for comparison. This case is especially interesting, since it demonstrates the conservation of spatial resolution through the multiscale approach. The results shown below show that the obtained quantified maps of X-ray yield keep atomic resolution even when reducing the acquisition time by a factor 3. As can be observed in Figure 1 a–f, the spots in the Fourier transform of the calculated maps are still clearly visible for the BMS analysis at the lowest acquisition time, while they are lost for the spatial filtering of the Velox analysis, proving that our method enhances

spatial resolution even under the most challenging conditions. (We note that these are not absolute maps of atomic columns, owing to scattering processes such as channeling and dechanneling.)

In summary, we present a novel strategy for the denoising of atomic-resolution EDX spectrum images, that incorporates both knowledge of spectral shape and Bayesian multiscale analysis. Testing of this algorithm on experimental data sets acquired from a range of samples shows a consistently better performance compared to quantification and denoising using state-of-the-art commercial software.

Figure 1 Left) Simulated EDX maps results: abundance maps mean error as a function of simulated acquisition time. Right) Overlaid elemental maps of Dy (green). Sc (red), La (orange) and V (Blue) from an $LaVO_3$ thin film on $DyScO_3$ substrate. Rows represent different acquisition times (obtained by reducing the number of frames used), while columns represent the different analysis methods tested: raw integrated peak counts, Velox quantification with 10 pixel Gaussian smoothing, and Bayesian multiscale approach. Fourier transform panels a, c, e correspond to the BMS analysis at the corresponding acquisition times, while b, d, f correspond to the Velox-filtered maps.

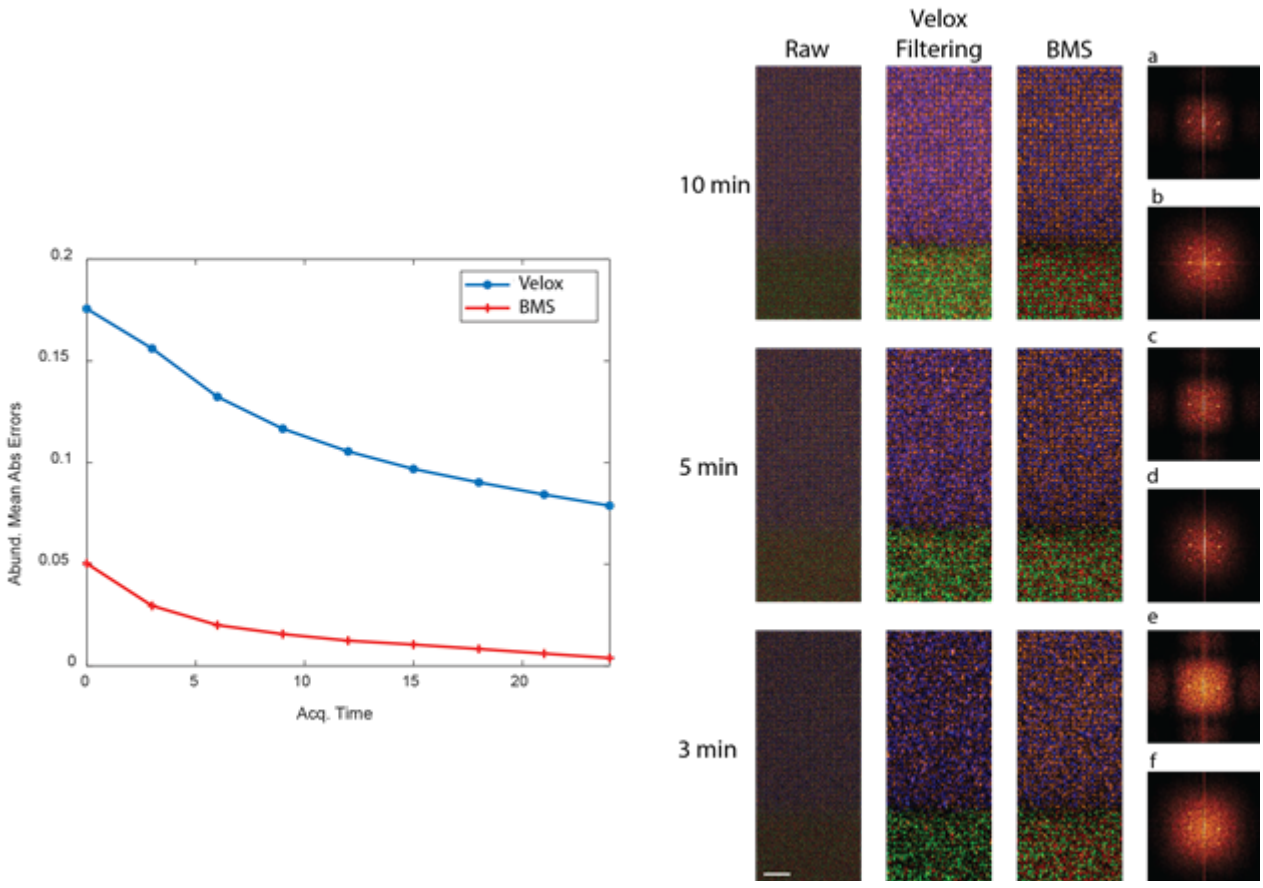

Keywords:

EDX, Bayesian analysis, atomic-resolution STEM-HAADF

Reference:

1. A. Halimi, A. Maccarone, R. Lamb, G. Buller, S. McLaughlin, "Robust and Guided Bayesian Reconstruction of Single-Photon 3D Lidar Data: Application to Multispectral and Underwater Imaging," IEEE Trans. Computational Imaging, vol. 7, p 961-974, Sept. 2021
2. Teurtrie, A. et al. espm: A Python library for the simulation of STEM-EDXS datasets. Ultramicroscopy 249, (2023).
3. Alexander, D. T. L. et al. Switching plane: A novel crystalline interface in orthorhombic perovskite films. (2024). https://arxiv.org/abs/2401.08798

372

Reducing user-interaction in the processing of electron energy-loss spectra

Mr. Daen Jannis[1,2], Dr. Wouter Van den Broek[3], Mr. Jo Verbeeck[1,2]
[1]University of Antwerp, Electron Microscopy for Materials Research (EMAT), Antwerp, Belgium, [2]University of Antwerp, Nanolab Center of Excellence, Antwerp, Belgium, [3]Thermo Fisher Scientific, Eindhoven, Netherlands

Poster Group 1

Background
Conventional processing of electron energy-loss spectra (EELS) relies heavily on user-determined parameters, like for instance location and width of a background window, or choice of fine structure region. This makes results operator-dependent, more subjective and harder to reproduce.
Here we introduce a model-based processing of EEL spectra that relies on a linear model for which physical constraints are derived and subsequently imposed with the aid of quadratic programming. The model's linearity ensures fast convergence and the absence of local optima. Since the model includes all relevant EELS-features---background, atomic cross sections, fine structure, and multiple scattering---minimal user-interaction is required.
Methods
The background is described as a sum of 4 to 5 power-laws with fixed exponents ranging from -1 to -5. During the fit the coefficients are subjected to constraints that ensure non-negativity, monotonous descent and convexity. This background was proven to hold for energy ranges up to 1500 eV and to be superior to the conventional power-law background model [1].
The atomic cross sections are taken from a data base [2] that contains all edges of all elements up to atomic number 108. They were obtained from numerical relativistic solutions to the Dirac equations.
The fine structure is modeled as a quadratic spline with either linearly or quadratically spaced sample points. Working out the Bethe sum rule, assuming independent atomic shells and the dipole approximation, shows that the fine structure must have a weighted sum of zero. This constraint, too, is enforced through quadratic programming.
Results
In the figure the elemental maps of a TbScO3 sample are shown, in order to compare our approach to three alternative methods:
1. Unconstrained fit, with fine structure, no energy ranges excluded from fit.
2. Unconstrained fit, without fine structure, fine structure region excluded from fit.
3. Conventional approach: background region in front of each edge, background extrapolated and subtracted.
These 3 methods require a substantial amount of user choices, which we made to the best of our abilities. In comparison, our unsupervised approach yields the highest-contrast elemental maps, while offering a better precision, as demonstrated in the concentration histograms in the figure.
Conclusions
Imposing physical constraints on the EELS model through quadratic programming---in this case non-negativity, monotonous descent and convexity for the background, and the Bethe sum rule for the fine structure---greatly improves the quality of the result and removes most of the user-dependent input from the fitting process.

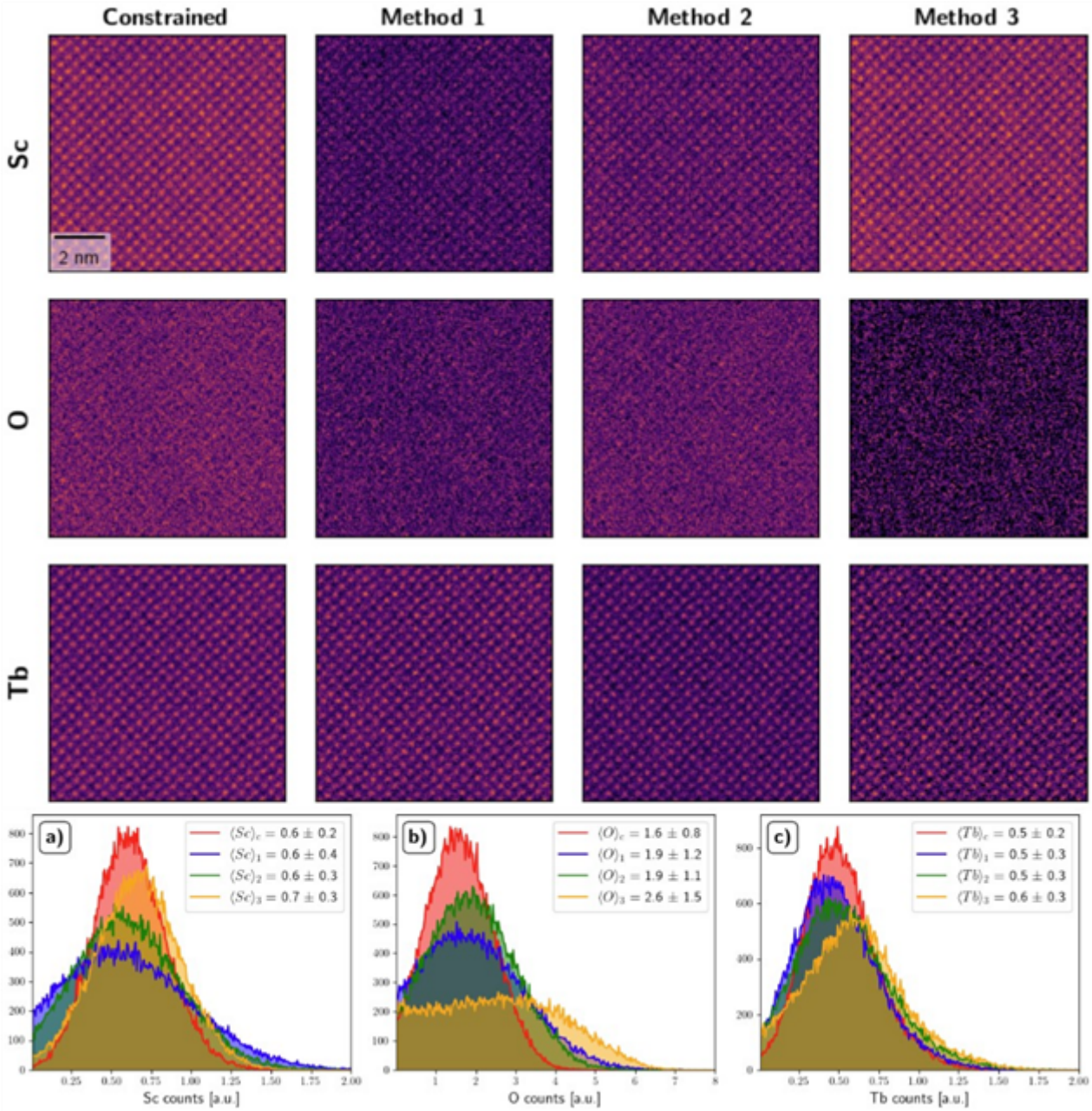

Keywords:

EELS; Constrained optimization; Background; Fine-structure

Reference:

[1] W. Van den Broek et al. Ultramicroscopy 254 (2023) p. 113830
[2] Z. Zhang et al. https://zenodo.org/records/7729585

374

Relativisitic EELS cross-sections for all elements

Dr Zezhong Zhang[1,2,3], Dr. Ivan Lobato[4], Dr. Hamish G. Brown[5], Dr. Daen Jannis[1,2], Prof. Johan Verbeeck[1,2], Prof. Dirk Lamoen[1,2], Prof. Sandra Van Aert[1,2], Prof Peter D. Nellist[3]
[1]EMAT, University of Antwerp, Antwerp, Belgium, [2]NANOlab Center of Excellence, University of Antwerp, Antwerp, Belgium, [3]Department of Materials, University of Oxford, Oxford, United Kingdom, [4]Rosalind Franklin Institute, Oxfordshire , United Kingdom, [5]Ian Holmes Imaging Centre, Bio21 Molecular Science and Biotechnology Institute, University of Melbourne, Victoria, Australia

Poster Group 1

Background incl. aims

The rich information obtained from EELS originates from the complex inelastic scattering process, wherein fast electrons transfer energy and momentum to atoms, exciting bound electrons to higher unoccupied states. To quantify compositions using EELS, the common practice is to fit the observed spectrum with the scattering cross-sections calculated from experimental parameters and the general oscillation strength (GOS) database [1]. A common commercial solution uses GOS tables obtained from the Hartree-Fock solution of atomic orbitals [2]. Here, almost 40 years after, we attempt to go beyond some of the limitations of this database by including the full relativistic effects and making use of dramatically improved computation capabilities in calculating a tabulated GOS solving the Dirac equation (Dirac-Hartree-Slater method within the local density approximation).

Methods

We calculated the transition density matrix using Fermi's golden rule, with the core orbital's bound state as the initial state and the continuum state as the excited state.

We assume a single independent atom, ignoring the solid state effects on the density of states and therefore the rich fine structure that is present in experimental EELS cross sections. We use the frozen core approximation, which assumes the potential remains unchanged after ionizing the core-shell electron to the continuum state, to ensure the orthogonality of the initial and final states. Both large and small components of the Dirac solution are needed to compute the transition matrix element. The convergence is checked by including the final states until the contribution of GOS of the last three states falls below 0.1%.

Results

A complete GOS database was constructed for all elements with atomic number Z=1-118 and all shells, which resulted in 2143 entries for which we store a tabulation of the GOS as a function of energy and momentum with fine sampling. We chose an energy range sampling from 0.01 - 4000 eV with 128 sampling points and a momentum range of 0.05-50 with 256 sampling points, both using a logarithmic sampling scheme. The database was saved in HDF5 file format [3] and will be supported in various software (e.g. Digital Micrograph, Hyperspy and pyEELSModel) so that users could switch easily between different flavours of GOS. As shown in Fig.1(a), the newly developed database has a much larger coverage of energy-momentum space with fine sampling for EELS cross-section quantification. It includes the effects of spin-orbital coupling, e.g. for the Ti L shell [Fig. 1(b)] and shows a good agreement with experimentally measured ionization energies across the periodic table [Fig. 1(c)]. We evaluated the computed spectrum based on different atomic calculations for the experimental spectrum fitting and elemental mapping [Fig. 1(d-f)]. We also considered the relativistic electrodynamics of the fast incoming electron on the orbital transition when computing the EELS cross-sections.

Conclusion

The accuracy of EELS quantification relies on the accuracy of the cross-section calculations represented in the GOS database as a function of energy loss and momentum transfer. In this study, we developed an open-source Dirac-based GOS database for all elements and shells for large energy and momentum space with fine sampling. The open-source Dirac-based GOS database [4] is expected to bring benefits to the EELS community for both academic use and industry integration.

Fig.1 (a) The sampling of Dirac-based GOS compared to Hartree-Fock-based commercial database for K-edge ionization of a C atom, with white grids indicating the sampling; (b) Example of the Ti L2/3 ionization energies comparison; (c)Plots of the experimental (from EELS Atlas) and calculated ionization energies for different elements and orbitals; (d-f) Spectrum fitting and elemental mapping with GOS computed by different atomic calculation methods.

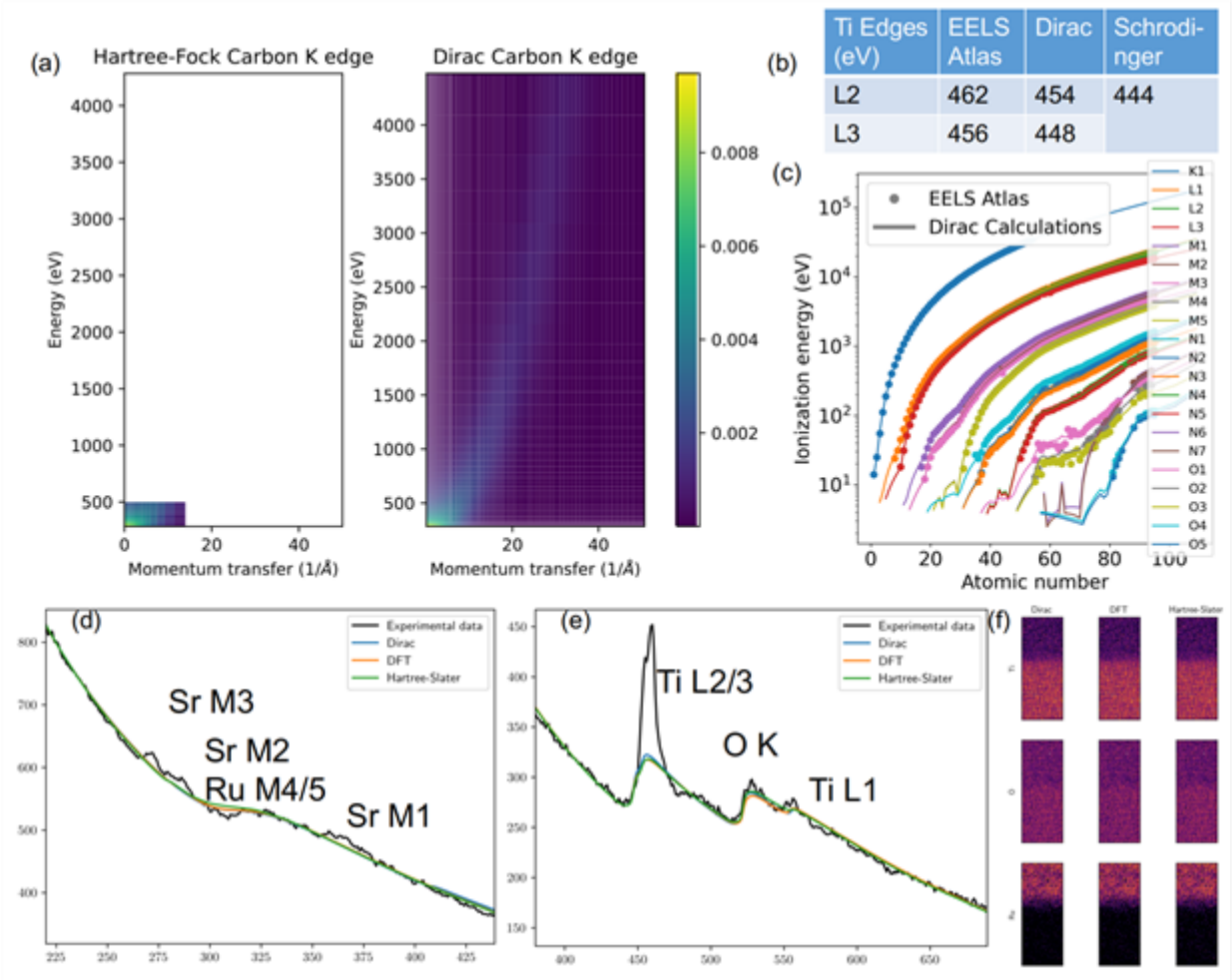

Keywords:

Quantitative EELS, General oscillation strength

Reference:

[1]Verbeeck, J., and S. Van Aert. Ultramicroscopy 101.2-4 (2004): 207-224.
[2]Leapman, R. D., Rez, P. & D. F. Mayers. (1980). The Journal of Chemical Physics, 72.2, 1232-1243.
[3]Guzzina,G. (2023), GOSH: Generalised Oscillator Strengths in HDF5.
[4]Zhang, Z., Lobato, I., Brown, H., Jannis, D., Verbeeck, J., Van Aert, S., & Nellist, P (2023). Dirac-based GOS on Zenodo [under CC-BY 4.0 International license], doi.org/10.5281/zenodo.8360240
The authors acknowledge financial support from the Research Foundation Flanders (FWO, Belgium) through Project No. G.0502.18N. This project has received funding from the European Research Council ((Grant Agreement No. 770887 PICOMETRICS).

396

Molecular Microscopy by Thermo-Fisher-Scientific: FTIR-Imaging of a Tintoretto-Fresco and Raman-Imaging of the Strain-Distribution in Semiconductors

Dr. Maximilian Ries[1,2], Barbara Bravo[1], Eleonora Balliana[3], Fabian Heisinger[2], Imad Limame[2]
[1]Thermo Fisher Scientific, , Germany/Italy, [2]Technische Universität Berlin, , Germany, [3]Ca' Foscari University of Venice, , Italy

Poster Group 1

Background incl. aims
Molecular spectroscopy tools are employed to investigate the vibrational properties of a wide variety of samples. The chemical composition and physical properties of materials are stored in the molecular bonds and can be read from the vibrational spectrum. Fourier transform infrared (FTIR) spectroscopy has long been utilized to investigate materials present in artwork. This study of Tintoretto's work at the Scuola Grande di San Rocco (Venice, Italy) aims to understand the composition of its pictorial layers. The second part of this talk is dedicated to the influence of a buried stressor on the strain-dependent site control of InGaAs quantum dots. Raman spectroscopy is highly sensitive to subtle changes in the crystal lattice structure. Under strain, its molecular bonds shift slightly, altering the vibrational frequencies of the lattice. The resulting shifts in Raman peaks contain information about the amount and type of strain present.

Methods
The cross-section of the Tintoretto painting sample was embedded in resin to assess the five layers. The sample was analyzed in several regions using a Thermo Scientific Nicolet RaptIR FTIR microscope in corroboration with scanning electron microscopy with energy-dispersive x-ray spectroscopy. All mappings were performed in ATR mode with a Germanium micro-ATR. The quantum dot sample was analyzed with a Thermo Fisher Scientific DXR3xi Raman imaging microscope and a 532 nm laser. The results are correlated with atomic force microscopy assessments of the sample height profile.

Results
The cross-section of the painting revealed the existence of a lipidic preparation layer and finishing layer. The preparation layer contains traces of proteins, pointing to the use of animal glue. The sandwiched layers contain different pigments and filler materials. The study confirmed assumptions and knowledge on the use of materials and techniques in the 16th century. In contrast, semiconductor nanostructures are state-of-the-art technology of the 21st century. InGaAs quantum dots grow at sites exhibiting a considerably larger strain than their surrounding. Tuning of the buried stressor size results in the precise control of the distribution, emission, and density of the quantum dots. The overlay of Raman strain mappings with atomic force microscopy height profiles allows for a deeper understanding of the physical properties. In combination with computational simulations, the results forecast the design of new devices with distinct emission patterns.

Conclusion
All materials that were expected to be found in the paint sample were successfully identified using the Nicolet RaptIR FTIR Microscope, combined with the multicomponent search function of OMNIC Paradigm Software. Besides the chemical composition, Raman spectroscopy is powerful in assessing the physical properties such as the strain in semiconductors. The power and beauty of these spectroscopic techniques are pivotal in the creation, conservation, consolidation, and understanding of materials across all scientific fields.

Graphics
(left) Cross section of a Tintoretto painting, highlighting the five layers.
(center) Tintoretto fresco at the Scuola Grande die San Rocco in Venice, Italy.
(right) 3D recreation of a quantum dot sample from Raman imaging. False color image of the vibrational frequency translating into the amount of strain in the material.

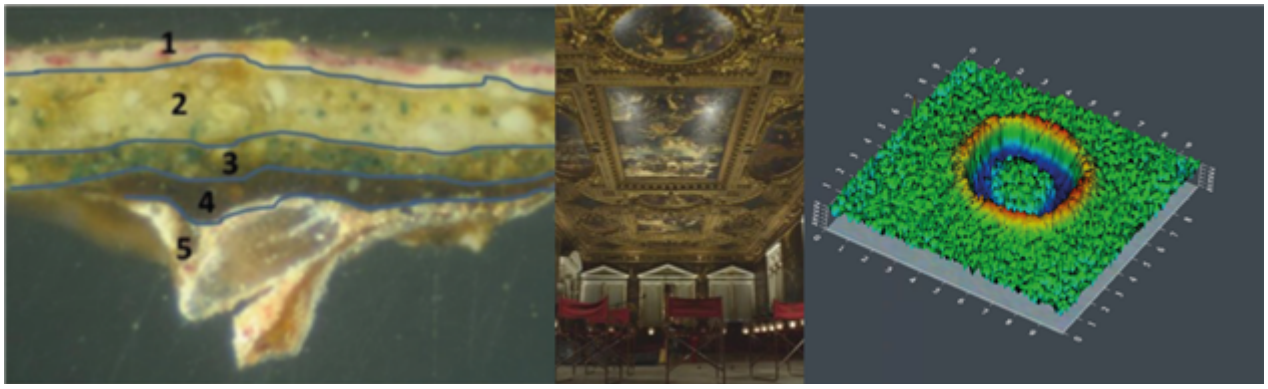

Keywords:

FTIR, Raman, Semiconductor, Material-Identification, Composition

Reference:

[1] Bravo, B.; Izzo, F.C.; Zendri, E.; Balliana, E. „Analysis of a Tintoretto stratigraphy with micro-FTIR spectroscopy," Thermo Fisher Scientific, Application Note:56373, 2023
[2] Ries, M; Heisinger, F., "Using Raman spectroscopy to determine the strain in semiconductor samples," Thermo Fisher Scientific, Application Note: 1023, 2024
[3] Limame, I.; Heisinger, F. et al., "Epitaxial growth and characterization of multi-layer site-controlled InGaAs quantum dots based on the buried stressor method," Applied Physics Letters, vol. 124, no. 6, Feb. 2024, doi: 10.1063/5.0187074.

416

WhatEELS upgrade: the software tool based in Python for EELS analysis

Vanessa Costa-Ledesma[1], Daniel del-Pozo-Bueno[1], Francesca Peiró[1], Sònia Estradé[1]
[1]LENS-MIND, Dept. d'Enginyeria Electrònica i Biomèdica and Institute of Nanoscience and Nanotechnology (IN2UB), Universitat de Barcelona, Barcelona, Spain

Poster Group 1

BACKGROUND INCLUDING AIMS
Electron Energy Loss Spectroscopy (EELS) employing a Scanning Transmission Electron Microscope (STEM) offers precise elemental characterization with exceptional spatial resolution. Multiple Linear Least Squares fits are one of the approaches with short convergence times that are typically favoured for spectral unmixing in the quantitative analysis due to the complexity and sizes of the EELS spectrum pictures datasets collected by the state-of-the-art instruments. However, Non-Linear Least Squares (NLLS) fitting could be a better option for analysis in some circumstances, since it does not need calibrated reference spectra and yields information for each of the constituent parts of the fitted model. For efficient analysis of complex datasets, combining clustering segmentation with Non-Linear Least Squares fitting enhances parameter control and accommodates mixed-composition samples. To facilitate this approach, integrating clustering, and NLLS, a modular software solution implemented in Python by J. Blanco-Portals was developed and open for the public in 2022, WhatEELS [1]. In the present work, we update the WhatEELS software with elemental quantification tools [2] using full relativistic cross-sections [3].
METHODS
The interactive shell of WhatEELS is based on Python and, in particular, in the following modules: Panel and Holoviews, and the graphical backend on Bokeh. Below the surface, the NLLS fitting, and background removal are based on a library called lmfit, which expands the SciPy fitting capabilities. The machine learning analysis is based on Hierarchical Density-Based Spatial Clustering of Applications with Noise, Uniform Manifold Approximation and Projection and Support Vector Machines, which the first and the last one are packages from the Scikit-learn library. The full relativistic cross-sections are calculated from Quantum Mechanics following Salvat [3].
RESULTS
We successfully implemented the relativistic elemental quantification in WhatEELS, This testing was applied to iron oxide core-shell nanocubes and iron and manganese oxide core-shell nanoparticles, obtaining the expected results for the quantification.
CONCLUSIONS
WhatEELS is a software tool designed to analyze multiple-pixel EELS datasets by combining clustering algorithms for image segmentation and NLLS fitting routines for improved workflow efficiency. WhatEELS is advantageous for scientists and students who are just starting in EELS data analysis for materials science because of its open-source nature and low programming requirements.

Keywords:

STEM, EELS, software

Reference:

[1] J. Blanco-Portals, P. Torruella, F. Baiutti, S. Anelli, M. Torrell, A. Tarancón, F. Peiró, S. Estradé, WhatEELS. A python-based interactive software solution for ELNES analysis combining clustering and NLLS, Ultramicroscopy, Volume 232, 2022.
[2] F. Salvat, "Inelastic collisions of fast charged particles with atoms. Relativistic plane-wave Born approximation" Report Universitat de Barcelona, Barcelona 2021, unpublished.
[3] R.F. Egerton, Electron Energy-Loss Spectroscopy in the Electron Microscope, Springer, 2011.

512

Atom-counting for heterogeneous nanostructures using multimodal STEM

Dr Annick De Backer[1], Dr Zezhong Zhang[1], Dr Ana Sánchez-Iglesias[2], Prof Luis M. Liz-Marzán[2,3], Prof Peter D. Nellist[4], Prof Sara Bals[1], Duygu G. Şentürk[1], Dr Yansong Hao[1], Prof Scott Findlay[5], Prof Sandra Van Aert[1]
[1]EMAT & NANOlab Center of Excellence, University of Antwerp, Antwerp, Belgium, [2]CIC biomaGUNE, Basque Research and Technology Alliance (BRTA), Donostia-San Sebastián, Spain, [3]Ikerbasque, Basque Foundation for Science, Bilbao, Spain, [4]Department of Materials, University of Oxford, Oxford, United Kingdom, [5]School of Physics and Astronomy, Monash University, Melbourne, Australia

Poster Group 1

Background incl. aims

To understand the structure-property relationship of nanostructures, reliably quantifying parameters, such as the number of atoms along the projection direction, is important. Advanced statistical methodologies made it possible to count the number of atoms for monoatomic crystalline nanoparticles from a single annular dark field scanning transmission electron microscopy (ADF STEM) image [1]. For this purpose, the so-called ADF STEM scattering cross-sections (SCSs), which correspond to the total intensity of electrons scattered by a single column, are a useful measure. Those SCSs scale with the number of atoms and the atomic number Z. Because of the presence of this Z-contrast, for mixed columns, different elements will contribute differently to the SCSs thus significantly complicating a quantitative interpretation. Progress was made to extend atom-counting from homogeneous to heterogeneous nanostructures by combining ADF STEM with energy dispersive X-ray (EDX) spectroscopy [2]. Although this method can be used to unscramble elements even when the difference in atomic number is only one, EDX measurements may not always be the most viable option for beam-sensitive materials due to the substantial electron dose needed to achieve a sufficiently high signal-to-noise ratio in the EDX elemental maps. As an alternative, we investigated multimode atomic resolution ADF STEM [3]. In this technique, distinct scattering behaviours in different annular detector collection regions will help to unscramble the composition and thickness. Both approaches will be discussed and in addition, the feasibility of novel dose-efficient 4D STEM techniques will be explored for atom-counting, since the simultaneous acquisition of both light and heavy elements remains challenging based on ADF STEM images [4].

Methods

As a first step to count the number of atoms, the atomic columns in the ADF STEM image are modelled by a superposition of Gaussian functions. The volume under each Gaussian corresponds to the scattering cross-section. When counting the number of atoms in heterogeneous nanostructures by combining EDX and ADF STEM, EDX STEM SCSs are also derived by integrating the intensity over the atomic column positions from the noisy elemental maps. Since both ADF STEM and EDX imaging are incoherent techniques, a linear relationship between the EDX and ADF STEM SCSs exists. By exploiting this linear relationship, the experimental SCSs are matched to the simulated SCSs by estimating normalisation constants for the EDX SCSs, using an iterative weighted least squares minimisation. Similarly, with multimode atomic resolution ADF STEM, the nanoparticle SCSs are matched with simulated SCSs by minimising the uniformly weighted sum of squared differences in the SCSs from multiple ADF STEM images. The latter method only considers ADF STEM images, i.e. images obtained by integrating from regions in the convergent beam electron diffraction (CBED) pattern with angles larger than the convergence angle of the probe. When using the flexibility of the 4D STEM datasets, the electrons scattered at low angles can also be employed, facilitating the quantification of light elements. To this end, first-moment STEM images, which measure the centre

of mass (COM) position from the CBED pattern are quantified by modelling the COMx(y) image as a superposition of 2D Lorentzian derivatives.

Results

The combination of EDX and ADF STEM images to count atoms is applied to experimental EDX and ADF STEM images of an Au@Ag core-shell nanorod. For this purpose, the EDX mapping was done for 60 minutes, with the results stored every 5 minutes followed by the acquisition of a calibrated ADF STEM image. This resulted in a times series of 12 EDX Ag and Au elemental maps and 12 ADF STEM images. The counting results for both types of elements agree well with the expected results for a symmetrical Au@Ag core-shell nanorod. The average error on the number of atoms in a column equals ±5.6, ±2.5, and ±3.2 atoms for respectively the number of Ag, Au and total number of atoms. With this methodology we also explored the possibility of characterising a simulated Au@Pt nanorod, with adjacent atomic numbers. Those analyses quantitatively demonstrate the opportunities to count the number of atoms corresponding to each specific element, even when the difference in atomic number is only one.

As a more dose-efficient method to reveal the thickness and composition information, we counted the number of atoms of a simulated Au@Ag core-shell nanoparticle based on multiple STEM images originating from non-overlapping detector regions retrieved from a 4D STEM dataset. When using a set of SCSs obtained from 3 independent ADF STEM images, the average root mean squared error for the atom-counting results is ±5.4, ±2.2, and ±3.5 atoms for respectively the number of Ag, Au, and total number of atoms. This is the same order of magnitude as for the EDX analysis, although the incident electron dose was much lower, i.e. 10^5 e/Å² in a single frame, whereas for the EDX experiment the incident electron dose per frame was approximately $4x10^4$ e/Å² and $4x10^6$ e/Å² for ADF and EDX respectively, clearly highlighting the dose-efficiency of multimode ADF STEM.

For light elements and COMx(y) imaging, the possibilities for atom-counting are explored using a simulation of an aluminium crystal. By fitting the 2D Lorentzian derivatives, the integrated intensities of the atomic columns as a function of thickness are calculated. A monotonic increase up to a thickness of 30 atoms is observed, suggesting that the COMx(y) images can be used for atom-counting.

Conclusions

In conclusion, different multimodal strategies are presented to count the number of atoms in heterogeneous nanocrystals. When combining EDX and ADF STEM imaging the number of atoms can be counted even for elements with adjacent atomic numbers, albeit at the expense of high incident electron doses. The analysis of images obtained from processed 4D STEM datasets will be more dose efficient. Given the promising results, it is a viable alternative for atom-counting of beam-sensitive materials.

This work was supported by the European Research Council (Grant 770887 PICOMETRICS and Grant 815128 REALNANO), the Research Foundation Flanders (FWO, Belgium), and partly under the Discovery Projects funding scheme of the Australian Research Council (project no. FT190100619). SVA acknowledges funding from the University of Antwerp Research fund (BOF).

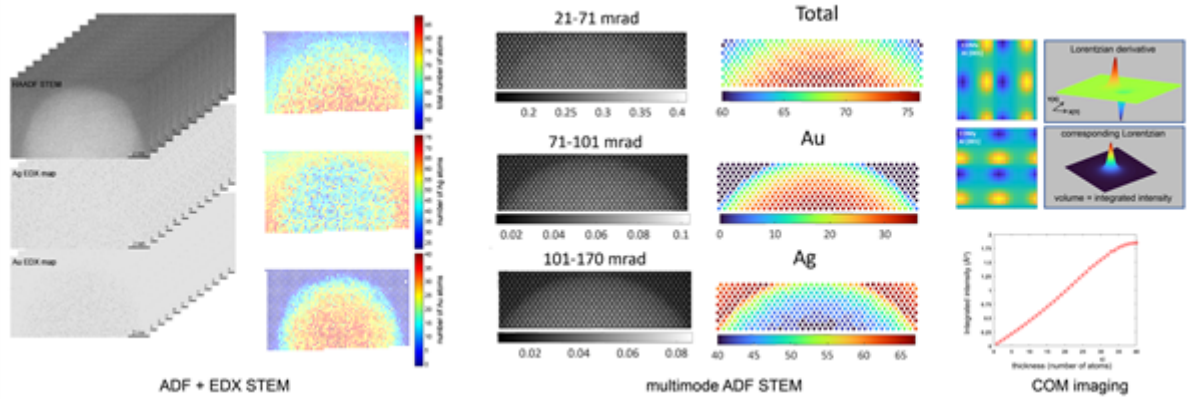

Keywords:

atom-counting, multimodal STEM, heterogeneous materials

Reference:

[1] A. De Backer et al., Ultramicroscopy 247, 113702 (2023).
[2] A. De Backer et al., Small Methods 6, 2200875 (2022).
[3] D.G. Sentürk et al., Ultramicroscopy 259, 113941 (2024).
[4] R. Close et al, Ultramicroscopy 159 124–137 (2015).

591

Development and applications of backscattered electron and X-ray detector

Dr Katherine Macarthur[1], Haithem Mansour[1], John Zhang[1], Anthony Hyde[1], Simon Burgess[1], Philippe Pinard[1]
[1]Oxford Instruments NanoAnalysis, High Wycombe, United Kingdom

Poster Group 1

Electron microscopical analysis frequently suffers from the criticism that we're only investigating a small region, a small percentage, of the whole material. When we only investigate minute regions of the sample, how can we make sure we're not biased by what we find or haven't found? How can we make sure that we're achieving a realistic overview of the sample? One strategy to increase the sampling is to acquire a large area mapping, where secondary electron (SE), backscattered electron (BSE) and X-ray signals are collected over 100 to 10,000's of fields by moving the stage to cover the entire sample. The rate limiting factor is usually the throughput and sensitivity of the energy dispersive spectrometry (EDS) detector(s) to collect enough X-rays to achieve an acceptable signal-to-noise ratio (SNR) for all elements in the sample.

One solution is to increase the solid angle of the EDS detector, by moving it under the pole piece of the scanning electron microscope (SEM), while keeping the ability to acquire SE and BSE signals simultaneously. In 2023, we introduced a detector which combines both X-ray and BSE sensors into one device (Unity, Oxford Instruments, UK). The head features two circular silicon drift detector X-ray sensors, two custom shaped BSE sensors and two cutouts to give unobstructed line-of-sight to conventional EDS detectors. Here, we will lift the lid on some of the important developments required to bring together the backscattered electron and X-ray (BEX) detector system. Figure 1 shows the type of data which achievable with this detector.

Firstly, the integrated BSE. Having two distinct sensors means both Z-contrast and topography can be produced. The unusual shape of the detectors maximises the collection area of the detector and therefore SNR, whilst still maintaining compatibility with additional standard EDS detectors. The Z-contrast is possible because the sensors are symmetrically positioned around the pole piece and cover a large solid angle. Combined experiments with a BSE signal is important because this has a much higher signal to noise and better resolution than x-ray elemental maps. In the overlaid results, Figure 1, the BSE is providing a sharpness to the image that wouldn't be present in the x-ray maps alone.

Secondly, the Unity detector is designed to work in parallel with a standard EDS. The Unity detector has a protective membrane over each of the X-ray sensors to help extend their life and cope with the high count rates an under pole piece detector is exposed to. Due to this membrane, there is limited detection of light elements, combining with a traditional EDS detector resolves this. Counterintuitively, having a second detector with a lower count rate is much better for mapping light elements, as it allows for the use of a longer process time, leading to improved energy resolution and therefore by association improved deconvolution of the lower energy X-ray lines. The BEX detector does not need to process low energy signals which means it can run faster and be optimised for the higher energies. This set up is technologically slightly tricky as it means the combination of two X-ray sensors which differ in size, shape, and sensitivity, in addition to the simultaneously acquired BSE signal. Unity is designed to maximise the throughput and achieve the optimal mapping resolution, whilst the ideal process time for the conventional EDS detector can be selected based on the relative solid angle, detector sensitivity and geometry. A similar ratio and comparison of the variance optimizes the selection of the optimum X-ray map for each element. Map selection has also been

optimized for a multidetector system, making sure the best results are being displayed, for each element.

BSE experiments are typically run with a constant dwell time where are EDS experiments are run with a variable dwell time but maintaining and constant live time. This must be taken into account when designing a synchronized experiment. We will present on the technology behind an improved workflow for synchronized multi-sensor and multi-signal experiments, including the importance of acquisition synchronization, combined processing and displaying of the final data.

Figure 1: Showing example results taken with a BEX detector, with a combined overlay of the BSE and several elemental maps (a). A larger view of (a) is shown in (b) emphasizing the sharpness of contrast which is achievable by this technique.

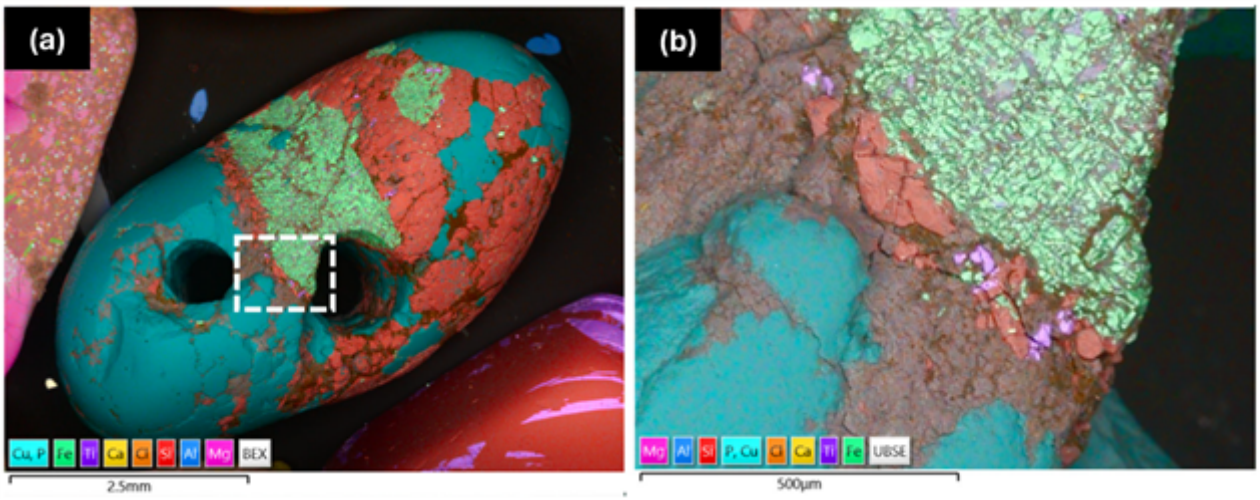

Keywords:

BSE, EDS, Multi-signal, Synchronization, hyperspectroscopy

592

Uranium reduction by magnetite and mechanism of UO2 formation monitored by low-dose STEM-EELS

Dr. Barbora Bártová[1,2], Thomas LaGrange[3], Zezhen Pan[1,4], Gregory Leinders[5], René Bes[6], Nicolas Jacquemin[1], Katharina Reinhold[1], Jacopo Carbone[1], Rizlan Bernier-Latmani[1]
[1]Environmental Microbiology Laboratory (EML), École polytechnique fédérale de Lausanne (EPFL), Lausanne, Switzerland, [2]Interdisciplinary Center for Electron Microscopy (CIME), EPFL, Lausanne, Switzerland, [3]Laboratory for Ultrafast Microscopy and Electron Scattering (LUMES), EPFL, Lausanne, Switzerland, [4]Department of Environmental Science and Engineering, Fudan University, Shanghai, China, [5]Institute for Nuclear Materials Science, Belgian Nuclear Research Centre (SCK CEN), Mol, Belgium, [6]Center for X-ray Spectroscopy, University of Helsinki, Helsinki, Finland

Poster Group 1

Background incl. aims
Uranium (U) is a ubiquitous element in the Earth's crust, and its biogeochemical behavior is primarily constrained by its redox transformation from soluble uranium (U) hexavalent species (U(VI)) to sparingly soluble tetravalent species (U(IV)) under anoxic conditions. U(VI) reduction by mineral phases, most commonly ferrous iron-bearing minerals, has been shown to produce crystalline U in the form of UO_2 as the end-product at circumneutral pH values. However, there is increasing evidence for the presence of pentavalent U (U(V)) in these minerals. Our work [1] has evidenced the presence of U(V) during U(VI) reduction by preformed magnetite and its persistence for days to weeks prior to the formation of fully reduced U(IV)O_2 nanoparticles. Despite this evidence, uncertainty about the mechanistic role of U(V) in uranium reduction pathways remains.
We reported the formation of single U oxide nanocrystals (1-5 nm) followed by the formation of nanowires that extended from the magnetite surface outward. Over time, the nanowires collapsed into ordered UO_2 nanoclusters, resembling those previously reported for the final product after U(VI) reduction by magnetite [2]. U(IV) was suggested as the dominant valence state in the nanowires based on both Fast Fourier Transform (FFT) on specific regions of HAADF-STEM images of the nanowires and the branching ratios (BR) obtained from M4/M5 peaks from U TEM-EELS spectra. However, due to the sensitivity of U(V) under the beam, the presence of mixed valence states may be overlooked by using the BR acquired from U TEM EELS spectra under high beam current. Differences between UO_2 and uranium oxides with mixed valence states, such as U_3O_8, are too small to be robustly differentiated with FFT analysis of HRSTEM images. Current work aims to measure O K-edge EELS STEM spectra of the nanoparticles within the nanowires and compare the edge feature to that of U oxides reference standards to characterize the valence state of nanocrystals.
Methods
We gathered low-loss and high-loss spectrum images of O-K edge and U N edges for UO_2+x standards and time-resolved U(VI) reduction samples. Solutions with magnetite (0.25 or 5 mM Fe) and U(VI) (30 or 200 uM) were prepared anoxically at neutral pH, and samples at various reduction stages were collected. Both U oxide standards and U nanowires formed during the reduction process are susceptible to electron beam-induced damage and reduction, changing the electronic structure of the samples. Thus, it is necessary to use ultra-low beam currents of 10-50 pAs, and we adapted the Gatan Continuum-K3 spectrometer-detector alignments to optimize sensitivity, dose rate per pixel, and the signal-to-noise ratio (SNR) at such low beam doses. We processed the EELS Data cubes with zero loss alignment, denoising, deconvolution, background subtraction, and spectral smoothing. Then, spectra from nanocrystals within the nanowires and in nanoclusters were extracted and compared with those from UO_2+x standards. We also fit the O K-edge of these spectra with data from UO_2+x standards to determine the valency and state of sample reduction.

Results

STEM-EELS measurements were performed for the following U oxide standards that contain the three main U oxidation states or mixtures thereof: UO_2 U(IV), U_4O_9 2xU(IV)+2xU(V), U_3O_7 U(IV)+2xU(V), KUO_3 U(V), and $BaUO_4$ U(VI). The O K-edges of standards were compared with the corresponding simulations based on DFT calculations, see Fig.1(a). The U(IV) containing standards O K-edge (UO_2, U_4O_9, and U_3O_7) have a lower intensity at peak 1 (533 eV), whereas peak 2 (539 eV) has a higher intensity. In contrast, U(V)- and U(VI)-containing standards O K-edges (KUO_3 and $BaUO_4$) have a different electronic structure, with a higher intensity of peak (labeled 1) at 534 eV and a lower intensity peak (2) at 541 eV. The measured U oxides standards correspond well with their simulations, and averaged spectra of each standard (at least 8 measurements) are used for the multiple linear least fitting within the region of O K-edge (520-620 eV) in nanowire samples. Figure 1(b-f) shows that the experimental setup allows us to obtain high-quality spectra from a single pixel even though the thickness of the nanowires does not exceed 10 nm. Fitting shows the presence of mixed valence state oxides U_4O_9 and U_3O_7 within the nanowires, thus confirming the presence of U(V).

Conclusion

We measured O K-edges of U oxide standards with various valence states and samples comprising nanowires composed of 1-5 nm size particles with as low as a 50 pA dose. The fits of reduced nanowire samples and comparison UO2+x standards O K-edge spectra confirm the presence of mixed valence state particles in nanowires, thus evidencing the presence of U(V).

Fig.1: (a) Comparison of O K-edge spectra for measured (M) U oxides standards and its respective simulations (S) that show varying peak 1 and 2 heights and their eV shift that reflects distinct U oxidation states. (b) Sample containing nanowires. (c) Detail of approximately 30 nm long nanowire sitting between 2 magnetite grains. (d) High loss spectrum imaging (SI) of the selected region with background subtraction, the red square represents 8 angstrom-sized pixels. (e) EELS spectrum from selected pixel (red square) of SI shows the quality of data. (f) Multiple linear least square fitting (MLLS) map shows the presence of mixed valence state U oxides U_4O_9 and U_3O_7.

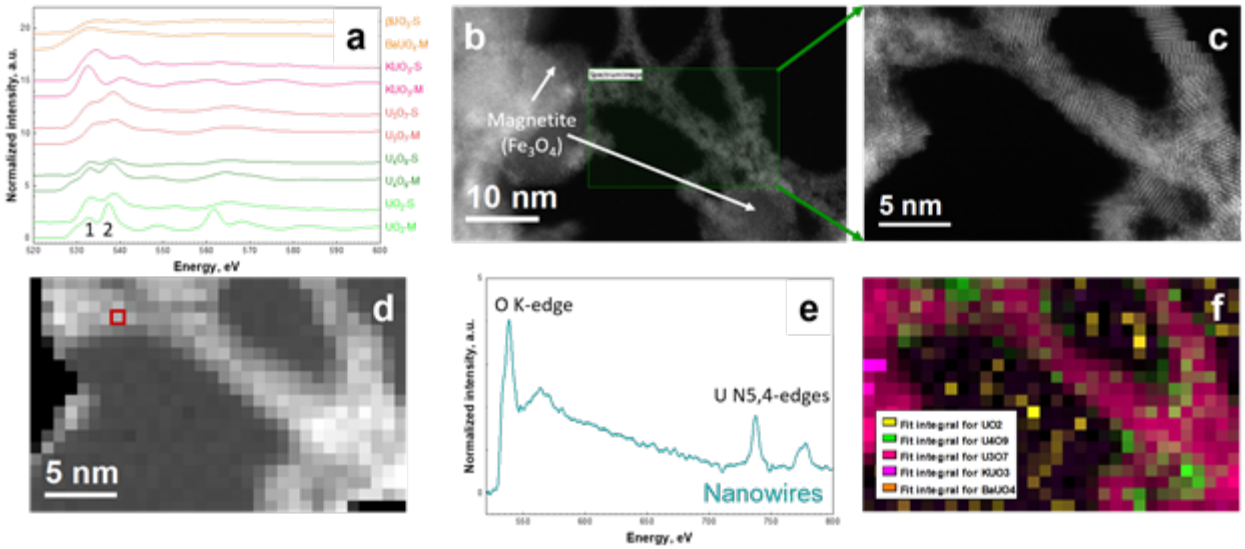

Keywords:

Uranium reduction, low-dose STEM-EELS

Reference:

[1] Pan et al., Nat Commun 11, 4001 (2020)
[2] Latta et al., Environ. Sci. Technol. 2014, 48, 3, 1683–1691
[3] Collela et al., Phys Chem Minerals (2005) 32: 52–64

709

The significance of the phonon polarization vector in vibrational EELS

Paul Zeiger[1], Jan Rusz[1]
[1]Uppsala University, Uppsala, Sweden

Poster Group 1

Background incl. aims
Phonons are the quasiparticles of lattice vibrations. They influence a variety of material properties such as for example the heat conductivity and play a major role in physical effects of technological importance such as for example superconductivity and the phonon Hall effect. Phonons are thereby wave excitations of the entire lattice of a material in the solid state, so-called normal modes, which can be distinguished by the wave vector q and the phonon branch v. Each mode (q, v) has a definite frequeny ω(q,v) and phonon polarization vector e(q,v). Knowledge of both of these quantities fully characterizes a phonon mode (q, v).
Vibrational Electron Energy Loss Spectroscopy (EELS) is establishing itself as an important tool to characterize phonons at the nano- and atomic-scale [1]. In this contribution we discuss the role of the phonon polarization vector in vibrational EELS from different perspectives.
Methods
As the first step we consider the analytical expression for the vibrational EELS cross section in first-order Born approximation, which scales with the phonon frequency ω(q,v) in a simple manner and depends on the scalar product of the momentum transfer Q and phonon polarization vector e(q,v). Here we focus on the richer dependence with respect to the phonon polarization e(q,v). In the second step we consider explicit simulations of vibrational EELS with the Frequency-Resolved Frozen Phonon MultiSlice method and comparison with experiments.
Results
The scalar product dependence of vibrational EELS is the key to the phonon polarization vector. It governs the visibility of phonon modes and is responsible for an interesting modulation of the intensity of the phonon EELS as a function of the detector placements, both for small and large off-axis detectors. The effects have been observed in recent experiments [3,4].
Conclusion
The phonon polarization vector leads to an intricate modulation of vibrational EELS, which can be exploited to gather information on the direction of the phonon polarization vector.

Keywords:

phonon polarization, EELS, simulation, theory

Reference:

1. P M Zeiger and J Rusz, Physical Review Letters 124 (2020), 025501.
2. P M Zeiger and J Rusz, Physical Review B 104 (2021), 104301.
3. A. Li et al., arXiv:2402.11275 (2024).
4. X. Yan et al., arXiv:2312.01694 (2023).

795

Application of secondary electron hyperspectral imaging to the analysis of pharmaceutical materials

Stuart Micklethwaite[1], Rastra Basnet[1], Joseph Ma[1], Daniel Hopper[1], James Nohl[2], Nicholas Farr[2], Cornelia Rodenburg[2], Dr Nicole Hondow[1]
[1]University of Leeds, Leeds, UK, [2]University of Sheffield, Sheffield, UK

Poster Group 1

Background

The importance of pharmaceuticals to the health and wellbeing of society is clear, and it is of upmost importance to have reliable characterisation techniques applicable to the pharmaceutical manufacturing process. Pharmaceutical materials are often complex mixtures, containing multiple organic and possibly inorganic components. The stability and longevity of tablets can be increased through the addition of a coating, and this is evident in many commercially available pain relief medications. The effectiveness of the coating is linked to its surface coverage, and nanoscale characterisation is useful to determine this.
Secondary electron hyperspectral imaging (SEHI) is a recently developed novel electron microscopy technique that provides enhanced surface characterisation. Spectra sensitive to composition, chemical bonding and structure can be formed by collection of the secondary electrons that are emitted from a material following irradiation by an electron beam in the SEM. A variety of materials have been examined by SEHI, not limited to perovskites [1], polymer blends [2] and biomaterials [3], and various carbon materials [4]; however, the technique has not previously been applied to pharmaceutical materials.

Methods

SEM images and SEHI were collected using an FEI Helios G4 CX, a dual beam scanning electron microscope. The hyperspectral images were collected using a monochromated 1 kV accelerating voltage, a typical vacuum pressure of 10^-6 mbar, and a range of probe currents. Complimentary EDX spectroscopy has been undertaken using an Oxford Instruments 150 mm^2 EDX detector. An example commercially available pain relief tablet, Nurofen Plus, has been examined, in addition to reference materials ibuprofen, anatase and rutile. Samples have been prepared by both embedding in Field's metal and by FIB-prepared lamellae.

Results

Sample preparation is a particular challenge in this work, with the non-conductive pharmaceutical samples charging and causing anomalous features in the produced secondary electron spectra. Various sample preparation methods have been compared, each with advantages and disadvantages, with guidance from previous work with sample preparation of powder materials utilised [5]. The chosen commercially available pain relief tablet has a coating containing an inorganic pigment (TiO_2) which has led to the analysis of the different structures, anatase and rutile. The applicability of SEHI to the damage and integrity of the coatings has been examined, to assess this technique for the nanoscale characterisation of formulated pharmaceutical products.

Conclusions

In conclusion, this work will present the first analysis of pharmaceutical materials by secondary electron hyperspectral imaging. The advantages and challenges associated with this technique when applied to these materials will be detailed.

Keywords:

SEM; SEHI; pharmaceuticals

Reference:

1. V. Kumar, W.H. Schmidt, G. Schileo, R.C. Masters, M. Wong-Stringer, D.C. Sinclair, I.M. Reaney, D. Lidzey and C. Rodenburg, ACS Omega 2017, 2, 2126.
2. R.C. Masters, A.J. Pearson, T.S. Glen, F.-C. Sasam, L. Li, M. Dapor, A.M. Donald, D.G. Lidzey and C. Rodenburg, Nature Communications 2015, 6, 6928.
3. N.T.H. Farr, S. Pashneh-Tala, N. Stehling, F. Claeyssens, N. Green and C. Rodenburg, Macromolecular Rapid Communications 2020, 41, 1900484.
4. N.T.H. Farr, S.F. Hamad, E. Gray. C.M. Magazzeni, F. Longman, D.E.J. Armstrong, J.P. Foreman, F. Claeyssens, N.H. Green and C. Rodenburg, Polymer Chemistry 2021, 12, 177.
5. J.F. Nohl, N.T.H. Farr, Y. Sun, G.M. Hughes, S.A. Cussen and C. Rodenburg, Micron 156, 2022, 156, 103234.

804

Denoising 4D STEM datasets with PCA

Leonid Potapov[1], Mingjian Wu[2]
[1]temDM, Dresden, Germany, [2]IMN&CENEM, Friedrich-Alexander Universität, Erlangen-Nürnberg, Germany

Poster Group 1

Background incl. aims
4D Scanning Transmission Electron Microscopy (4D STEM) provides crucial insights into materials structures by utilizing Differential Phase Contrast (DPC), ptychography, orientation and strain mapping. However, 4D STEM datasets often suffer from noise, hindering accurate analysis. It would be desired to denoise 4D STEM data by Principal Component Analysis (PCA) as it was successfully applied for EELS and EDX STEM datasets [1]. Additionally, PCA allows for accurate separation of the constituting compounds by clustering in the latent PCA factor space.

Methods
The sample used for this demonstration is organic solar cell blend DRCN5T:PC71BM solvent vapour annealed in chloroform. The 4D STEM dataset was obtained in micro-probe STEM (convergence angle ~1 mrad) with a Titan Themis microscope operating at 300kV. The data was collected using a OneView IS detector operating at frame rate of 400 fps (2.5 ms frame time) and probe current of about 5 pA.

We developed a Python-based PCA routine and integrated it into the temDM in-house developed 'Spectrum Imager' tool. This tool, originally designed for visualizing and denoising EELS and EDX spectrum-images [2], is presently adapted for 4D STEM datasets processing, including re-centring, clipping, viewing with virtual circular/ring apertures et cet. [3].

Results
When scanning the focussed beam across a sample, a shift of the diffraction pattern inevitably occurs, known as the pivot effect. While this effect can be minimized through accurate instrument tuning, it cannot be eliminated completely. We found that even a slight pivot effect dramatically influences PCA results, overriding any structural variations. In the considered example, the pivot shift within the scanned field of view was less than 2 pixels. Nevertheless, the data variation in the PCA factor space predominantly reflected the pivot variation rather than the structural changes in the sample (Fig.2, upper).

The diffraction shift was measured with the sub-pixel precision in each individual diffraction pattern using the centre-of-mass method. It important to note that simply centring the patterns is not an option as this would preclude any DPC measurements. Instead, we assumed that the pivot shift changes linearly along both x- and y- directions and calculated this by the least-square fit. The diffraction patterns were then shifted with the cubic-spline interpolation to account for the linear pivot. After the consequent PCA, the principal components clearly revealed the structural changes in the sample (Fig.2, lower).

Conclusion
4D STEM datasets can be successfully denoised by PCA, however it requires precise data pre-processing, particularly addressing the pivot shift. The sub-pixel interpolation is mandatory for the accurate subtraction of the pivot shift.

Figure caption
Impact of pivot correction on PCA results. The clusters are selected as hypercylinders in the latent PCA factor space. Without correction, instrumental pivot shift dominates in the PCA factor space. After correction, clustering in the factor space clearly reveals the structural compounds.

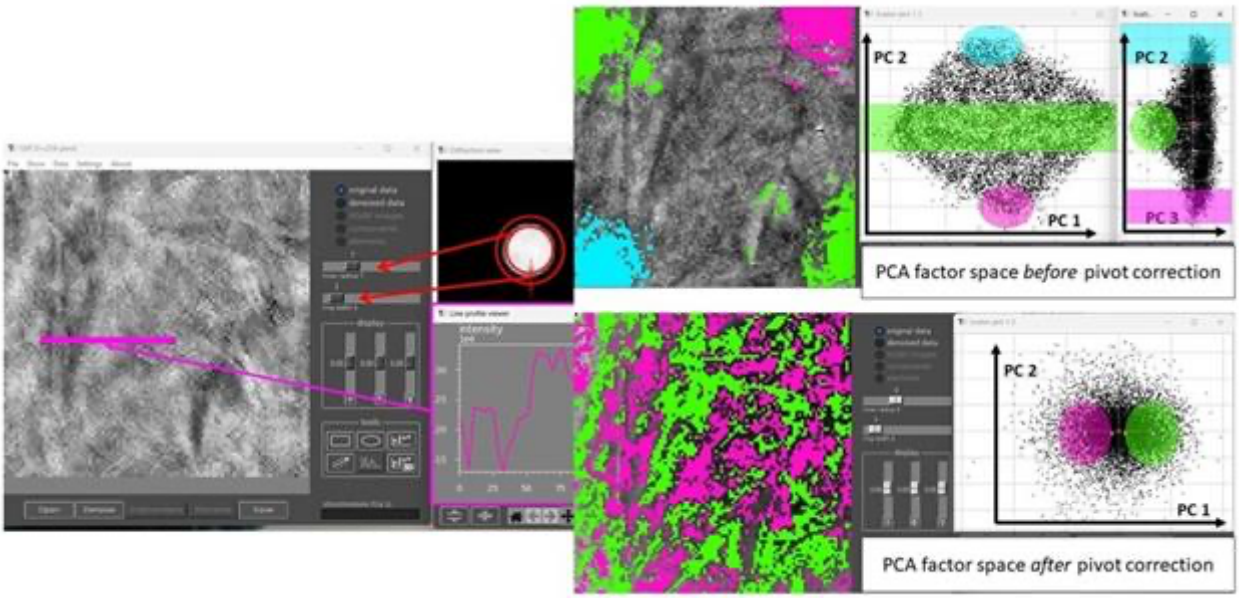

Keywords:

4D STEM, software, PCA, denoising

Reference:

[1] M. Watanabe et al. Microsc. Microanal. 11, 5, 2009.
[2] P. Potapov et al. #0132. Proc. Int. Microscopy Congress, Sept. 2023, Bussan, Korea.
[3] The self-installing package can be free downloaded at https://temdm.com/msa/. Its application is discussed in the blog at https://temdm.com/news.

834

Sub-nanometer mapping of strain-induced band structure variations in different semiconductor device configurations

Marc Botifoll[1], Dr. Sara Martí-Sánchez[1], Dr. Eitan Oksenberg[2], MSc. Christian Koch[1], MSc. Carla Borja[1], Dr. Maria Chiara Spadaro[1], Dr. Valerio Di Giulio[3], Prof. Quentin Ramasse[4,5], Prof. F. Javier García de Abajo[3,6], Prof. Ernesto Joselevich2[2], Prof. Jordi Arbiol[1,6]
[1]Catalan Institute of Nanoscience and Nanotechnology (ICN2), CSIC and BIST, Bellaterra, 08193 Barcelona, Spain, [2]Department of Molecular Chemistry and Materials Science, Weizmann Institute of Science, Rehovot 76100, Israel, [3]ICFO-Institut de Ciencies Fotoniques, The Barcelona Institute of Science and Technology, 08860 Castelldefels, Barcelona, Spain, [4]SuperSTEM Laboratory, STFC Daresbury Campus, Daresbury WA4 4AD, United Kingdom, [5]School of Chemical and Process Engineering & School of Physics and Astronomy, University of Leeds, Leeds LS2 9JT, United Kingdom, [6]ICREA, Passeig Lluís Companys 23, 08010 Barcelona, Spain

Poster Group 1

Over the last three decades, heterostructured semiconductor nanowires (NWs) have been in the spotlight because of their potential as nanoengineered building blocks for a new generation of electronic, photonic and plasmonic, devices for quantum, sensing, and energy-harvesting applications [1]. The nanometer-scale lateral dimensions and resulting quasi one-dimensional morphology of the NWs facilitate the release of the inherent epitaxial strain, preserving high crystal quality even when interfacing highly mismatched materials. Therefore, the characterization of plastic and elastic strain relaxation mechanisms is key to understand and gain control over the optoelectronic properties of epitaxially grown planar structures. Here we propose a methodology to correlate these optoelectronic properties, namely the bandgap, with the structural properties, namely the strain, and prove its concept with ZnSe/ZnTe core-shell nanowires as radial p-n junctions, used as electro-optic detectors among other applications. The method is based on electron energy loss spectroscopy (EELS) to take advantage of sub-nanometric spatial resolutions.
To go through this correlation, we first evaluate the strain, by means of Geometrical Phase Analysis (GPA), in different ZnSe/ZnTe planar systems, which modulate their strain relaxation mechanisms and morphology depending on the substrate (sapphire) plane exposed, determining the final epitaxy of the system. Afterwards, the low-loss EELS regime is acquired, and our methodology is applied to extract and spatially map the bandgap energy, which can be linked with the previous strain measurements [2].
The proposed novel methodology for low-loss EELS analysis can get over limiting scenarios which are affected by parasitic signals such as Cherenkov radiation and surface modes. Until now, these contributions to the low-loss regime that hide valuable signals such as phonons, bandgap and plasmons, hampered more ambitious experimental setups and limited them to low refractive index materials or off-axis EELS [3]. Interestingly, our methodology allows the data cleaning and removal of parasitic modes in any acquisition condition and for materials with any dielectric description. In summary, the method uses unsupervised machine learning for spectrally mapping distinct regions and later applies a spectrum-wise theory-supported correction. These corrections based on classical electrodynamics enable the removal of the percentage of signal attributed to parasitic signals, therefore ensuring the remaining signal is only composed of intrinsic properties of the materials.
The present proof of concept focused on bandgap mapping, which is key knowledge in optoelectronics. However, the methodology is thought to be reproducible to any property if the adequate level of theory is applied. Importantly, this methodology and EELS high spatial resolution proved its sensitivity by allowing us to distinguish a strain-induced direct to indirect bandgap transition at the interface between the ZnSe core and the ZnTe shell of one of the studied systems.

In addition, although the original methodology was developed in the ZnSe/ZnTe heterojunction, preliminary results will be shown on Ge/SiGe quantum wells for holding spin qubits [4] and Ge/Si nanowires aiming towards topological quantum computing, which push the method to more challenging scenarios with bandgaps below 1eV.

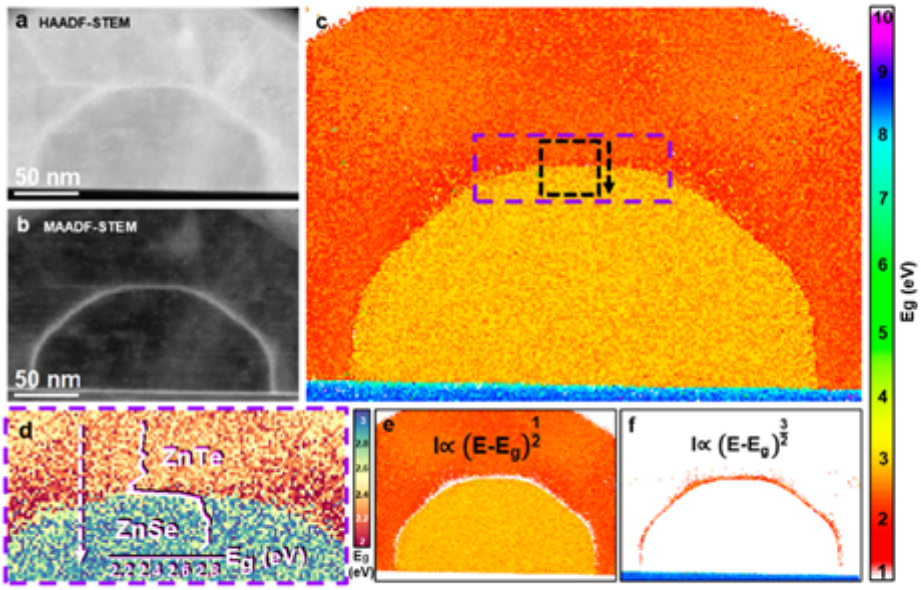

Figure 1: Bandgap maps obtained from applying the proposed methodology to a ZnSe/ZnSe core-shell nanowire

Keywords:

EELS, bandgap, strain, methodology

Reference:

1. Oksenberg, E., et al. Surface-Guided Core-Shell ZnSe@ZnTe Nanowires as Radial p-n Heterojunctions with Photovoltaic Behavior. ACS Nano 11, 6155–6166 (2017).
2. Martí-sánchez, S.*, Botifoll, M.* et al. Sub-nanometer mapping of strain-induced band structure variations in planar nanowire core-shell heterostructures. Nat. Commun. 13, 4089 (2022).
3. Korneychuk, S. et al. Exploring possibilities of band gap measurement with off-axis EELS in TEM. Ultramicroscopy 189, 76–84 (2018).
4. Jirovec, D. et al. A singlet-triplet hole spin qubit in planar Ge. Nat. Mater. 20, 1106–1112 (2021).

852

Nanoscale structural and spectroscopic characterization of hard carbons for Na-ion batteries

Tatiana Kormilina[1], Harald Fitzek[1], Daniel Knez[2], Ilie Hanzu[3], Gerald Kothleitner[1,2], Georg Haberfehlner[2]
[1]Graz Centre for Electron Microscopy, Graz, Austria, [2]Institute of Electron Microscopy and Nanoanalysis, Graz University of Technology, Graz, Austria, [3]Institute for Chemistry and Technology of Materials, Graz University of Technology , Graz, Austria

Poster Group 1

Background incl. aims
Sodium-ion batteries are one of the best candidates to replace lithium-ion batteries for stationary applications, as a cost-effective and sustainable alternative. [1] A key role in their development and integration is the use of renewable carbon sources. Here we are characterizing the structure and chemical composition of bio-derived hard carbons, used as anodes in sodium ion batteries. We aim at a fundamental understanding of parameters that may influence Na storage in these materials.
Methods
Several samples of hard carbon materials were investigated by means of scanning transmission electron microscopy (STEM), employing annular dark field (ADF), integrated differential phase contrast (iDPC) and electron energy loss spectroscopy (EELS), as well as by vibrational spectroscopy, namely, Fourier-transform infrared (FTIR) and Raman spectroscopy.
Raman and IR measurements were carried out on powder samples. TEM samples were prepared by dispersing hard carbon powders in ethanol and drop-casting solution onto a holey carbon film grid.
Results
Previously, bright field imaging in (S)TEM has been prefered for this type of structures.[2] We show that the use of iDPC in combination with ADF STEM imaging at low voltage (80kV) has paramount benefits for the investigation of hard carbons, while no significant beam damage is observed. In iDPC STEM, graphitic layers could be readily imaged, as demonstrated by Graphic A. Moreover, measurements of the d002-spacing are feasible, either directly within images or by analysing their FFT, where also the d100- and d110-spacing of graphite can be measured. In addition, we can observe nanosized pores, which are confirmed in particular by the correlation of iDPC and ADF images. EELS spectra reveal a fine structure of the C K edge that lies between the typical signatures of graphite and amorphous carbon. Both the d002-spacing and the nanoscale pores are supposed to be the key to Na storage capabilities of hard carbons.
FTIR measurements of hard carbons using a diamond ATR crystal face challenges in achieving total reflection condition due to the similarity of refractive indexes. Using Ge with much higher refractive index should be adapted instead for accurate spectra acquisition. FTIR and Raman measurements (exemplary spectra B and C in the Graphic, respectively) allow us to detect differences in crystallinity and surface groups of hard carbon samples with prospects of using Raman in-situ during the Na loading process.
Conclusions
The microscopic and spectroscopic methods chosen for hard carbon characterization have been tested and optimized to meet the specific needs of the material. Next, the characterization results will be compared to electrochemistry measurements to see if certain morphological or chemical characteristics are influencing the Na storage properties. [3]

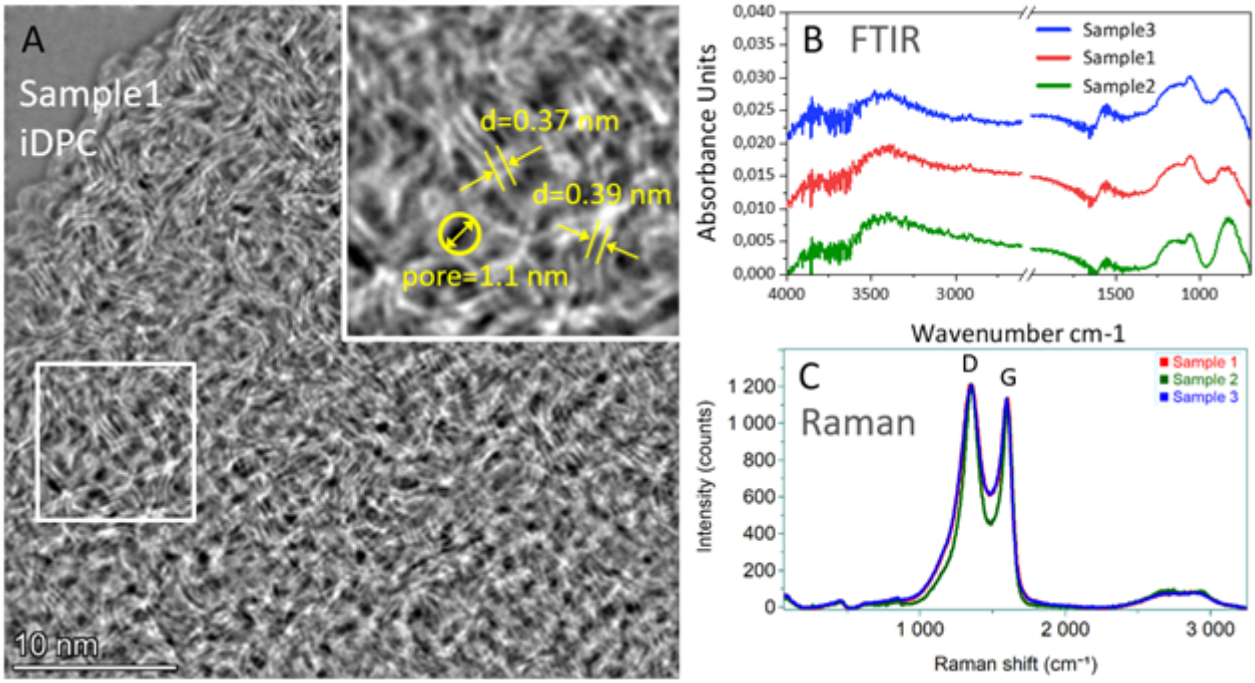

Keywords:

Na-ion battery, iDPC, Raman, FTIR

Reference:

[1] K. Chayambuka et al., “From Li-Ion Batteries toward Na-Ion Chemistries: Challenges and Opportunities,” Adv Energy Mater, vol. 10, no. 38, p. 2001310, Oct. 2020, doi: 10.1002/AENM.202001310.

[2] A. Beda et al., “Hard carbon key properties allow for the achievement of high Coulombic efficiency and high volumetric capacity in Na-ion batteries,” J Mater Chem A Mater, vol. 9, no. 3, pp. 1743–1758, Jan. 2021, doi: 10.1039/D0TA07687B.

[3] Authors thank Corina Taeubert, Rudolf Grasberger and Klaus Höll from Schunk Carbon Technology GmbH for providing hard carbon samples and FFG Austria for funding under the SAM4SIB project (FFG-BRIDGE; project number: 903691).

879

FTIR-Imaging of a Tintoretto-Fresco

Dr. Maximilian Ries[1], Barbara Bravo[1], Eleonora Balliana[2]
[1]Thermo Fisher Scientific, , Germany/Italy/USA, [2]Ca' Foscari University of Venice, Venice, Italy

Poster Group 1

Background incl. aims
Molecular spectroscopy tools are employed to investigate the vibrational properties of a wide variety of samples. The chemical composition and physical properties of materials are stored in the molecular bonds and can be read from the vibrational spectrum. Fourier transform infrared (FTIR) spectroscopy has long been utilized to investigate materials present in artwork. This study of Tintoretto's work at the Scuola Grande di San Rocco (Venice, Italy) aims to understand the composition of its pictorial layers.
Methods
The cross-section of the Tintoretto painting sample was embedded in resin to assess the five layers. The sample was analyzed in several regions using a Thermo Scientific Nicolet RaptIR FTIR microscope in corroboration with scanning electron microscopy with energy-dispersive x-ray spectroscopy. All mappings were performed in ATR mode with a Germanium micro-ATR.
Results
The cross-section of the painting revealed the existence of a lipidic preparation layer and finishing layer. The preparation layer contains traces of proteins, pointing to the use of animal glue. The sandwiched layers contain different pigments and filler materials. The study confirmed assumptions and knowledge on the use of materials and techniques in the 16th century. In contrast, semiconductor nanostructures are state-of-the-art technology of the 21st century.
Conclusion
All materials that were expected to be found in the paint sample were successfully identified using the Nicolet RaptIR FTIR Microscope, combined with the multicomponent search function of OMNIC Paradigm Software. The power of spectroscopic techniques is pivotal in the creation, conservation, consolidation, and understanding of materials across all scientific fields.

Keywords:

FTIR, Imaging, Art&Conservation, Spectroscopy, ATR

Reference:

[1] Bravo, B.; Izzo, F.C.; Zendri, E.; Balliana, E. „Analysis of a Tintoretto stratigraphy with micro-FTIR spectroscopy," Thermo Fisher Scientific, Application Note:56373, 2023

880

Raman-Imaging of the Strain-Distribution in Semiconductors

Dr. Maximilian Ries[1,2], Fabian Heisinger[2], Dr. Imad Limame[2]
[1]Thermo Fisher Scientific, , Germany/USA, [2]Technische Universität Berlin, Berlin, Germany

Poster Group 1

Background incl. aims
Molecular spectroscopy tools are employed to investigate the vibrational properties of a wide variety of samples. The chemical composition and physical properties of materials are stored in the molecular bonds and can be read from the vibrational spectrum. This poster is dedicated to the influence of a buried stressor on the strain-dependent site control of InGaAs quantum dots. Raman spectroscopy is highly sensitive to subtle changes in the crystal lattice structure. Under strain, its molecular bonds shift slightly, altering the vibrational frequencies of the lattice. The resulting shifts in Raman peaks contain information about the amount and type of strain present.
Methods
The quantum dot sample was analyzed with a Thermo Fisher Scientific DXR3xi Raman imaging microscope and a 532 nm laser. The results are correlated with atomic force microscopy assessments of the sample height profile.
Results
InGaAs quantum dots grow at sites exhibiting a considerably larger strain than their surrounding. Tuning of the buried stressor size results in the precise control of the distribution, emission, and density of the quantum dots. The overlay of Raman strain mappings with atomic force microscopy height profiles allows for a deeper understanding of the physical properties. In combination with computational simulations, the results forecast the design of new devices with distinct emission patterns.
Conclusion
Besides the chemical composition, Raman spectroscopy is powerful in assessing the physical properties such as the strain in semiconductors. The power of spectroscopic techniques is pivotal in the creation, conservation, consolidation, and understanding of materials across all scientific fields.

References:
[1] Ries, M; Heisinger, F., “Using Raman spectroscopy to determine the strain in semiconductor samples,” Thermo Fisher Scientific, Application Note: 1023, 2024
[2] Limame, I.; Heisinger, F. et al., “Epitaxial growth and characterization of multi-layer site-controlled InGaAs quantum dots based on the buried stressor method,” Applied Physics Letters, vol. 124, no. 6, Feb. 2024, doi: 10.1063/5.0187074.

Keywords:

Raman, Spectroscopy, Semiconductor, Strain, AFM

Reference:

[1] Ries, M; Heisinger, F., “Using Raman spectroscopy to determine the strain in semiconductor samples,” Thermo Fisher Scientific, Application Note: 1023, 2024
[2] Limame, I.; Heisinger, F. et al., “Epitaxial growth and characterization of multi-layer site-controlled InGaAs quantum dots based on the buried stressor method,” Applied Physics Letters, vol. 124, no. 6, Feb. 2024, doi: 10.1063/5.0187074.

933

Annular silicon drift detector for advanced EDS on SEM applications

Dr. Igor Németh[1], Dr. Yang Yang
[1]Bruker Nano GmbH, Berlin, Germany

Poster Group 1

Background incl. aims
Energy dispersive X-ray spectroscopy in an SEM can be challenging in certain cases: if no sample preparation (cutting, polishing) is possible or allowed to generate a flat sample surface (which would be ideal for analysis). Furthermore, samples having low electrical conductivity or high electron beam sensitivity can only be investigated using low beam currents, which in turn results in a low X-ray signal. Under such conditions, trace elements cannot be analyzed using EDS within reasonable measurement times.
Methods
We present a solution for maximizing X-ray signal collection: an annular EDS detector, inserted between the pole-piece and the sample. High count rates can be reached even at low beam currents as the four separate X-ray detector segments cover a large solid angle (up to 1.1sr). Due to the high count rates, element distribution mapping (including trace elements) is orders or magnitudes faster than using conventional EDS detection geometry. This configuration is also ideal for the analysis of samples with high topography as shadowing effects are minimized by X-ray detection from all spatial directions.
Results
We present various examples benefiting from the annular acquisition geometry. Li-ion battery components (anode and cathode particles) or black mass material can be mapped with high spatial resolution without the need of any meticulous sample preparation. Contaminants and inhomogeneities in the submicron range can be visualized within the micrometer-sized particles. We will demonstrate that the annular EDS detector is capable of identifying and mapping contaminants in the range of only a few tens of ppm within a few minutes of measurement time. These findings will be compared to a classic trace element detection method (X-ray fluorescence).
Conclusion
The annular EDS detector in an SEM is a proven tool for challenging elemental analysis, such as unprepared samples with high topography and low conductivity (for example battery components: anode, cathode particles, black mass). Due to its maximized collection solid angle, this type of detector yields significantly higher count rates compared to conventional EDS detectors and thus considerably reduces the necessary electron dose or measurement time. EDS using annular detectors is an analytical method capable of detecting and mapping contaminants in the sensitivity range of X-ray fluorescence methods but with the advantage of having high spatial resolution.

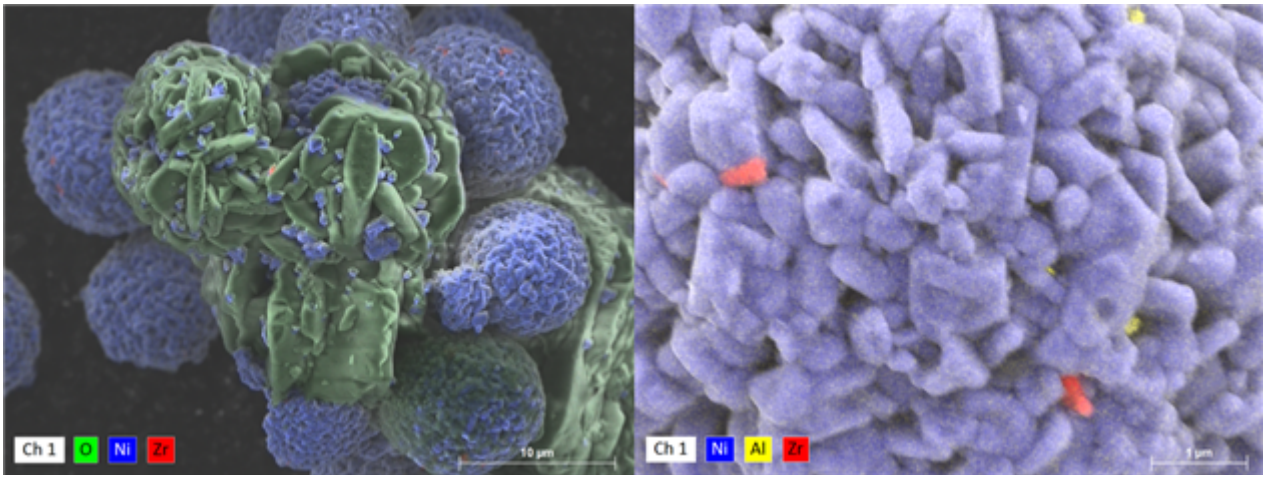

Keywords:

EDS, hyperspectral imaging, battery

968

Electron energy loss spectroscopy for differentiating of minerals polymorphs

Dr Vladimir Roddatis[1], Dr Elizaveta Kovaleva[1,2], Dr Marcin Syczewski[1], Anja Schreiber[1], Dr Richard Wirth[1], Prof Monica Koch-Müller[1]
[1]GFZ German Research Centre for Geosciences, Potsdam, Germany, [2]Department of Earth Sciences, University of the Western Cape, , South Africa

Poster Group 1

Background incl. aims
Nanoscale phase identification in transmission electron microscopy TEM involves selected area or nanobeam electron diffraction combined with electron energy loss spectroscopy (EELS) or energy dispersive X-ray (EDX) analysis. Scanning TEM (STEM) extends this versatility by applying 4D-STEM and precession electron diffraction (PED) for orientational analysis. Recently, $CaCO_3$ polymorphs, calcite and aragonite, were characterized by STEM-EELS in the valence region (< 50 eV, VEELS) and the obtained results were verified by density functional theory (DFT) [1]. It was demonstrated that the near edge fine structures of spectra in the VEELS range closely relate to the electronic structure of materials and their crystal symmetries [1]. Moreover, VEELS is rather independent on crystallographic orientation which makes it a versatile technique even for nanoscale phase identification and mapping of 2D-materials [2].

In this study we applied Cs-corrected STEM and EELS mapping to visualize the distribution of (i) the $ZrSiO_4$ polymorphs zircon and reidite within the natural sample and distribution and structural relation of (ii) the coexisting SiO_2 polymorphs coesite and stishovite in synthetic high-pressure run products.

Methods
TEM foils of approx. 15 x 10 µm were prepared by a lift-out method using a focused ion beam (FIB). Phase distributions were visualized by applying HAADF imaging as well as the EELS and PED methods. Samples containing zircon and reidite were collected from the 70.3 Ma Kara impact structure crater-infill suevite breccias. Coexisting SiO_2 phases were synthesized in high-pressure multi-anvil experiments.

Results
Low magnification HAADF image (see Graphic section) shows reidite lamellae having various apparent thickness inside zircon matrix. Both phases were identified using SAED and high-resolution imaging. VEELS spectra of zircon and reidite were collected in the blue and green points, respectively. The difference (~ 2.3 eV) between position of the main peak at ~25 eV in zircon and at ~27 eV in reidite as well as other small features marked with the grey dashed lines were used to map the distribution of both phases. Corresponding EDX maps of zirconium, oxygen and silicon demonstrate uniform chemical elemental distribution in both phases. The phase distribution was also imaged using the PED data collected using a DigiSTAR device and the ASTAR software (NanoMEGAS SPRL, Belgium). In order to test applicability of the method, additional experiments were carried out to visualize distribution of stishovite and coesite (polymorphs of SiO_2), and kyanite (Al_2SiO_5) in a few FIB-prepared TEM specimens.

Conclusion
Our data demonstrate that phases having identical chemical composition may have distinct spectra in both low-loss and core-loss regions. This difference can be used to map their distribution in TEM

specimens, which can be done at a very high spatial resolution, precision and acquisition speed. This allows minimizing the electron dose and thus the electron irradiation damage, hence, the presented EELS technique could also be applied to a variety of electron beam-sensitive materials. Moreover, a procession time for EELS mapping is much shorter comparing with e.g. PED. Thus, this approach has a great potential for phase mapping with unsurpassed spatial resolution for a series of geoscience applications.

We acknowledge the European Union's Horizon 2020 research and innovation programme under grant agreement No 101005611 (EXCITE) for Transnational Access conducted at Helmholtz-Zentrum Potsdam Deutsches GeoforschungsZentrum (GFZ).

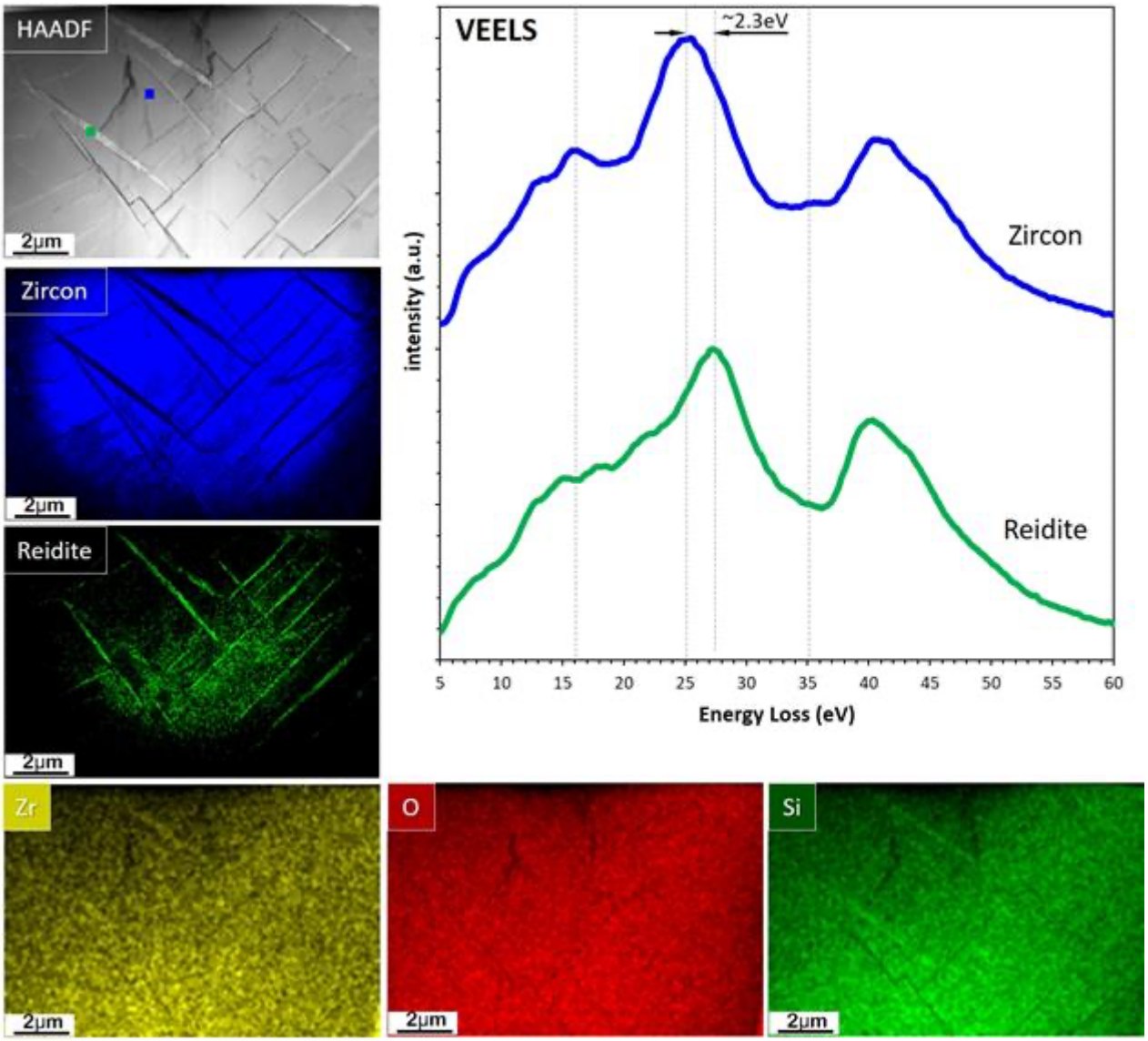

Keywords:

Zircon, reidite, EELS, phase mapping

Reference:

[1] Y-W. Yeh, S. Singh, G. Cheng, N. Yao, K.M. Rabe, D. Vanderbilt, P.E. Batson, L. Pan, G. Xu, S. Xu, Acta Materialia 257 (2023) 119191
[2] C. Chen, M. Dai, C. Xu, X. Che, C. Dwyer, X. Luo, and Y/ Zhu, Nano Lett. 24 (2024) 1539−1543

996

2D and 3D Oxidation State Mapping in FeO/Fe3O4 Nanocubes Using the Fe-M2,3 EELS Edge

Dr Mario Pelaez-Fernandez[1,2,3], Daniel del-Pozo-Bueno[4,5], Dr Maya Marinova[6], Dr Adrien Teurtrie[1], Prof. Hugues Leroux[1], Prof. Francesca Peiró[4,5], Prof. Sonia Estradé[4,5], Dr Francisco De la Peña[1]
[1]Unité Matériaux et Transformations (UMET UMR 8207), Université de Lille, Bâtiment C6, Cité Scientifique, Villeneuve d'Ascq, France, [2] Instituto de Nanociencia y Materiales de Aragon (INMA), CSIC-U. de Zaragoza, Zaragoza, Spain, [3]Laboratorio de Microscopias Avanzadas, Universidad de Zaragoza, Zaragoza, Spain, [4]LENS-MIND, Departament d'Enginyeria Electrònica i Biomèdica, Universitat de Barcelona, Barcelona, Spain, [5]Institute of Nanoscience and Nanotechnology (IN2UB), Universitat de Barcelona, , Spain, [6]Univ. Lille, FR 2638-IMEC-Institut Michel-Eugène Chevreul, , France

Poster Group 1

Background

EELS in the STEM is capable of oxidation state quantification by analyzing the fine structure of the elemental ionization edges. The exact analysis procedure has been1 and continues to be2 a major focus of EELS research. In the last decade, oxidation state mapping at the atomic level 3 has become common and advances in data analysis have enabled 3D oxidation state mapping through tomographic reconstruction of EELS oxidation maps tilt-series4.

To date, most methods of oxidation state analysis involve ionization edges with onset energies above 100 eV. For example, the standard method for iron oxidation state analysis is based on the fine structure of the Fe-L2,3 ionization edges at ~708 eV. However, the small ionization cross-section of these ionization edges presents serious experimental challenges for beam-sensitive samples. For instance, beam damage and contamination issues limited the EELS tilt series in 4 to just half of the angles needed to obtain a full tomograph.

In this context, we explore the new possibilities for oxidation state analysis offered by the new generation of hybrid-pixel direct electron detectors5. Thanks to their almost-perfect DQE and zero read-out noise, using the standard oxidation state analysis methods, the same results can be obtained with a lower electron dose. Less obviously, we show that these detectors' high speed, large dynamic range and small point spread function facilitate EELS analysis using ionization edges that lie below 100 eV. This comes with mainly two advantages with respect to edges situated at higher energies: a much higher signal-to-noise ratio for the same electron dose, and the simultaneous acquisition of the full low-loss spectrum needed for accurate absolute quantification.

To demonstrate the novel oxidation state analysis method, we perform EELS oxidation state tomography on the FeO/Fe3O4 core-shell nanoparticles from 4 by analyzing the Fe-M2,3 ionization edges at ~54 eV.

Methods

FeO/Fe3O4 core-shell nanoparticle EELS spectrum images were acquired on an FEI TITAN Themis 300 S/TEM with a dwell time of 1 ms and a pixel size ranging from 0.2 nm for single maps to 0.4 for tomography studies. EELS maps were taken at 9 different angles ranging from -70 to 70 degrees for these tomographic studies.

Spectrum images were then analyzed using a combination of SVD decomposition of the four-dimensional dataset, blind source separation, and curve fitting EELS quantification.

Results

Figure 1 shows the EEL Fe-M2,3 spectra and maps corresponding to Fe3+ (in blue) and Fe2+ (in green) extracted from the dataset by blind source separation, which has proven successful. Furthermore, the 3D reconstruction of both oxidation states has been achieved, showing a

differentiation between the core and the shell of the particle, and with minimal damage to the sample. A frame from this reconstruction can also be seen in Figure 1.

Conclusion

The combination of direct electron detection and the extension of oxidation state analysis to low-energy ionization edges has proven successful in performing EELS oxidation state tomography in beam-sensitive FeO/Fe3O4 core-shell nanoparticles, with a much lower electron dose than standard methods, notably minimizing sample damage and increasing the acquisition speed. This method sets a new standard for EELS analysis of suitable beam-sensitive materials.

Acknowledgments

Authors thank Marta Estrader and Germán Salazar-Alvarez for the synthesis of these samples.

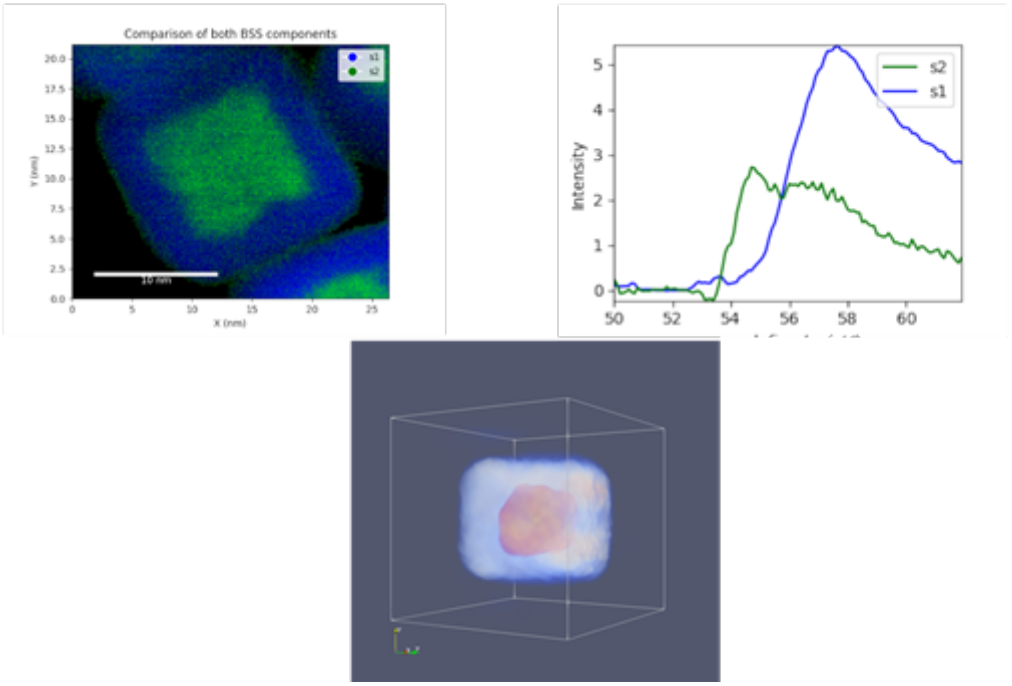

Keywords:

EELS, oxidation states, tomography

Reference:

1 L. A. J. Garvie and P. R. Buseck, Nature, 1998, 396, 667–670.

2 D. del-Pozo-Bueno, F. Peiró and S. Estradé, Ultramicroscopy, 2021, 221, 113190.

3 A. Gloter, V. Badjeck, L. Bocher, N. Brun, K. March, M. Marinova, M. Tencé, M. Walls, A. Zobelli, O. Stéphan and C. Colliex, Mater. Sci. Semicond. Process., 2017, 65, 2–17.

4 P. Torruella, R. Arenal, F. de la Peña, Z. Saghi, L. Yedra, A. Eljarrat, L. López-Conesa, M. Estrader, A. López-Ortega, G. Salazar-Alvarez, J. Nogués, C. Ducati, P. A. Midgley, F. Peiró and S. Estradé, Nano Lett., 2016, 16, 5068–5073.

5 M. Tencé, J.-D. Blazit, X. Li, M. Krajnak, E. N. Del Busto, R. Skogeby, L. Cambou, M. Kociak, O. Stephan and A. Gloter, Microsc. Microanal., 2020, 26, 1940–1942.

1039

Resolving short-range order in Carbon Nitride-based catalysts using EELS

Mr. Teodor Jianu[1], Mr. Horațiu Szalad[1], Dr. Baile Wu[1], Dr. Vladimir Rodatis[2], Prof. Dr. Dr. h.c. Markus Antonietti[1], Dr. habil. Nadezda V Tarakina[1]
[1]Department of Colloid Chemistry, Max Planck Institute of Colloids and Interfaces, Potsdam, Germany, [2]German Research Centre for Geosciences GFZ, Helmholtz Centre Potsdam, Potsdam, Germany

Poster Group 1

Background and aims
Carbon Nitrides (CNs) attract great attention as promising materials for water remediation, gas sorption, energy storage devices and photocatalysis, among others. This variety of applications stems from a set of specific properties of CNs: chemical inertness, biocompatibility, high thermal and mechanical stability, and non-toxicity [1,2]. Tuning the functionalities of carbon nitrides requires precise control over their structure and composition. Many CNs are poorly crystalline or even amorphous materials, thus requiring specific methods to describe their local structure (short- and medium-range order). In this work, we explore the possibility of obtaining quantitative information about the local structure of CN-based compounds using electron energy loss spectroscopy (EELS) in (S)TEM. Element-specific radial distribution functions (RDFs) can be derived from the extended energy loss fine structure (EXELFS) of EELS spectra [3]. Taking into account that modern analytical microscopes are much easier to access than spectroscopic beamlines at synchrotrons, this method holds great potential for fast analysis and prescreening of high amounts of samples. Here we investigate two challenging CN systems to establish the limitations of RDF analysis from EELS spectra in application to polymeric compounds: (1) the heterojunction of two photocatalysts (poly(triazine imide) (PTI) and potassium poly(heptazine imide) (K-PHI)) is used to check the ability to distinguish between two structurally closely related polymeric materials; (2) Ce-doped CNs (Ce-CNs) are used to check the limitations regarding sensing the local environment around single-atom catalysts.
Methods
All samples were first investigated using high-resolution (scanning) transmission electron microscopy (HRTEM) and electron energy loss spectroscopy (EELS) using a double aberration-corrected Jeol JEM ARM200F equipped with a cold field emission gun and a Gatan Imaging Filter (GIF) Quantum spectrometer. HRTEM images were acquired on an Oneview (4k × 4k) camera, EELS spectra were collected on a US1000 (2k × 2k) camera. EELS spectra for the PHI/PTI sample were collected using a monochromated TFS Themis Z 80-300 microscope operated at 80 kV and equipped with a GIF Continuum 1065ER spectrometer (convergence and collection angles of 22 mrad) at energy dispersion of 0.15 eV/ch. For all EELs spectra, a power law model was used for background subtraction. Multiple scattering effects were removed using the Fourier-ratio method, implemented in the Gatan Digital Micrograph Suite (GMS), version 3.4. EXELFS data were normalized and Fourier-transformed using the Athena software package. FEFF9 was used for fitting of the experimental data.
Results
The results will be described in two sections following the scientific questions defined above.
(1) Samples of PTI, K-PHI and a heterojunction between them (PTI/K-PHI) were analyzed [5]. Our study confirmed the formation of a heterojunction between the PTI and the K-PHI phase. The RDF obtained from the EXELFS part of the N K-edge of the PHI/PTI sample shows five prominent peaks. The first peak at around 1.3 Å arises due to scattering from the nearest carbon neighbors in both PTI and K-PHI. The second and third peaks correspond to the N-N (2.1 Å) and N-C (2.75 Å) distances within the aromatic rings. The fourth peak represents the summed contribution of the shortest N-N (3.3 Å) and N-C (3.58 Å) distances between adjacent layers of K-PHI. The fitting of RDFs obtained from

individual phases and the heterojunction is in progress and should allow us to quantify the amount of each phase.
2. We investigated Ce-CNs employed in photocatalytic wastewater dephosphorylation. By varying the amount of Ce(NO3)3·6H2O precursor, samples with different concentration of Ce were obtained (9.5, 17.0, 30.5 and 39.8 wt.%). HAADF-STEM images of the samples showed that Ce is present in the CN matrix in different forms: single atoms, clusters and nanoparticles. To resolve the average coordination around Ce atoms and distinguish between the aforementioned types of structures, RDFs obtained from the EXELFS part of the M4,5-edge of Ce and from EXAFS at the Ce L2,3-edge were compared. The EXELFS signal obtained from the 9.5 wt.% doped sample was found to be too low in intensity to perform reliable RDF analysis. The position (~2.5 Å) and the high intensity of the first peak on RDFs obtained from the Ce-CNs samples with 17.0, 30.5 and 39.8 wt.% suggest that Ce atoms bind to C or N and that a considerable fraction of Ce forms single atoms. On the RDFs from the CeO2 reference the most intense peak, at 3.5 Å, corresponds to the Ce-Ce distance. Different structural models for Ce incorporated into the CN matrix were constructed and the refinement of these models is currently in progress. In addition, we collected X-ray absorption spectra from these samples in order to compare RDFs obtained from bulk samples and locally from EXELFS spectra.
Conclusion
The local structure in two soft polymeric systems utilized in energy-conversion (K-PHI/PTI heterojunction) and photocatalytic water treatment (Ce-doped CNs) was studied using element-specific RDFs obtained from EELS spectra. The results suggest that a clear discrimination between the structurally closely related PHI and PTI phases is challenging; accurate data fitting (which is currently in progress) is required to make a final conclusion. The formation of Ce single atoms manifests itself by considerably higher intensity of the C/N-Ce peak on RDFs. Conclusions about the possibility to quantify the amounts of co-existing phases (CeO2, Ce-clusters and Ce-single atoms) can only be made after accurate fitting of RDFs.

Keywords:

EELS, Carbon Nitrides, short-range order.

Reference:

1. A Wang et al., Nano-Micro Lett. 9, 47 (2017). https://doi.org/10.1007/s40820-017-0148-2
2. A. Savateev et al., Angewandte Chemie International Edition (2020), 59, 15061.
3. J.B.J. Souza et al., Matter 4,2 (2021), https://doi.org/10.1016/j.matt.2020.10.025.
4. R. F. Egerton. Electron energy-loss spectroscopy in the electron microscope. 3rd ed. Boston, MA: Springer (2011).
5. H. Szalad et al., submitted to Applied Catalysis B: Environment and Energy (2023).

Max Planck Society is gratefully acknowledged.

1069

WDS-supported Bayesian Peak Deconvolution for optimized Standardless EDS-Quantification

Jörg Nissen[1], Frank Eggert[2], Dirk Berger[1], Ulrich Gernert[1]
[1]Technische Universität Berlin, Center for Electron Microscopy (ZELMI) , Berlin, Germany,
[2]Microanalyst.net, Berlin, Germany

Poster Group 1

EDS software often has the weakness that the (standardless) quantitative measurement result depends strongly on the energy calibration when peaks with evident overlap have to be deconvoluted. A typical solution is that the elements with the overlapping peaks are quantified using a WDS-analysis with much improved energy resolution and results are integrated into the EDS software via K-ratio values. Unfortunately, this WDS-analysis is then not standardless but standard based.
A combined EDS-/WDS-quantification method that is completely standardless is presented here. The novalty is that net-count ratios of the lines measured with WDS are taken into account in the Bayesian deconvolution for the standardless EDS-analysis. The by WDS measured net count ratios are used as additional boundary conditions of the probability theory based (Bayesian theorem) EDS spectrum deconvolution [1]. In this way, uncertain deconvolution of the EDS spectra is supported by additional real measured values. We use the software Benchmark-EDS and its standardless quantification model eZAF. In the latest program version Benchmark-EDS 2.01, an accuracy with relative result deviations of < ±10% was achieved (for 95% of all results) through dedicated model adjustments by empirical databases for ZAF method [2]. We will present additional EDS measurements on challenging samples on the poster, which are particularly suitable for evaluating the accuracy of standardless EDS-analysis.
The example of PbS (figure) shows how well the WDS supported deconvolution works. The spectra were measured with EDS and WDS spectrometers on a JEOL microprobe JXA-8530F. By varying the energy calibration from 5.00 eV/channel to 4.97 eV/channel, the pure EDS evaluation provides quite varying results (between 29 and 57 at% for S and 71 and 43 at% for Pb). The correct EDS quantification (50:50 at%) is achieved with 4.98 eV. With the WDS measurement support this influence of energy calibration can be eliminated. The normalised result (and at% then also) for this binary sample is determined exclusively by the deconvolution of the overlapping S- and Pb-lines. By taking into account the WDS measured line ratios, the quantification result is then stable at 50.64 at% / 49.36 at% . Uncertainties in the energy axis or other systematic errors of deconvolution of the pure EDS spectrum are then suppressed or, as in this case (binary sample, no other elements), no longer have any effect at all. It is worth noting that an EDS evaluation is still performed, but with additional WDS measurement knowledge and a probability-theory based deconvolution. The method works independently of different detection efficiencies of EDS- and WDS-detectors since peak-ratios are regarded only and the efficiency differences can be neglected since the line energies are similar. The method works even with more than 2 elements in the specimen and also if only a part of all elements is measured with WDS spectrometer, if applied only for selected EDS peak overlap problems. Additional application examples are included in the poster presentation.
In conclusion, the integration of standardless WDS-spectra acquired net-counts-ratios of lines that overlap in EDS spectra improves their peak deconvolution and makes the standardless EDS-quantification for EDS bad resolved line series independent from systematic peak deconvolution errors like the energy calibration.

Figure 1: EDS-/WDS-spectrum evaluation of PbS; a plot of deconvolution results [cps] depending on energy calibration w/wo WDS measurement support (the related quantitative results in at%)

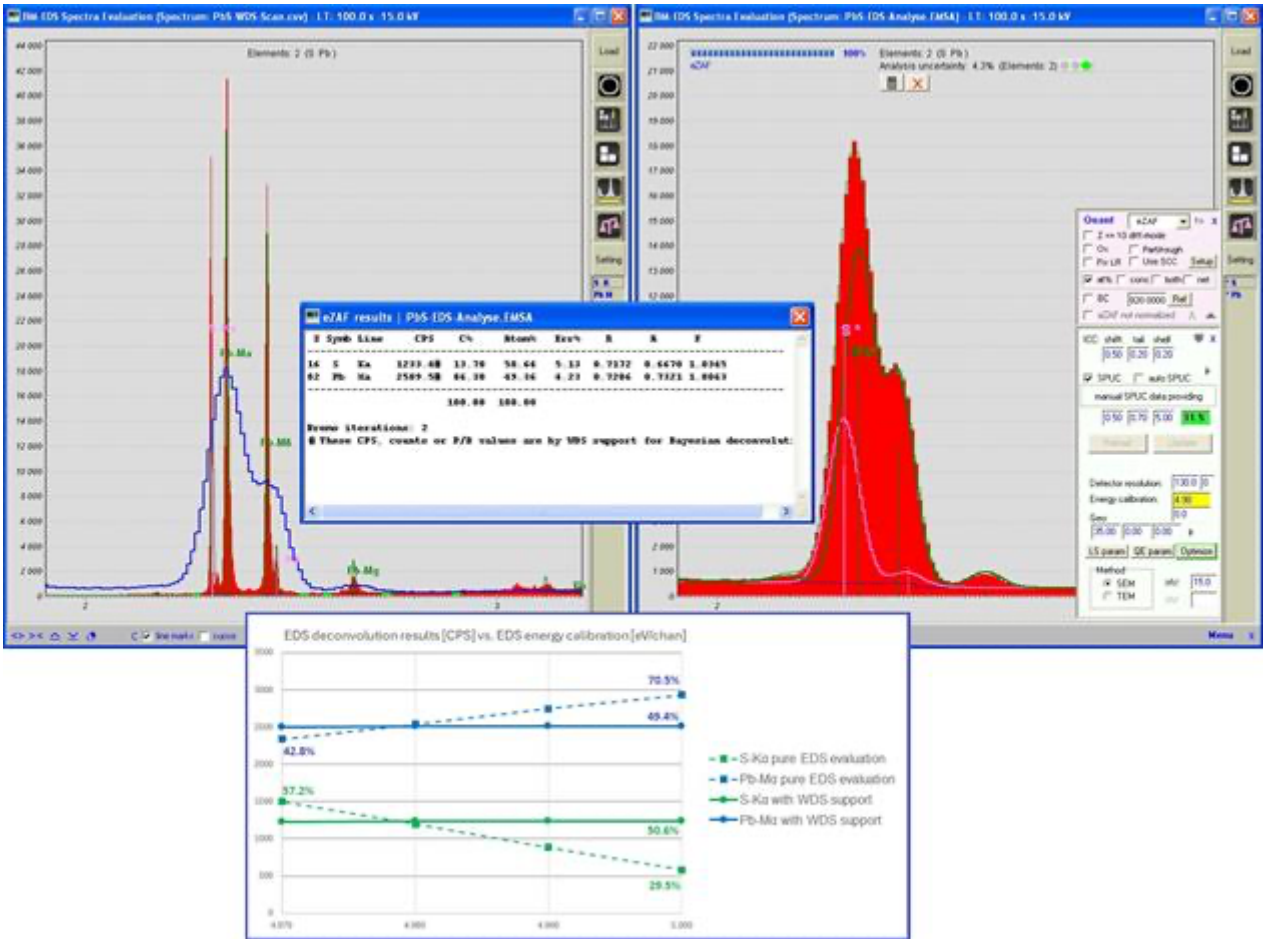

Keywords:

Bayes-Deconvolution, standardless EDS-Quantification, standardless WDS-application

Reference:

[1] F. Eggert, P.P. Camus, J. Rafaelsen (2022), Microsc. Microanal. 28 (Suppl 1) 532 DOI: 10.1017/S1431927622002732

[2] F. Eggert DOI: 10.13140/RG.2.2.26778.04804

1075

Measurement of EELS standards and application on oxidation state determination of a MeOH catalyst

Dr. Daniela Ramermann[1], Dr. Elisabeth H. Wolf[1], Dr. Michael Poschmann[1], Dr. Christoph Göbel[1], Dr. Lukas Pielsticker[1], Dr. Holger Ruland[1], Dr. Walid Hetaba[1]
[1]Max Planck Institute for Chemical Energy Conversion, Department of Heterogeneous Reactions, Mülheim an der Ruhr, Germany

Poster Group 1

Background & aims
Electron energy loss spectroscopy (EELS) is a powerful technique, foremost allowing determination of the elemental composition, but furthermore investigation of electronic properties like chemical bonding and oxidation states. This information can be collected with high spatial resolution on today´s scanning transmission electron microscopes. Most common for the analysis of EELS data is the use of cross-section models. These are often sufficient for determination of the elemental composition, but to extract information like oxidation states, a different analysis approach is necessary: Spectra of well-known reference materials (standards) improve the quantification results and allow fitting of the edge shapes to investigate and map oxidation states. These reference spectra can either be obtained by measuring well-defined materials or by using EELS reference databases [1-3]. Since their content is mostly not exhaustive to provide a set of reference spectra for each element and oxidation state for a given material, the process of obtaining commercially available materials, evaluating them for their ability to be usable as standards and using the obtained set of standards to map the oxidation states of a Cu-based MeOH catalyst [4] post-catalysis is presented.
Methods
The investigated catalyst [4] consists of Cu, ZnO and Al_2O_3. The standard materials needed to cover possible oxidation states are Cu, Cu_2O, CuO, Zn, ZnO and Al_2O_3. Of each material a commercially available sample has been obtained and investigated for its purity and oxidation state via XRD and in the TEM using EDX and EELS. Storage and sample transfer under inert conditions are considered mandatory for all samples that could oxidise further. Sample parts suitable for the measurement of standard spectra are identified, measured and spectra extracted and then imported into Gatan GMS3 as references. An EELS map of the MeOH catalyst [4] after catalytic reaction, that has been transferred under inert conditions into the microscope to preserve the oxidation states, has been acquired. This map is evaluated for materials and oxidation states based on the measured standard spectra.
Results
First it was tested via XRD if the bought materials are as described, with a focus on additional phases that can result from trace metals or different oxidation states than expected. Two materials show a deviation, Cu showed ~5% oxidation and ZnO exhibited an additional unknown phase. EDX maps of each material led to the following results: We found ~3-5% O in Cu, non-homogeneous oxidation and a slightly less O content in Cu_2O, while CuO was homogeneous as described. Some oxidation of ~5-7% was found in the Zn sample and additional O in the ZnO. The oxidation layer on the Zn appears to be amorphous, otherwise it would have been detected in the XRD. Trace elements in all cases are Al, Si and Zn for the Cu-based materials, and Al, Si and Cu for the Zn-based materials, with each amount less than 0,2 at.%. They do not explain the additional phase in the ZnO, so additional bulk EDX has been measured in SEM at low magnification, again revealing no additional elements present. Due to the O excess likely resulting from the production process, there is a high probability that this phase determined by XRD consists of zinc hydroxides.
In all EDX maps a region on the sample can be found, where the desired material in the specific state is likely to be present. Therefore, EELS spectrum images have been acquired and evaluated as

elemental mappings, allowing to identify a region of this spectrum image where the material has the desired composition and oxidation state. Of this region the standard spectra for each element and oxidation state have been obtained, integrating over several single spectra. The concurrent standards fit using these spectra on the spectrum image of the MeOH catalyst is able to differentiate between elements and oxidation state, resulting in a detailed, spatially resolved map for each (figure 1).

Conclusions

By careful combination of analysis techniques, it is possible to obtain self-measured EELS standards from commercially available standard materials. These allow to evaluate EELS data also for oxidation states with high quality, allowing deeper insight in the properties of catalysts.

Figure 1: a) HAADF image of the MeOH catalyst, from the EELS spectrum image. b) Fit result for the O K edge using self-measured standards for CuO, Cu_2O, ZnO and Al_2O_3. Mostly ZnO is present, some Al_2O_3 and very few Cu oxides. c) Fit result for the Cu $L_{2,3}$ edges using self-measured standards for Cu, CuO and Cu_2O. It shows mostly pure Cu, slightly oxidised. The region from which the line profile in e) is obtained is highlighted in this image. d) Fit result for the Zn $L_{2,3}$ edges using self-measured standards for Zn and ZnO. e) Line profile across the calculated maps, quantifying the fit result.

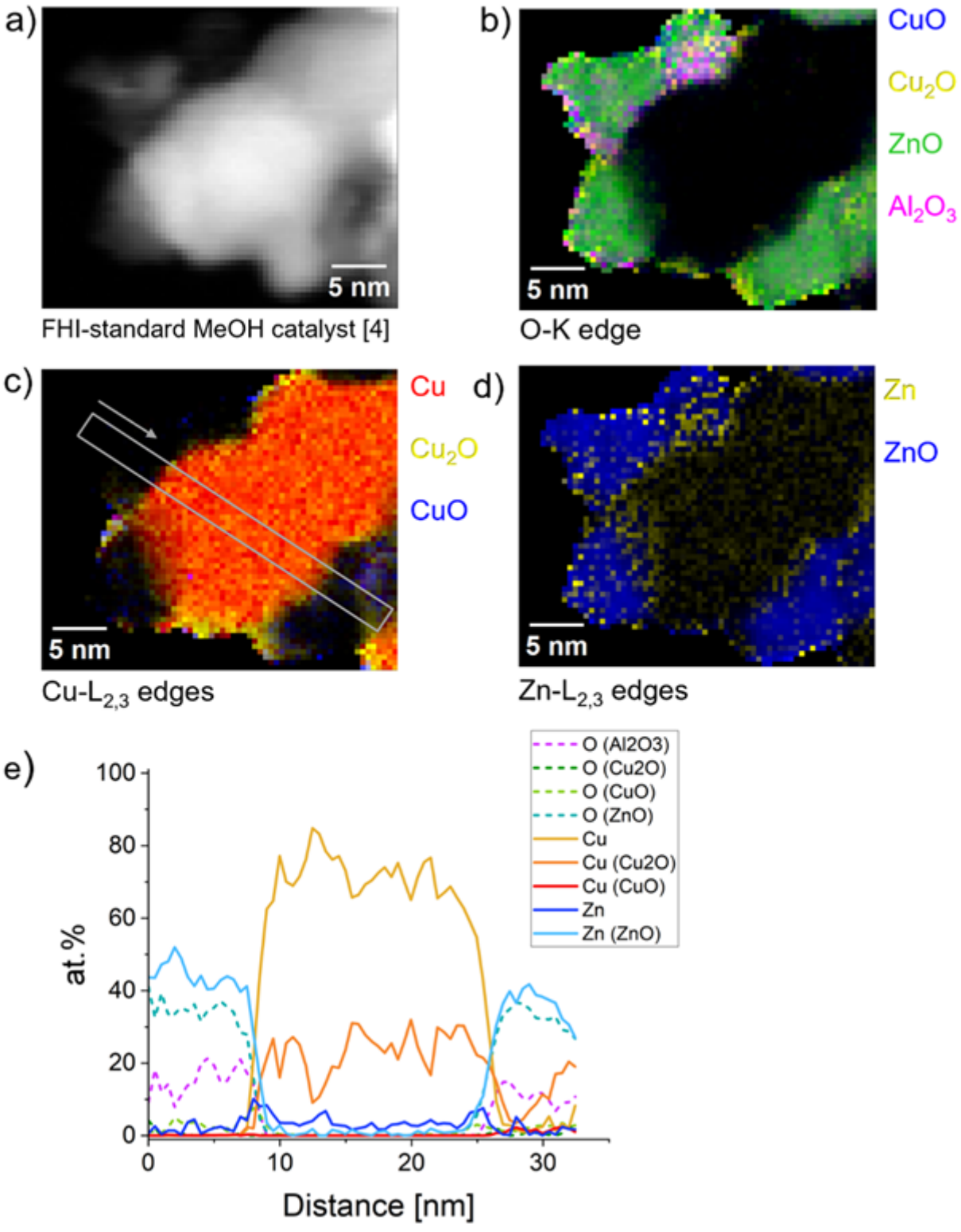

Keywords:

EELS, Oxidation state, Standards, catalysis

Reference:

[1] Philip Ewels, Thierry Sikora, Virginie Serin, Chris P. Ewels and Luc Lajaunie.
“A Complete Overhaul of the Electron Energy-Loss Spectroscopy and X-Ray Absorption Spectroscopy Database: eelsdb.eu.”
Microscopy and Microanalysis, 22, 717–724 (2016), doi:10.1017/S1431927616000179.
[2] https://eels.info/atlas

[3] Chae, J., Kim, JS., Nam, SY. et al. Introduction to the standard reference data of electron energy loss spectra and their database: eel.geri.re.kr. Appl. Microsc. 50, 2 (2020). https://doi.org/10.1186/s42649-019-0015-3
[4] Schumann et al. 2014, „Synthesis and Characterisation of a Highly Active Cu/ZnO:Al Catalyst“ ChemCatChem, 6: 2889-2897. https://doi.org/10.1002/cctc.201402278

1076

Numerical Analysis of Temperature Calibration using Plasmon Energy Expansion Thermometry

Lucas Pedersen[1], Yi-Chieh Yang[2], Mads Sørensen[3], Joerg Jinschek[4]
[1]Department of Applied Mathematics and Computer Science, Technical University of Denmark (DTU), Kgs. Lyngby, Denmark, Kgs. Lyngby, Denmark, [2]National Center for Nano Fabrication and Characterization, Technical University of Denmark (DTU), Kgs. Lyngby, Denmark, , , [3]Department of Applied Mathematics and Computer Science, Technical University of Denmark (DTU), Kgs. Lyngby, Denmark, , , [4]National Center for Nano Fabrication and Characterization, Technical University of Denmark (DTU), Kgs. Lyngby, Denmark, ,

Poster Group 1

Background incl. aims
Transmission electron microscopy (TEM) has become an important tool for characterizing the microstructure in materials [1]. However, to gain access to the underlying structure-property relationships, real-time observations in TEM experiments are required to study the material's microstructure under operating or process conditions, e.g. at elevated temperature in in-situ heating experiments. And, with the advent of TEM nanoheaters that utilize microelectromechanical systems (MEMS) technology [2,3], atomic-scale studies at elevated temperatures became feasible.
However, the exact local temperature of a TEM sample itself remains rather uncertain, limiting the interpretation of observed structural phenomena observed in in-situ TEM heating experiments. Here, we explored how accurately plasmon energy expansion thermometry (PEET) [4] can be used to determine the local temperature. .

Methods
As our model system, a tungsten (W) sample, prepared using a ThermoFisher Hydra plasma focus ion-beam (PFIB), was placed on a DENS Wildfire nanoheater [3]. For the PEET experiment, low-loss energy electron loss spectroscopy (EELS) was performed using ThermoFisher Spectra Ultra at 300kV with an energy resolution of 1 eV and a Gatan Continuum GIF with Dual-EELS functionality.
The site-specific temperature (T) within the W lamella was estimated by measuring the T-dependent energy shift of the W bulk plasmon in the low-loss EELS. The energy dispersion of 0.01 eV was used for an increased precision for detecting the plasmon energy shift.
To accurately estimate the temperature profile within the W lamellas with uniform sample thickness, we used the finite element method (FEM) in COMSOL. Further, the GPAW package [5] was used to simulate EELS spectra, based on the dielectric function. The temperature-dependent energy of the W bulk plasmon was estimated in the GPAW environment by implementing the temperature-dependent thermal expansion of the lattice constant.

Results
The COMSOL simulation models the heat flow and the temperature distribution in our W sample with increasing nanoheater temperature, providing an estimation to simulate corresponding low-loss EELS spectra. Our simulated EELS spectra using GPAW predicted a shift of the W bulk plasmon energy ΔE of ~0.236 eV when the temperature was increased from RT to 1000℃. The value of the simulated W bulk plasmon energy is at the same order of magnitude as our experimental PEET data (ΔE ~ 0.38 eV) when increasing the temperature from RT (25.11 eV) to 1000℃ (24.73 eV) in our in-situ heating TEM experiment.
However, the deviation between our simulation and experiments indicated that more details need to be considered. One approach in the simulation is that the precision of PEET has been evaluated in our simulated EELS data from the uncertainties of the coefficient of thermal expansion and of the

lattice constant at the reference temperature. Another reason could be that we have to take varying sample thickness into account in our COMSOL simulations.

Conclusion

Our study shows that PEET with W is able to measure local TEM sample temperatures in a quantitative way. The COMSOL/GPAW simulation can be used to predict the T-dependent plasmon energy and estimate the uncertainties for spectra in such experiments. This advances our approach in determining the local temperature across the sample in in situ TEM heating experiments.

Keywords:

Thermal expansion, EELS, PEET, Tungsten

Reference:

[1] K. Jungjohann et al., Transmission Electron Microscopy: Diffraction, Imaging, and Spectrometry (2016), 17-80. doi:10.1007/978-3-319-26651-0_2
[2] L. Mele, et al. Microscopy Research and Technique 79 (2016), 239-250. doi:10.1002/jemt.22623
[3] J.T. van Omme, et al., Ultramicroscopy 192 (2018), 14-20. doi:10.1016/j.ultramic.2018.05.005
[4] M. Mecklenburg et al., Physical Review Applied, 9, 014005 (2018). doi: 10.1103/PhysRevApplied.9.014005
[5] J. Mortensen et al., J. Chem. Phys. 160, 092503 (2024). doi:10.1063/5.0182685

1120

Multimodal imaging accelerates the analysis of composition in bone implant sites

Joshua Lea[1], Pedro Machado[1], Zhidao Xia[2], Dr Louise Hughes[1]
[1]Oxford Instruments NanoAnalysis, High Wycombe, United Kingdom, [2]Centre for Nanohealth, Institute of Life Science, Swansea University Medical School, Swansea , United Kingdom

Poster Group 1

Multimodal imaging approaches are essential for the characterisation of biomaterials and tissue-biomaterials interactions. We focused on multi-modal imaging techniques to acquire combined structural, molecular, and chemical information.
Confocal Raman imaging uses the inelastic scattering of photons to provide molecular bonding information and chemical identification. Hyperspectral Raman mapping gives the discrete distribution of chemical compounds within a material. Backscattered Electron and X-ray (BEX) imaging is the combined acquisition of backscattered electron (BSE) and x-ray data in a scanning electron microscope (SEM). BEX provides fast and automated mapping across a large area, collecting ultrastructural and composition data simultaneously.
We used a multimodal approach that combines Raman, SEM and BEX for investigating the interface regions between hydroxyapatite implants and bone tissue, connecting materials and tissue analysis. Resin embedded bone samples were polished to expose the implant regions. For SEM imaging we used a Zeiss 460 (Carl Zeiss Microscopy GmbH, Germany) operated at 10kV, 800pA - 1nA probe current, at 8.5mm WD, in variable pressure mode (30 Pa). BEX imaging was collected in the SEM with Unity (BEX detector, Oxford Instruments, UK) combined with an Ultim 100 (Oxford Instruments, UK). Implant areas were collected automatically, using cartography mode.
Regions of interest (ROIs) were identified with low magnification (500x magnification), large field of view (2 x 1.5mm ROIs, 30min acquisition time) rapid mapping using BEX (Fig 1a, b). High resolution images (2500x magnification) show that the implants are heterogenous, with distinct higher contras foci, rich in phosphate (Fig 1d, e). The same ROIs were subsequently imaged with Raman mapping using a 785 nm laser at 50 mW focused using a 100x objective with a spatial resolution of less than 500 nm.
We observed differences in electron density between bone and implant, as well as variability within the implant itself (Fig 1a, d). The combination of BEX and Raman analysis of the ROIs shows that electron density variation is explained by differences in concentration of calcium and phosphate (Fig 1g) and molecular composition, apatite vs hydrogenphosphate (Fig1 f, h).
The fast mapping of large samples using BEX was vital for an efficient selection of multiple ROIs of implant-bone interface. In addition, the speed of data acquisition using BEX permits the imaging of beam sensitive samples with compatibility for Raman imaging (no coating and lower electron dose related damage). The compositional information from BEX and Raman provides valuable context for the interpretation of bone and implant ultrastructure.

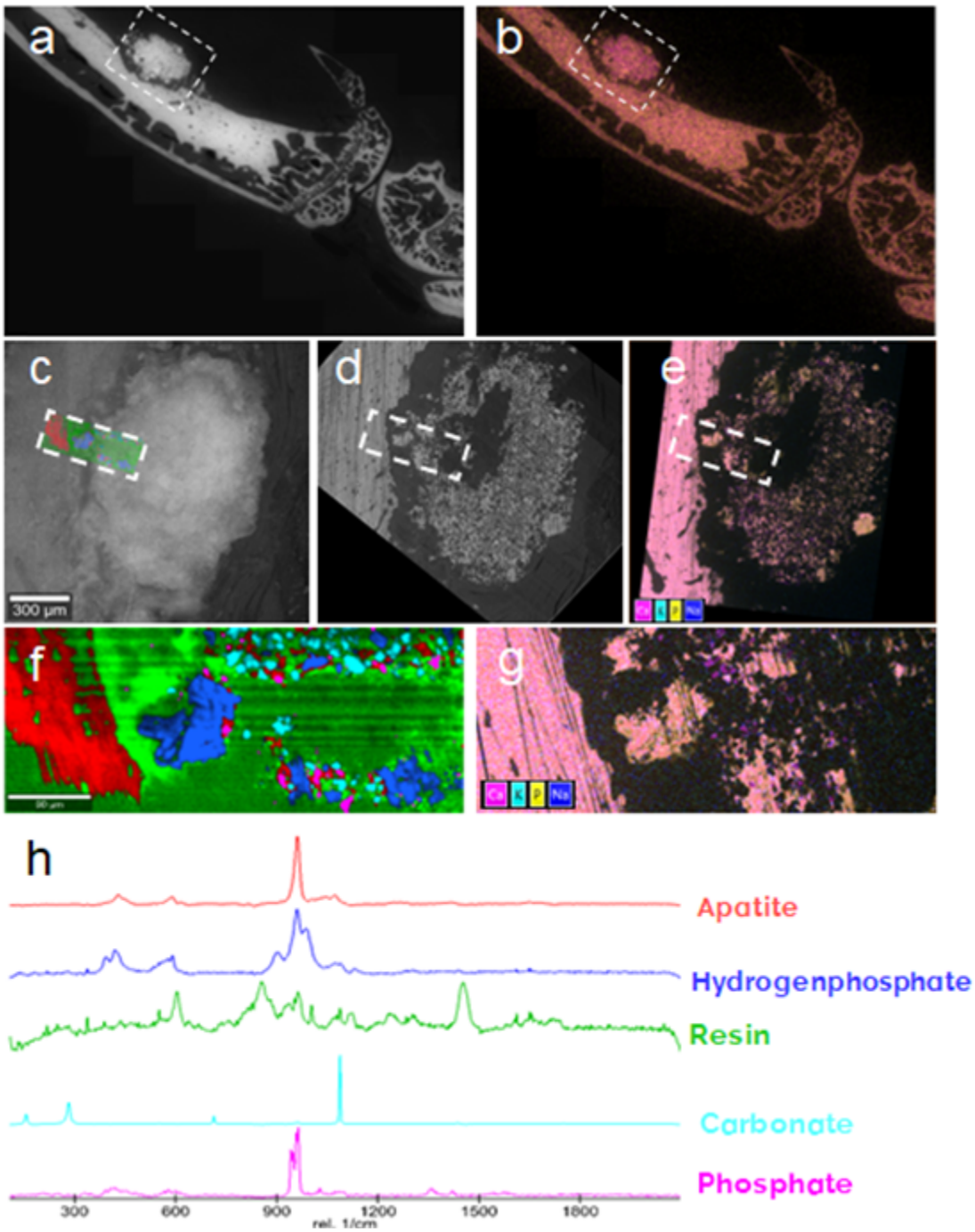

Keywords:

Multimodal imaging, Raman, BEX imaging

1271

Atomic Structure and Electron Magnetic Circular Dichroism of Individual Rock-Salt Structure Antiphase-Boundaries in Spinel Ferrites

Associate Professor Xiaoyan Zhong[1]
[1]TRACE EM Unit and Department of Materials Science and Engineering, City University of Hong Kong, Kowloon, Hong Kong SAR, China, [2]City University of Hong Kong Matter Science Research Institute (Futian), , Shenzhen, China, [3]Nanomanufacturing Laboratory (NML), City University of Hong Kong Shenzhen Research Institute, Shenzhen , China

Poster Group 1

Background incl. aims
Functional oxides are ubiquitous and exhibit a wide range of electric, magnetic, optical, and structural properties. Controlling the defects and interfaces in thin-film devices is the new challenge in multifunctional oxides. Antiphase boundaries are the interfaces between two crystallographically identical regions with shifted phases. Based on previous studies, the correlation between the existence of antiphase boundary and decreased saturation magnetization in oxides has been discussed [1]. Due to the resolution limitation of magnetism measurement, it is difficult to investigate the structure-property relationship at high spatial resolution.
Methods
EMCD, first experimentally verified by Schattchneider et al. [2], is a magnetism measurement method in a transmission electron microscope and is confirmed with the ability to reach spatial resolution better than 2 nm using a convergent beam [3]. This significant breakthrough enables us to study the magnetic properties of interfaces and boundaries on the nanometer scale. In the meanwhile, our group has developed site-specific EMCD [4] and atomic plane resolved EMCD [5] in complex oxides such as spinel and double perovskite.
Results
Intensity analysis of antiphase boundary (APB) in HAADF (high angle annular dark-field imaging) STEM (scanning transmission electron microscopy) images suggests that only half of the octahedral interstices are occupied at the rock salt structure interlayer of a new type APB in $NiFe_2O_4$ with a relative translation of (1/4)a[011]. High-spatial-resolution EMCD has been used to demonstrate experimentally reductions of ~46.8%±8.2% and ~38.8%±14.5% in the EMCD strengths of Fe and Ni in APB, respectively, compared to perfectly ordered $NiFe_2O_4$ [6]. DFT and dynamical diffraction calculations suggest that the reduced EMCD strengths result from the fact that Fe ions at the APB interlayer are antiferromagnetically coupled with each other. In contrast, Ni ions show a significant decrease in magnetic moment as a result of the formation of low-spin state Ni^{4+} (d^6) ions.
Conclusion
Our combined approach of using element-specific EMCD under high-spatial-resolution and first-principles calculations to resolve and identify the atomic structure and magnetic coupling of an individual APB in spinel ferrite is applicable to studies of a broad spectrum of other defects in magnetic materials.[7]

Keywords:

Antiphase-boundary, Electron-magnetic-circular-dichroism, Spinel ferrites

Reference:

Reference:
[1] D. T. Margulies et al., Phys. Rev. Lett., vol. 79, no. 25, pp. 5162, 1997.
[2] P. Schattschneider et al., Nature, vol. 441, pp. 486, 2006.

[3] L. Jin et al., Adv. Mater. Inter., vol. 3, pp. 1600414, 2016.
[4] Z. Q. Wang et al., Nat. Commun., vol. 4, no. 1395, 2013.
[5] Z. C. Wang et al., Nat. Mater. vol. 17, pp. 221, 2018.
[6] Z. Li, et al., Adv. Funct. Mater., vol. 31, no. 21, 2021.
[7] This work was financially supported by NSFC (52171014), Science, Technology and Innovation Commission of Shenzhen Municipality (JCYJ20210324134402007), Guangdong Provincial Department of Science and Technology (2024A1515012303), Sino-German Center for Research Promotion (M-0265), RGC (C1013-23EF, C1018-22E, CityU 11302121, CityU 11309822), European Research Council (856538, “3D MAGiC”), and CityU (9610484, 9680291, 9678288, 9610607，7020043).